Monitoring soil moisture dynamics and energy fluxes using geostationary satellite data

Dissertation zur Erlangung des Doktorgrades
an der Fakultät für Geowissenschaften
der Ludwig-Maximilians-Universität München

Vorgelegt von
Yawei Wang

München, den 16.02.2021

Erstgutachter: Prof. Dr. Ralf Ludwig

Zweitgutachter: Prof. Dr. Jian Peng

Tag der mündlichen Prüfung: 07.06.2021

Preface

Throughout the journey related to this thesis, I have received a great deal of support and assistance. First, I would like to express my deepest appreciation to my supervisor Prof. Dr. Ralf Ludwig, who educated me valuable scientific knowledge at each of our meetings and fully trusted me and in my work for the entire process of my study. He gave me the largest freedom to work and encouraged me to explore my interests with his endless support and encouragement. I also appreciate that he spent large time on improving my manuscripts and supported me to travel abroad to participate numerous conferences and workshop. I also want to express my deepest gratitude to Prof. Dr. Alexander Löw, who was my supervisor. He kindly offered me a chance to join his team and was always kind to me. I am sincerely grateful for his scientific guidance. With his so many wonderful memories, I believe he will be with us forever. I would like to thank Prof. Dr. Jian Peng from Helmholtz Centre for Environmental Research (UFZ), who provided tremendous help to figure out the difficulties and revised my manuscripts, with revision word by word.

I owe my deepest gratitude to the China Scholarship Council (CSC) and the KliMoBay project (funded under the European Regional Development Fund (ERDF)) for their financial support, a help without which I would never have been able to complete this work.

Many thanks to my nice colleagues from the LMU. I miss the office working days with Yueli Chen, Dr. Lingxiao Wang, Amarachi Kalu and Batnyambuu Dashpurev, especially during the corona time. I particularly want to thank Yueli Chen, who is a sweet girl, helped me and encouraged me a lot. I am also thankful to Benjamin Müller and Thomas Ramsauer who helped me to solve some python problems, Vera Erfurth who managed the logistical affairs. A special thanks goes to the whole AG Ludwig for their support and joyful moments that we shared in the group.

Besides, I would like to thank Prof. Dr. Pei Leng from Institute of Agricultural Resources and Regional Planning, Chinese Academy of Agricultural Sciences. He revised my manuscripts and provided many helpful feedbacks.

Last but not least, my deepest appreciation goes to my parents and grandparents who, not only during my studies, but throughout my entire life have always been there for me and always encouraged me in everything I am doing.

Summary

Soil Moisture (SM) is a key variable in global climate change, hydrology and water resources, digital agriculture and other relevant domains. Many factors affect the spatial variability of SM, such as topography, soil characteristics, vegetation and climate. These factors place obstacles in the estimation of continuous spatial and temporal SM at regional and global scales. Though the traditional methods based on in-situ observations/networks provide the most accurate SM, they are expensive, time consuming, labor intensive, as well as inferior in spatial extent. These features make the in-situ measurements more suitable to validate SM data derived from satellite retrievals instead of direct applications in various investigations. The last few decades witness the advent of satellite-based remote sensing creating profound progression of determining spatially explicit maps of SM from space.

SM at coarse spatial resolution with long time coverage and high temporal resolution would benefit the continental or global applications. SM at high spatial resolution (i.e. <=5 km) is commonly required in applications, particularly on regional and local scales.

Due to the characteristics of optical/thermal infrared data, many high spatial resolution SM retrieval approaches have been proposed. Most optical/thermal infrared-based SM retrieval methods are based on a SM-related index or proxy of SM (e.g. the Temperature Vegetation Dryness Index (TVDI) and the Apparent Thermal Inertia (ATI)). Generally, numerous in-situ SM measurements for the empirical/statistical relationships or soil field capacity/wilting point are required to retrieve SM in regional scale. These methods are naturally empirical with many limitations, including necessity of underlying soil texture or in-situ SM measurements, lack of transferability to other regions, weakness of describing physical processes, inapplicability under cloudy conditions. In this cumulative thesis, a new SM retrieval method has been proposed, which overcomes the drawbacks of traditional optical/thermal infrared-based approaches mentioned above. This SM retrieval method can directly estimate the quantitative volumetric soil water content without soil texture or empirical relationships between ground-based SM measurements and satellite-derived proxies of SM. The method developed in this thesis relies on the synergistic use of the diurnal cycles of Land Surface Temperature (LST) and Net Surface Shortwave Radiation (NSSR) from geostationary satellite allowing to provide land surface parameters at much higher frequencies (48-96 times per day). First, LST was

derived based on a generalized split-window algorithm using the two thermal infrared channels data from geostationary satellite (FY-2E). The validation proved its applicability to SM estimation by the fact that the LST retrieval show great consistent with in-situ measurements and Moderate-resolution Imaging Spectroradiometer (MODIS) LST product. Second, based on the simulated data from the Common Land Model (CoLM), including diurnal LST and NSSR cycles as well as synergistic SM variation, a simple stepwise linear regression was performed to acquire the ellipse parameters derived from the elliptical relationship between diurnal LST and NSSR cycles, thereby developing the daily average SM retrieval model. A good concordance with the ellipse model-based SM retrievals was discovered, with a correlation coefficient (R) of 0.845, a RMSE of 0.064 m^3/m^3 and a bias of 0.017 m^3/m^3 when comparing with the in-situ measurements.

The combination of high spatial resolution remote sensing data with low spatial resolution SM products has recently caught significant scientific attention in the context of improving the assessment of the spatial variability of SM. However, most optical/thermal infrared-based disaggregation methods are only available for cloud-free days. In this thesis, a new downscaling approach has been developed to disaggregate a low spatial resolution microwave SM product with optical/thermal infrared data from geostationary satellite. This method not only successfully downscales microwave SM data by using temporal information, but also avoids the failure of traditional instantaneous observations-based downscaling procedure obstructed by clouds. Until now, only two blended microwave SM products, namely the Climate Change Initiative (CCI) from the European Space Agency (ESA) and the Soil Moisture Operational Product System (SMOPS) from the National Oceanic and Atmospheric Administration (NOAA), are available with either better temporal or spatial coverage than that of other microwave SM products derived from a single sensor. However, a proper assessment and, in particular, a synchronous comparison of these two products is still lacking. Since these two blended products show big discrepancy in temporal intervals, spatial coverages, data sources and merging methods, three important conclusions have been drawn: 1) CCI has better errors statistics than SMOPS over most areas worldwide; 2) SMOPS can provide SM with acceptable accuracy over the gaps remaining by CCI; 3) Two SM products can complement each other for applications. Therefore, the new downscaling method has been developed to disaggregate the 25 km CCI SM product to 3 km spatial resolution. Similar to the ellipse method, it is based on the temporal variation of geostationary satellite-derived LST and NSSR over the mid-morning period, which is expected to enhance the temporal coverage of land surface parameters related to SM in the downscaling procedure. As a result, the multi-observations from the geostationary

satellites can potentially avoid cases in which the traditional instantaneous observation from the polar-orbit satellite is not available. Specifically, the downscaling method is based on the fact that the rate of change of LST with respect to NSSR over the mid-morning period is more sensitive to SM as shown in several previous studies. Last, the results in this thesis indicated that the downscaled SM agreed well with in-situ measurements and had comparable accuracy to the original microwave CCI SM product.

In summary, the two proposed methods in this thesis overcome some limitations of the traditional methods. They not only successfully obtained high spatial resolution SM by using temporal information, but also avoid the failure of traditional instantaneous observations-based downscaling procedure obstructed by clouds. Neither numerous in-situ SM measurements nor soil information is required. Additionally, the ellipse model can directly estimate SM without the necessity of establishing empirical relationships between in-situ SM measurements and remotely sensed parameters, which overcomes the drawbacks of traditional optical/thermal infrared-based approaches.

Zusammenfassung

Bodenfeuchte (soil moisture, SM) ist eine Schlüsselvariable für den globalen Klimawandel, die Hydrologie und die Wasserressourcen, die Landwirtschaft und andere relevante Bereiche. Viele Faktoren beeinflussen die räumliche Variabilität von SM, wie z. B. Topographie, Bodentypen, Vegetationsbedeckung und Klima. Diese Faktoren erschweren die räumlich und zeitlich kontinuierliche Schätzung von SM auf regionaler und globaler Ebene. Obwohl die traditionellen Methoden, die auf In-situ-Beobachtungen basieren, die genaueste Abschätzung von SM erlauben, sind sie teuer, zeitaufwändig, arbeitsintensiv und räumlich begrenzt. Daher eignen sich in-situ-Messungen vor allem zur Validierung der aus Satellitendaten gewonnenen SM Daten a, die eine immer höher aufgelöste flächenhafte Abdeckung ermöglichen. In den letzten Jahrzehnten hat die satellitenbasierte Fernerkundung für die räumlich explizite Kartierung der Bodenfeuchte zunehmend an Bedeutung gewonnen und sich methodisch etabliert.

Bei der Bodenfeuchtemessung aus Satellitendaten kann man unterschiedliche Skalen differenzieren: für Anwendungen auf globaler bis kontinentaler Ebene sind SM-Daten mit grober räumlicher Auflösung, hoher zeitlicher Auflösung und langer Zeitabdeckung nützlich; auf regionaler und lokaler Ebene wird üblicherweise auch eine hohe räumliche Auflösung (d.h. <= 5 km) erforderlich.

Basierend auf den Eigenschaften von sichtbarem Licht und thermischem Infrarot sind viele SM-Ableitungsverfahren mit hoher räumlicher Auflösung entstanden. Die meisten auf optischen Daten und thermischen Infrarotdaten basierenden SM-Ableitungen basieren auf einem SM-bezogenen Index oder Proxy v (z.B. dem temperature vegetation dryness index (TVDI) oder der apparent thermal inertia (ATI)). Im Allgemeinen sind zahlreiche In-situ-SM-Messungen für die empirischen / statistischen Beziehungen oder die Bodenfeldkapazität / den Welkepunkt erforderlich, um SM auf regionaler Ebene bestimmen zu können. Diese empirischen Methoden unterliegen naturgemäß zahlreichen Einschränkungen, wie beispielsweise der mangelnden Information zur Bodentextur oder der In-situ-SM-Messungen, einer nicht gesicherten Übertragbarkeit auf andere Regionen, die Schwäche bei der Beschreibung physikalischer Prozesse oder die Limitierung auf wolkenfreie Bedingungen.

In dieser kumulativen Dissertation wird ein neues SM-Abrufverfahren vorgeschlagen, das die oben erwähnten Nachteile der traditionellen, auf optischen Daten/thermischen Infrarotdaten basierenden Ansätze überwindet. Diese SM-Ableitung kann den volumetrischen Bodenwassergehalt direkt abschätzen, ohne die Bodentextur oder empirische Beziehungen zwischen bodengestützten SM-Messungen und satellitengestützten Proxys von SM zu berücksichtigen. Die in dieser Arbeit entwickelte Methode basiert auf der synergistischen Nutzung der Tageszyklen von Landoberflächentemperatur (land surface temperature LST) und kurzwelligen Strahlungsbilanz an der Landoberfläche (net surface short-wave radiation NSSR) von geostationären Satelliten, die es ermöglichen, Landoberflächenparameter in deutlich höherer Frequenz (48-96 Mal pro Tag) bereitzustellen. Zunächst wurde LST basierend auf eines verallgemeinerten Split-Window-Algorithmus unter Verwendung von Daten der beiden thermischen Infrarotkanäle des geostationären Satelliten (FY-2E) ermittelt. Die Validierung bewies ihre Anwendbarkeit auf die SM-Schätzung durch die Tatsache, dass der LST-Abruf in hohem Maße mit In-situ-Messungen und dem LST-Produkt des Moderate Resolution Imaging Spectroradiometer (MODIS) übereinstimmt. Zweitens wurde basierend auf den simulierten Daten aus dem Common Land Model (CoLM), einschließlich der täglichen LST- und NSSR-Zyklen sowie der synergistischen SM-Variation, eine einfache schrittweise lineare Regression durchgeführt. Somit werden die Parameter erfasst, die sich aus der elliptischen Beziehung zwischen den täglichen LST und NSSR-Zyklen ergeben; auf dieser Grundlage wird schließlich das SM-Modell in täglicher Auflösung entwickelt. Die auf Ellipsenmodellen basierenden SM-Ableitungen zeigen einen hohen Grad an Übereinstimmung mit den In-situ-Messungen, mit einem Korrelationskoeffizienten (R) von 0,845, einem RMSE von 0,064 m^3/m^3 und einem Bias von 0,017 m^3/m^3.

Die Kombination von Fernerkundungsdaten mit hoher räumlicher Auflösung und SM-Produkten mit niedriger räumlicher Auflösung hat kürzlich erhebliche wissenschaftliche Aufmerksamkeit im Zusammenhang mit der Verbesserung der Bewertung der räumlichen Variabilität von SM erregt. Die meisten auf optischen Daten/thermischen Infrarotdaten basierenden Disaggregationsmethoden sind jedoch nur für wolkenfreie Tage verfügbar. In dieser Arbeit wurde ein neuer Downscaling-Ansatz entwickelt, um Mikrowellen-SM-Produkte mit niedriger räumlicher Auflösung unter Verwendung von optischen Daten/thermischen Infrarotdaten von geostationären Satelliten zu disaggregieren. Diese Methode ist nicht nur erfolgreich beim Downscaling der Mikrowellen-SM-Daten mithilfe zeitlicher Information, sondern vermeidet auch das Bewölkungsproblem der traditionellen, auf Sofortbeobachtungen basierenden Downscaling-Verfahren. Bisher sind nur zwei synergistische Mikrowellen-SM-

Produkte erhältlich, nämlich die Climate Change Initiative (CCI) der Europäischen Weltraumorganisation (ESA) und das Bodenfeuchteprodukt Soil Moisture Operational Products System (SMOPS) der National Oceanic and Atmospheric Administration (NOAA). Beide können eine bessere zeitliche oder räumliche Abdeckung anbietenals Mikrowellen-SM-Produkte, die von einem einzelnen Sensor abgeleitet werden. Eine ordnungsgemäße Bewertung und insbesondere eine direkte Gegenüberstellung dieser beiden Produkte fehlen jedoch noch. Da diese beiden Mischprodukte große Unterschiede in der zeitlichen Auflösung, der räumlichen Abdeckung, der grundlegenden Datenquellen und der Methodik der Zusammenführung von Bilddaten aufweisen, werden drei wichtige Schlussfolgerungen gezogen: 1) CCI weist in den meisten Gebieten weltweit eine bessere Fehlerstatistik als SMOPS auf; 2) SMOPS kann jedoch für die verbleibenden Lücken von CCI SM-Produkte mit akzeptabler Genauigkeit liefern; 3) die Kombination der beiden SM-Produkte kann sich für mehrere Anwendungen gut ergänzen. Daher wurde die neue Downscaling-Methode entwickelt, um das 25 km CCI SM-Produkt auf eine räumliche Auflösung von 3 km zu disaggregieren. Ähnlich wie bei der Ellipsenmethode basiert diese Methode auf der zeitlichen Variation von geostationären satellitengestützten LST und NSSR über den Vormittag. Die zeitliche Abdeckung von Landoberflächenparametern, die mit der SM in Verbindung stehen, soll in der Downscaling-Methode verbessert werden. Infolgedessen können Fälle, in denen die herkömmliche Sofortbeobachtung von Satelliten mit polarer Umlaufbahn nicht verfügbar ist, durch die Mehrfachbeobachtungen von den geostationären Satelliten vermieden werden. Insbesondere basiert die Downscaling-Methode auf der Tatsache, dass die Änderungsrate von LST in Bezug auf NSSR vormittags empfindlicher auf SM reagiert, wie in mehreren früheren Studien gezeigt werden konnte. Schließlich zeigen die Ergebnisse dieser Arbeit, dass die verbesserten SM-Daten gut mit In-situ-Messungen übereinstimmen und eine vergleichbare Genauigkeit wie das originale Mikrowellen-CCI-SM-Produkt aufweist.

Zusammenfassend überwinden die beiden in dieser Arbeit vorgeschlagenen Methoden etliche Einschränkungen der traditionellen Verfahren. So erzieltder neue Ansatz nicht nur erfolgreich SM-Daten mit hoher räumlicher Auflösung durch Verwendung zeitlicher Informationen, sondern umgeht auch das Bewölkungsproblem der herkömmlichen, auf Sofortbeobachtungen basierenden Downscaling-Verfahren. Die Methodik wird dadurch besser einsetzbar, da auf zahlreiche In-situ-SM-Messungen oder die Bereitstellung von Bodeninformationen verzichtet werden kann. Darüber hinaus kann das Ellipsenmodell die SM direkt abschätzen; empirische Beziehungen zwischen In-situ-SM-Messungen und fernerkundeten Parametern müssen somit

nicht aufwendig hergestellt werden. Dadurch werden wesentliche Nachteile herkömmlicher VIS- und TIR-Verfahren überwunden.

Contents

List of Figures

List of Tables

Abbreviations

Abbreviation	Description
AMI-WS	Active Microwave Instrument Wind Scatterometer
AMSR2	Advanced Microwave Scanning Radiometer 2
AMSR-E	Advanced Microwave Scanning Radiometer
ASCAT	MetOp A/B Advanced Scatterometer
ATI	Apparent Thermal Inertia
AVHRR	Advanced Very High Resolution Radiometer
BWI	Basin Wetness Index
CCI	Climate Change Initiative
CDF	Cumulative Density Function
CoLM	Common Land Model
CSA	Canadian Space Agency
CWSI	Crop Water Stress Index
DCA	Dual Channel Algorithm
DEM	Digital Elevation Model
DISPATCH	Disaggregation based on Physical And Theoretical scale CHange
DLR	German Aerospace Center
EADS	European Aeronautic Defence and Space Company
ESA	European Space Agency
FVC	Fractional Vegetation Cover
GLEAM	Global Land Evaporation Amsterdam Model
GOM	Geometrical Optics Model
GPM	Global Precipitation Measurement
IEM	Integral Equation Model
LAI	Leaf Area Index

Abbreviation	Description
LPRM	Land Parameter Retrieval Model
LSM	Land Surface Model
LSMEM	Land Surface Microwave Emission Model
LST	Land Surface Temperature
MODIS	Moderate-resolution Imaging Spectroradiometer
NASA	National Aeronautics and Space Administration
NBMI	Normalized radar Backscatter soil Moisture Index
NDVI	Normalized Difference Vegetation Index
NOAA	National Oceanic and Atmospheric Administration
NSSR	Net Surface Shortwave Radiation
RFI	Radio Frequency Interference
RTM	Radiative Transfer Model
SAR	Synthetic Aperture Radar
SM	Soil Moisture
SMAP	Soil Moisture Active Passive
SMMR	Scanning Multichannel Microwave Radiometer
SMOPS	Soil Moisture Operational Product System
SMOS	Soil Moisture and Ocean Salinity
SPM	Small Perturbation Model
SPOT-2	Satellite pour l'Observation de la Terre -2
SSM/I	Special Sensor Microwave/Imager
SVAT	Soil Vegetation Atmosphere Transfer
TCI	Temperature Condition Index
TI	Thermal Infrared
TM	Landsat Thematic Mapper
TMI	Tropical Rainfall Measuring Mission Microwave Imager

Abbreviation	Description
TRMM	Tropical Rainfall Measuring Mission
TVDI	Temperature Vegetation Dryness Index
TWI	Topography-based Wetness Index
VCI	Vegetation Condition Index
VI	Vegetation Index
VOD	Vegetation Optical Depth
VTCI	Vegetation Temperature Condition Index
WCM	Water Cloud Model
WDI	Water Deficiency Index

1. Introduction of soil moisture

Soil Moisture (SM) is an essential variable in various scientific fields. It plays an important role in climate research and numerical weather prediction. SM is an integrator of climatic conditions and a driver of local weather and climate, which has been defined an essential climate variable by the global climate observing system (Wagner et al., 2012). SM is required to improve understanding the of land-atmosphere processes for climate researches. SM-atmosphere coupling is a vital process underlying climate variability and change over land (Berg and Sheffield, 2018). It regulates the partitioning of mass and energy fluxes between land and atmosphere and thus plays a key role in the assessment of the different components of the water and energy balance. SM is a source of water for the atmosphere through processes leading to evapotranspiration from land, mainly including soil evaporation and plant transpiration. Evapotranspiration is a key ingredient of the continental water cycle, as it returns up to 60% of all land precipitation back to the atmosphere (Oki and Kanae, 2006; Seneviratne et al., 2010). SM has been used in some weather prediction models to improve forecasts. For instance, the assimilation of Soil Moisture and Ocean Salinity (SMOS) SM into the European Centre for Medium-Range Weather Forecasts (ECMWF) Hydrology revised-Tiled ECMWF Scheme for Surface Exchanges over Land (H-TESSEL) model improved the forecast (Rodríguez-Fernández et al., 2019). Besides, the drought code from SM has been used in the detection of climate change influence on wildfire risk and for forecasting wildfire risks (Girardin and Wotton, 2009).

SM is also required in hydrology due to its substantial impacts on many processes, such as flooding, runoff, infiltration and ground water recharge (Brocca et al., 2017). Specifically, SM is the key variable for the partitioning of rainfall into runoff and infiltration, which plays a fundamental role in runoff modeling and flood forecasting (Brocca et al., 2010). For instance, SM is used for hydrological model calibrations, flood model initialization and flood simulation via data assimilation methods (Chen et al., 2011; Massari et al., 2014; Tramblay et al., 2010). Except for floods, SM is also important for many other natural hazards, such as landslide and erosion prediction. For example, some researchers analyzed the linkage between landslide occurrence and SM (Godt et al., 2006; Ponziani et al., 2012). Therefore, due to its effect on runoff and soil erosion in cropping systems, droughts or exposure to flood threats, changes in SM have substantial impacts on the socio-economic field (Wei et al., 2007).

For its vital role of water supply for plants, the knowledge of SM is required to optimize irrigation management and agricultural practices. Accurate high resolution SM is a requisite for precision farming applications to provide information for plant photosynthesis, agricultural irrigation, water management and crop yield forecasting (Engman, 1991). Besides, SM has been beneficial to assess and monitor of the epidemic risk. For example, based on an eco-hydrological model, Montosi et al. (2012) identified the factors affecting malaria dynamics and spotlighted the importance of SM.

As shown in Figure 1, SM is usually defined as the water contained in the unsaturated soil zone, expressed as either a dimensionless ratio of two masses or two volumes in %, or given as volumetric water content (m^3/m^3) adopting by most research communities (Petropoulos et al., 2015).

Volumetric SM θ(m^3/m^3) in the soil volume V is defined as follows:

$$\theta = \left(\frac{volume\ of\ water\ in\ V}{V}\right) \quad (1)$$

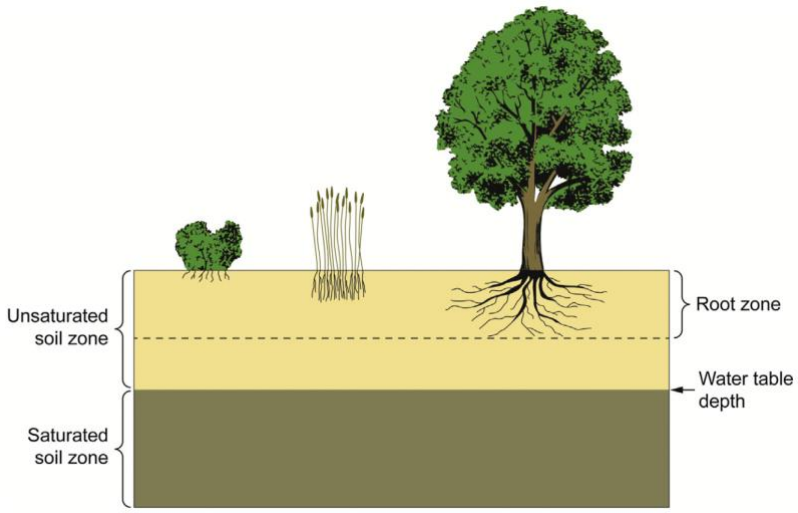

Figure 1. The saturated and unsaturated soil zones (adapted from Petropoulos et al. 2015)

Peng et al. (2020) summarized the requirements of SM depths across disciplines. In agriculture and ecosystem, only root zone SM is required for precision agriculture, erosion modelling, ecosystem monitoring and ecological modelling. While in numerical weather prediction, climate and hydrology fields, surface SM is needed. In particular, surface SM at high temporal resolution (i.e. daily or sub-daily) benefit for hydrological modelling, estimation of water cycle components, and assimilation in numerical weather prediction system. Except for P-band Synthetic Aperture Radar (SAR), remote sensing can only show its potential to provide spatially

explicit maps of the surface SM (i.e. 0-5 cm). Though P-band SAR has a deeper penetration depth than others, the increased antenna-length requirements and the influences of Radio Frequency Interference (RFI) make the construction of space-borne P-band SAR systems difficult (Peng et al., 2020).

This thesis focuses on the surface SM based on remote sensing methods. According to the spectrum, remote sensing SM are divided into four categories, including optical-, thermal infrared-, microwave-based methods, synergistic methods. The microwave-based methods consist of active and passive microwave-based methods according to the interaction between the surface of the Earth and the sensor. A comprehensive introduction of the commonly used methodologies for soil moisture estimation, including their physical principles, advantages and constraints is presented in chapter 2.

2. State of the art in remote sensing SM

2.1. Optical remote sensing of surface SM

The optical spectrum is generally defined to encompass electromagnetic radiation with frequencies in the range from 300 GHz to 3000 THz, or wavelengths in the range from 10^2 to 10^6 nm. The spectral reflectance varies by different SM in the reflectance for a range of soil types has been studied extensively over the years. In 1925, it was firstly found that the spectral reflectance decreased as SM increased using laboratory measurements (Ångström, 1925). Bowers and Hanks (1971) showed that the reflectance decreased and absorptance increased as moisture content increased. The plot of SM against reflectance indicated the possibility of using reflectance data to estimate SM. Idso et. al (1975) denoted that albedo and SM at depth of 2 cm had a linear function in drying bare soil, independent of season. It indicated that albedo could be used to estimate the SM of the very surface of the soil. The finding from Bowers and Hanks (1971) was proved by Liu et al. (2002) at low SM levels (Liu et al., 2002). Conversely, after a critical point related to soil hydrodynamic properties, reflectance increased with SM. Besides, some studies found some non-linear relationships between SM and reflectance, such as an exponential function (Lobell and Asner, 2002) and an inverted Gaussian function (Whiting et al., 2004).

Most above listed studies are based on laboratory measurements or model applications in bare soil. Gao et al. (2013) developed an empirical exponential model to estimate SM using visible (RED) and near-infrared (NIR) spectral band reflectance through removing the effect of vegetation. It was achieved through the linear decomposition of the mixed pixels in the RED-NIR spectral feature space approximately presented as a triangular shape (Figure 2), which has been applied to the regions in Beijing using satellite imagery from Landsat TM and ground-based measurements.

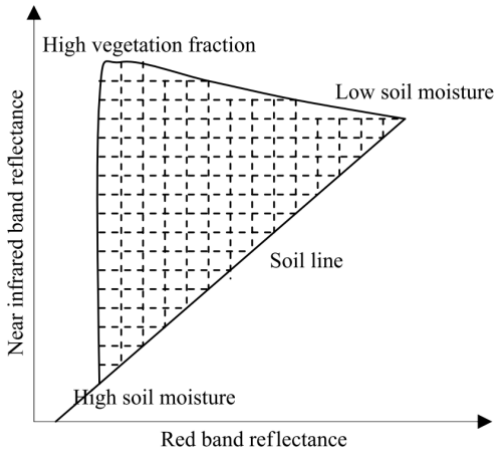

Figure 2. Red and Near infrared spectral feature space (adapted from Gao et al., 2013)

Except for SM estimation directly with empirical relationships from RED and NIR band spectral reflectance, many RED-NIR related indices have been proposed. As the most commonly used vegetation index in SM retrieval, Normalized Difference Vegetation Index (NDVI) can be calculated as (Carlson and Ripley, 1997; Myneni and Williams, 1994):

$$NDVI = \frac{NIR - RED}{NIR + RED} \quad (2)$$

NDVI was applied to drought monitoring (Peters et al., 2002; Wigneron et al., 2007) and exploration of the relationship between NDVI and SM over the U.S. Corn Belt (Adegoke and Carleton, 2002) or the Texas Gulf Coast region (Wang et al., 2007). The relationship between NDVI and SM is limited by many factors, such as vegetation types, soil types, climate conditions, topography and land cover.

Though many optical sensors are currently in orbit, fairly limited literature exists on the exploitation of quantitative SM estimation based on hyperspectral, shortwave infrared (SWIR), NIR or visible data. Some methods are based on laboratory measurements and are only applicable to bare soil. Most optical vegetation indices or drought monitoring indices are only able to present the drought status, but do not allow for quantitative SM estimates. Reflectance measurements are highly affected by cloud, incidence angle, vegetation and some inherent physical soil properties, including roughness, texture and organic matter content, which makes the exploitation of such techniques more difficult.

2.2. Thermal infrared sensing of surface SM

The Land Surface Temperature (LST) as a key variable in determining the land surface heat and water balance is affected by the fluxes of outgoing longwave, sensible, and ground heat which decide the latent heat flux, namely evapotranspiration by the energy balance principle (Lakshmi et al., 2003). The variation of LST influences SM and vice versa. Based on the relationship of energy and water, the SM retrieval methods using thermal infrared data are mainly partitioned into two group, Thermal Infrared (TI) methods and temperature index methods.

2.2.1. Thermal infrared methods

TI is a property of the soil that is defined by the volumetric heat capacity and thermal conductivity, both properties positive correlate with SM. For a given heat transfer, a high TI indicates small changes in temperature, while the opposite is true for a low TI. TI can be expressed:

$$P = \sqrt{k\rho c} \tag{3}$$

Where P is TI ($J \cdot m^{-2} \cdot s^{-1/2} \cdot K^{-1}$); ρ is density ($kg \cdot m^{-3}$); k is thermal conductivity ($J \cdot m^{-1} \cdot s^{-1} \cdot K^{-1}$); c is specific heat ($J \cdot kg^{-1} \cdot K^{-1}$) of the material.

Many initially developed TI models are based on diurnal/daily variation temperature. In 1973, Watson firstly developed a thermal model for exploring the diurnal temperature behavior which was originally created by Jaeger (1953) using an one-dimensional periodic heating model to simulate temperature variations of the lunar surface. With the advent of satellite technology, researchers started to focus on TI mapping using satellites data (Pohn et al., 1974; Price, 1977; Watson, 1982). A well-known TI approach was proposed by Price (1977). However, the method required various parameters, including diurnal temperature difference, surface albedo, solar constant, atmospheric transmittance in the visible spectrum and some meteorological data. Consequently, Xue and Cracknell (1995) proposed a simple and operational TI model by using the phase angle information of the diurnal temperature change, requiring the time of maximum temperature in the daytime for the calculation of real TI. Based on this model, Sobrino et al. (1998) developed a TI method only from remote sensing data, using three surface temperatures from National Oceanic and Atmospheric Administration (NOAA) satellite at different hours on the same day. From a different perspective, Verhoef (2004) developed a TI approach from

remote measurements of night-time net radiation and variation of surface temperatures between sunset and sunrise. However, this approach only works for bare soil and windless nights.

With the great development of TI, researchers have concentrated on the SM studies via TI approaches from 1970 onward. Based on laboratory measurements, some studies were conducted to analyze thermal parameters with variable SM (Idso et al., 1975; Reginato et al., 1976). Several researchers focused on the possibility of SM estimation by TI methods based on nature of the land surface. Pratt and Ellyett (1979) illustrated the influence of soil type and soil porosity on SM estimation. Using a simulation method, they analyzed the ability of the TI approach to estimate remotely both SM and soil type. But the limitations and complexity make TI methods difficult to derive SM. Consequently, a more easily calculated index, namely Apparent Thermal Inertia (ATI), has been initially proposed by Short and Stuart (1982). ATI is an approximation to the actual TI value which can be obtained by surface albedo and diurnal temperature as follows (Price, 1985):

$$ATI = N \times \frac{(1-A)C}{T_{max} - T_{min}} \tag{4}$$

$$N = 1000\pi \tag{5}$$

$$C = \frac{1}{\pi} \times \left[sin\alpha sin\beta\sqrt{1 - tan^2\alpha\ tan^2\beta} + cos^{-1}(-tan\alpha\ tan\beta) \times cos\alpha\ cos\beta\right] \tag{6}$$

where A is surface albedo; N is a scaling factor; C is a constant to normalize for solar flux variations with the solar declination (α) and latitude (β); T_{max} and T_{min} are the maximum and minimum surface temperatures during the diurnal cycle.

ATI as a related factor to the actual TI, it can be generated directly from remote sensing data. ATI correlates positive to SM. Because of its simple formulation, it has been widely used to map SM in the 21st century (Liu and Zhao, 2006; Scheidt et al., 2010; Van doninck et al., 2011; Verstraeten et al., 2006). Verstraeten et al. (2006) proposed a Soil Moisture Saturation Index (SMSI) from ATI series, including maximal ATI and minimal ATI, and estimated SM in the arid to semi-arid regions of north-western China using MODIS data (Veroustraete et al., 2012).

TI/ATI models are based on soil properties with great physical significance. However, TI/ATI can be converted to SM only if the soil properties are known (Minacapilli et al., 2009). If the soil texture changes or when the model is transferred to another study area, the fitting model parameters have to change accordingly. Another limitation of estimation SM based on TI/ATI

is that the accuracy diminishes over dense vegetation (Sohrabinia et al., 2014; Van Doninck et al., 2011). The precision of TI/ATI retrieval is affected by the sky conditions, especially clouds. In summary, TI/ATI methods for SM estimation are more effective in arid and semi-arid regions under clear-sky condition.

2.2.2. Temperature index methods

LST is a good indicator of the energy balance in the Earth's surface processes on a regional and global scale, which is one of the biophysical factors sensitive to surface water stress. From 1981, Crop Water Stress Index (CWSI) based on the canopy-air temperature difference has been widely used to detect plant water demand using multi-source thermal imagery including the hand-held radiometers, the Landsat Thematic Mapper (TM) and the Advanced Very High Resolution Radiometer (AVHRR) (Cohen et al., 2005; Jackson et al., 1981). Colaizzi et al. (2003) investigated the relationship between the CWSI and SM under low frequency surface irrigation. However, it is difficult to differentiate the surface soil temperature and canopy temperature. To overcome it, a Water Deficiency Index (WDI) was proposed by Moran et al. (1994), which works under two assumptions: 1) the LST difference varies linearly with the vegetation fraction; 2) the canopy temperature difference and the surface soil temperature have linear relations with the transpiration rate of the vegetation and the evaporation rate of the soil (Gao et al., 2013). Additionally, Kogan (1995) developed the Temperature Condition Index (TCI) based on time series data from the AVHRR daytime LST. This method is quite simple, since only daytime thermal remote sensing data is needed. But it is difficult to normalize the variation of daily meteorological conditions (McVicar and Jupp, 1998). TCI showed its potential to monitor drought (Tsiros et al., 2004). Though many temperature indices have been proposed, fairly limited literature exists on the exploitation of quantitative SM. Due to lack of soil and vegetation information, the quantitative relationships between most temperature indices and SM are difficult to be determined.

2.3. Passive microwave sensing of surface SM

Passive microwave remote sensing of SM spans over almost 40 years of history. In 1978, the Scanning Multichannel Microwave Radiometer (SMMR), which was launched onboard the National Aeronautics and Space Administration (NASA) Nimbus-7 satellite, was the first passive microwave satellite sensor that had the capability to estimate SM (Gloersen et al., 1984). The Special Sensor Microwave/Imager (SSM/I), a linearly polarized passive microwave

radiometer system with seven channels and four frequencies, was on board the satellites of the United States air force defense meteorological satellite program in 1987. Although it was not designed for SM sensing, a number of SM estimation studies have been conducted (Jackson, 1997). In December 1997, the Tropical Rainfall Measuring Mission (TRMM) Microwave Imager (TMI) began acquiring data with a nine-channel radiometer largely based on SSM/I technology. TMI is a dual polarization passive microwave conical scanning radiometer operating at 10.65, 19.4, 21.3, 37.0 and 85.5 GHz. The TMI observation at 10.65 GHz was used for deriving the surface wetness state. It has a spatial resolution of about 50 km and a wide swath that can provide data between $\pm$ 38° latitude (Bindlish et al., 2003). In December 2002, Advanced Microwave Scanning Radiometer (AMSR-E) of the Earth observing system was developed by the national space development agency of Japan and provided to the U.S. NASA for launch on its Aqua satellite. The AMSR-E provides daily SM measurements on a global scale with the exception of regions of snow, ice or frozen soil and dense vegetation from June 2002 to October 2011. In November 2009, the Soil Moisture and Ocean Salinity (SMOS) mission was launched to provide global SM and sea surface salinity observations from microwave L-band. As a successor instrument of AMSR-E on NASA's Aqua satellite, Advanced Microwave Scanning Radiometer 2 (AMSR2) was launched in 2012. It provides the SM product from July 2012 to present at 10 km resolution (Imaoka et al., 2010). In January 2015, Soil Moisture Active Passive (SMAP) mission was launched to provide SM every two to three days using an L-band radiometer and an L-band radar (active) (Chan et al., 2016; Entekhabi et al., 2010).

Passive sensors, in other words the so-called microwave radiometer, use very sensitive detectors to measure the naturally emitted intensity of the microwave emission from the Earth's surface at wavelengths of 1 to 30 cm, expressed as brightness temperature (TB). Similar to TIR remote sensing sensors, the emitted energy recorded by passive microwave radiometers contains the contributions from the land surface, atmosphere and reflected sky radiation. In contrast to TIR wavelengths, atmospheric effects, namely atmospheric transmission and upwelling radiation, can be ignored at frequencies below about 6 GHz. TB of the surface is related to its physical temperature, emissivity and contributions from the intervening atmosphere. TB observed by a radiometer at a height H above the ground can be expressed as (Jackson and Schmugge, 1989; Schmugge et al., 1986):

$$T_B = \tau(H) \times \left((1 - e_v)T_{sky} + e_V T_{surf}\right) + T_{atm} \quad (7)$$

$$e_v = 1 + \left(e_{surf} - 1\right) \exp(bW) \tag{8}$$

$$e_{surf} = 1 + (e_{soil} - 1) \exp(h) \tag{9}$$

$$e_{soil} = 1 - \left|\frac{\sqrt{k}-1}{\sqrt{k}+1}\right|^2 \tag{10}$$

where T_B is the TB; $\tau(H)$ is the atmospheric transmissivity; T_{sky} is the reflected sky brightness temperature; T_{surf} and T_{atm} are the thermal temperature of surface and direct atmospheric contribution separately; and e_V, e_{surf} and e_{soil} are the vegetation, rough surface and soil emissivity respectively; *b* is vegetation attenuation parameter; *W* is vegetation water content; *h* means surface roughness parameter and *k* is complex dielectric constant of the soil.

In general, passive microwave sensing of surface SM has two phases: 1) relating T_B and soil dielectric constant via a Radiative Transfer Model (RTM), 2) linking soil dielectric constant with SM through 'dielectric mixing' models.

Among the numerous retrieval algorithms, the first category is developed based on mono-configuration sensors, namely single polarization/frequency channel and view angle (Wang et al., 1990). These algorithms determine the SM only with the purpose of minimizing the error between observed and modeled TBs in the horizontal or vertical polarization. Parameters such as surface temperature, Vegetation Optical Depth (VOD) and roughness are either obtained from additional data/empirical sources or assumed to be constant (Karthikeyan et al., 2017). The Single Channel Algorithm (SCA) is an example using mono-configuration observations as the baseline retrieval algorithm for the SMAP mission and the Land Surface Microwave Emission Model (LSMEM) (Gao et al., 2004; Jackson and Schmugge, 1989).

Due to the capability of measuring multi frequency/angular dual polarization TB from the passive microwave satellite sensors, more "extra" observations are available to estimate additional parameters along with SM simultaneously, including vegetation water content through the VOD, surface roughness conditions and LST (Calvet et al., 1995; Njoku and Li, 1999; Parrens et al., 2017). The second category of passive retrieval algorithms are based on two-parameter retrieval (SM and VOD) or multi-parameter retrieval. Paloscia et al. (2001) proposed an SM retrieval algorithm using two dual polarized frequency measurements, including vegetation effects correction using X-band emission, from SMMR and SSM/I Satellites. SM retrieval methods from TMI observations are normally based on a physical model of microwave emission from a layered soil–vegetation–atmosphere medium using dual

polarization observations at 10.65 GHz (Bindlish et al., 2003; Wen et al., 2003). The baseline algorithm of AMSR-E SM product is based on three primary parameters, including SM, LST and vegetation water, from observations at four channels (Njoku and Li, 1999). As the most important variable in the retrieval process, VOD can be estimated via the 2-Parameter L-band microwave emission of the biosphere model (Wigneron et al., 2007, 2000), the Dual Channel Algorithm (DCA) (Owe et al., 2001), the Land Parameter Retrieval Model (LPRM) (Owe et al., 2008), or the revised Land Surface Microwave Emission Model (LSMEM) (Pan et al., 2014). Numerous studies have reported good accuracy and relatively low error distribution of the two/multi-parameter retrieval approaches validated with in-situ measurements (de Jeu et al., 2014; Li and Rodell, 2013; Mladenova et al., 2014).

In summary, the passive microwave SM estimation techniques have several important advantages and disadvantages. A particular advantage is that SM is the dominant parameter that influences the received signal over poorly vegetated land (Njoku and Entekhabi, 1996). In addition, the passive microwave techniques allowing day or night observation are not limited by the presence of clouds and weather. Passive microwave instruments are typically characterized by a wide spatial coverage and high temporal resolution, but also by coarse spatial resolutions normally over ~25 km. Therefore, passive microwave SM estimation is more suitable for global scale studies rather than watershed-scale applications (Moran et al., 2004). SM retrieval from TB is not straightforward as it is also affected by many factors such as vegetation cover, surface roughness and soil texture (Srivastava, 2017). Moreover, the operation of these instruments at low frequencies is limited by the effect of RFI, which influences the TB quality.

2.4. Active microwave sensing of surface SM

Due to the limitation by the coarse spatial resolution of the passive radiometer signal and the development of active sensors, some studies have focused on the radar signal, which is characterized by a higher spatial resolution and a longer revisit time. Active microwave sensors can be classified into imaging and non-imaging sensors. The most common imaging sensor is radio detection and ranging (radar), which has been used for SM retrieval since the 1970s (Jackson et al., 1981; Macdonald and Waite, 1971). As an advanced form of sensor, SAR has been designed for remote sensing purposes, such as onboard RADARSAT-1 from the Canadian Space Agency (CSA), Envisat and Sentinel-1 operated by the European Space Agency (ESA), TerraSAR-X by the German Aerospace Center (DLR) and European Aeronautic Defence and

Space Company (EADS), and SMAP developed by NASA. The non-imaging sensors include altimeters and scatterometers. Jason-1/2, Cryosat-2 and TOPEX/Poseidon are a few examples of satellites on board the altimeter. QuikSCAT, Remote Sensing Satellite (ERS) Scatterometer, NASA scatterometer and MetOp A/B Advanced Scatterometer (ASCAT) are some of the important scatterometers.

Active sensors send radiation pulses towards the Earth surface and then detect the reflected and scattered signals as backscatter coefficients. The backscatter coefficient is a function of physical and electrical properties of the soil surface and the radar characteristics including wavelength, polarization and incidence angle. It depends on the amount of radiation reflected from land surface. Generally, the models for the SM estimation using active sensors are divided into four groups: physical-based, semi-empirical, empirical and change detection models.

2.4.1. Physical-based models

The physical-based models are used to simulate backscatter coefficients according to soil dielectric constant, surface roughness and sensor properties. In principle, these physical-based models work similar to RTM of passive microwave SM estimation. Some widely used physical-based models include Small Perturbation Model (SPM) (Rice, 1951; Ulaby et al., 1986), Kirchhoff Approximation (KA) model (Ulaby, 1982), Small Slope Approximation (SSA) model (Voronovich, 1985), Michigan Microwave Canopy Scattering (MIMICS) model (Ulaby et al., 1990) and Integral Equation Model (IEM). IEM was developed by Fung et al. (1992). As one of the most widely used model, IEM calculates the backscatter coefficient given the surface characteristics of dielectric constant and surface roughness. Backscatter coefficient (σ_{pq}) is generally described by root-mean-square height (s), radar properties including frequency(f) and polarization, and local incidence angle (ϑ):

$$\sigma_{pq} = \frac{k^2}{2} e^{-2k_z^2 s^2} \sum_{i=1}^{\infty} s^{2i} \left| I_{pq}^i \right|^2 \frac{W^{(i)}(-2k_x, 0)}{i!} \tag{11}$$

where pq means the co-polarization (HH or VV) or cross-polarization (HV or VH); k is the radar wavenumber ($2\pi f$); k_z and k_x are determined by k and ϑ ($k_z = k\cos\vartheta$, $k_x = k\sin\vartheta$); $W^{(i)}(u, v)$ is the Fourier transform of ith power of autocorrelation function ρ (which is a function of correlation length L) given by

$$W^{(i)}(u, v) = \frac{1}{2\pi} \iint \rho^i(l, m) e^{(-jul - jvm)} dl dl dm \tag{12}$$

$$I_{pq}^{i} = (2k_z)^{i} w_{pq} e^{-k_z^2 s^2} + \frac{k_z^i}{2}[F_{pq}(-k_x, 0) + F_{pq}(k_x, 0)] \quad (13)$$

$$w_{HH} = -2R^H / \cos\vartheta \quad (14)$$

$$w_{VV} = -2R^V / \cos\vartheta \quad (15)$$

$$F_{HH}(-k_x, 0) + F_{HH}(k_x, 0) = -\frac{2\sin^2\vartheta\left(1+R^H\right)^2}{\cos\vartheta}\left[\left(1-\frac{1}{\mu_r}\right) + \frac{\mu_r k' - \sin^2\vartheta - \mu_r\cos^2\vartheta}{\mu_r\cos^2\vartheta}\right] \quad (16)$$

$$F_{VV}(-k_x, 0) + F_{VV}(k_x, 0) = -\frac{2\sin^2\vartheta\left(1+R^V\right)^2}{\cos\vartheta}\left[\left(1-\frac{1}{k'}\right) + \frac{\mu_r k' - \sin^2\vartheta - k'\cos^2\vartheta}{k'\cos^2\vartheta}\right] \quad (17)$$

where R^H and R^V are the reflectivities of smooth soil in horizontal and vertical polarization separately; k' is the dielectric constant of the soil; μ_r is the relative permittivity.

Based on fitting IEM numerical simulations, several models have been developed for a wide range of roughness and SM conditions, including neural networks (Satalino et al., 2002), the method of least squares (Baghdadi et al., 2002), the Bayesian approach (Paloscia et al., 2005) and look up tables (Rahman et al., 2007).

Overall, physical-based models can describe physical processes well, but they have several important disadvantages. These models are only applicable under specifically known roughness conditions. For instance, SPM only works for slightly rough surface. Zribi et al. (1997) and Baghdadi et al. (2011) found the IEM performed well over smooth surface. However, the result is bad when the IEM is applied to a real world simulation. The series of IEM models (including the Advanced IEM) are difficult to be used especially from a specific location to a large region (Bindlish and Barros, 2000). The main difficulty of using them on natural surfaces is related to the sensitivity of the models to surface roughness parameters and the difficulty associated with their correct measurement (Zribi and Dechambre, 2002). Additionally, IEM neglects scattering from the sub-surface soil volume, which may be important for dry soil conditions and long wavelengths (Schanda, 1987). Due to the drawbacks of the physical-based models, the semi-empirical models have been developed.

2.4.2. Semi-empirical models

Based on the conceptual background of physical models, semi-empirical models simplify the theoretical backscattering models with simulation or experiments. Therefore, the semi-empirical model is a good compromise between the complexity of the theoretical model and

the simplicity of the empirical model. The main advantages of semi-empirical models are that they are not site dependent and can also be used when the surface roughness cannot be measured. The most widely used semi-empirical models are the Oh model (Oh et al., 1992), Dubois model (Dubois et al., 1995) and Water Cloud Model (WCM) (Attema and Ulaby, 1978).

Based on truck-mounted network-analyzer-based scatterometer measurements, the Oh model relates the ratios of co-polarized and cross-polarized backscatter coefficients in separate polarizations to SM and surface roughness (Oh et al., 1992). The two main advantages of the Oh model are, first, only one surface parameter of surface roughness height is required; second, both surface roughness and dielectric constant can be obtained without the need for field measurements, if multi-polarized data are available. The drawbacks of the Oh model are, first, not considering multiple or secondary scattering processes, second, only applicable to the surfaces of the same type as in the experiment. Based on the original Oh model, Oh et al. (2002) further improved to take the full range of surface roughness into account for natural conditions. In contrast, Dubois model was only based on co-polarized backscatter coefficients and radar configuration parameters (namely wavenumber, wavelength, surface roughness height and incidence angle) using truck-mounted scatterometer experiments (Dubois et al., 1995). Subsequently, several evaluations of the two semi-empirical models were conducted. Zribi et al. (1997) and Baghdadi et al. (2011) indicated that Oh model simulated backscatter coefficients accurately over rough soil. Panciera et al. (2013) found that the Oh and Dubois models had comparable accuracies under HH polarization whereas the Oh model was superior in the case of VV polarization over Australia. Baghdadi and Zribi (2006) concluded that these models either overestimate or underestimate the backscatter coefficients when evaluated with C-band SAR data.

These aforementioned models are only applicable to bare soil. In the case of vegetated soil surface, the dielectric properties of vegetation (i.e., the water content of the leaves, branches, and trunk), as well as the physical structure of the vegetation, are two main determinants. Thus, to understand how vegetative structure affects microwave backscattering and to remove the impact from vegetation, the WCM as a semi-empirical model has been proposed to address this issue (Attema and Ulaby, 1978). The theoretical basis is that the co-polarized backscatter coefficient measured at the incidence angle can be expressed as the sum of the backscatter contributions from soil, vegetation, and the interaction of the radar radiation between vegetation and soil layers. Although WCM is a simple and widely used method, it is unsuitable for

vegetation with a certain height (e.g., sorghum and corn) because it ignores the multiple scattering process between the vegetation and the land surface (Song et al., 2014).

2.4.3. Empirical models

Except for the physical and semi-empirical models, various researches have been focused on the explicit relationships between the backscatter coefficients and SM. Many studies have shown a linear relationship between the backscattering coefficient and SM assuming under conditions with bare soil or constant vegetation and roughness (Kelly et al., 2003; Lakshmi, 2013; Shoshany et al., 2000; Ulaby et al., 1978). The coefficients of the linear relationship vary strongly from site to site that the model cannot be transferred from one region to other regions (Verhoest et al., 2008). Besides, some studies presented non-linear relationships between SM and the backscatter coefficient (Narayanan et al., 1999; Narvekar et al., 2015; Tomer et al., 2015; Ulaby et al., 1986). Overall, empirical models have two main drawbacks. 1) They are limited to the studies at the local level due to the lack of a physical basis. 2) The calibration of empirical models requires accurate numerous in-situ SM observation and roughness parameters. To expand the applicability of empirical models, the models must therefore contain data relating to different conditions of surface roughness and the seasons, collected over different spatial areas (Baghdadi et al., 2008).

2.4.4. Change detection approaches

While the physical, semi-empirical and empirical models are based on the backscatter coefficient obtained in a single period, it has been found that the active microwave data from multi-temporal passes in one location can be used to get the relative change in SM (Engman, 1994). Change detection approaches rely on the assumption that the temporal variability of vegetation biomass and surface roughness has a much longer time scale than that of SM. The change in the radar backscatter between repeat passes is caused by the change in SM. Therefore, multi-temporal radar data can minimize the effect of vegetation biomass and surface roughness and maximize the sensitivity of the backscatter to changes in the SM.

Several change detection approaches are widely used to estimate relative SM levels using active microwave data, including delta index approach (Thoma et al., 2004), alpha approximation method (Balenzano et al., 2011; He et al., 2017). Additionally, a Normalized radar Backscatter soil Moisture Index (NBMI) has been proposed by the backscatter measurements at two times (t_1 and t_2) over one location. By normalizing the effects of surface roughness, soil type, and

topography on the SAR backscatter, such ratio technique ($NBMI = \frac{\sigma_{t_1}+\sigma_{t_2}}{\sigma_{t_1}-\sigma_{t_2}}$) provides a relative SM index ranging between 0 and 1, based to distributed SM variations. Similarly, Wagner and Scipal (2000) estimated the relative SM by normalization of variations in backscatter coefficient with dry and wet soil surface conditions using six years of data. This methodology has been used in the soil water retrieval package algorithm to estimate SM using the data from the advanced scatterometer sensors onboard the MetOp-A and MetOp-B satellites (Lindell and Long, 2016; Wagner et al., 2013).

In summary, the active microwave SM retrieval method is fundamentally based on the large difference between the dielectric constants of water and the soil particles. The active microwave remote sensing over other spectral regions has three advantages. First, the atmosphere is effectively transparent and offers complete weather coverage in the decimeter range of wavelengths. Second, the measurement is independent of solar illumination and can be obtained in the day or at night. Third, it has much higher spatial resolution than passive data. However, active microwave instruments are typically characterized by a narrow spatial coverage and coarse temporal resolution. Both passive and active remote sensing SM retrievals are influenced by surface roughness and vegetation cover.

2.5. Synergistic methods

2.5.1. Synergistic methods of optical with thermal infrared observations

Given that the special features and limitations of each optical and thermal infrared observations, a significant number of investigations have been focused on exploring the potential for surface SM estimation from the synergistic use of optical and thermal infrared observations. Generally, most methods are based on a triangular or trapezoidal domain, namely a two-dimensional scatterplot (Figure 3) with satellite-derived surface temperature (T_s) and Vegetation Index (VI) (Petropoulos et al., 2009). Figure 3 shows the physical properties encapsulated in the T_s/VI feature space. The triangular or trapezoid domain is based on the fact that high sensitivity of T_s to SM variations over bare soil, but its reduced sensitivity over vegetated regions. The ‘dry edge’ as the border of the triangle or trapezoid is defined by the locus of highest temperature with varying from full vegetation covered land to bare soil, which represents the conditions of limited SM. Similarly, the ‘wet edge’ corresponds to the pixels of lowest temperature with maximum SM which contain differing amounts of vegetation and bare soil.

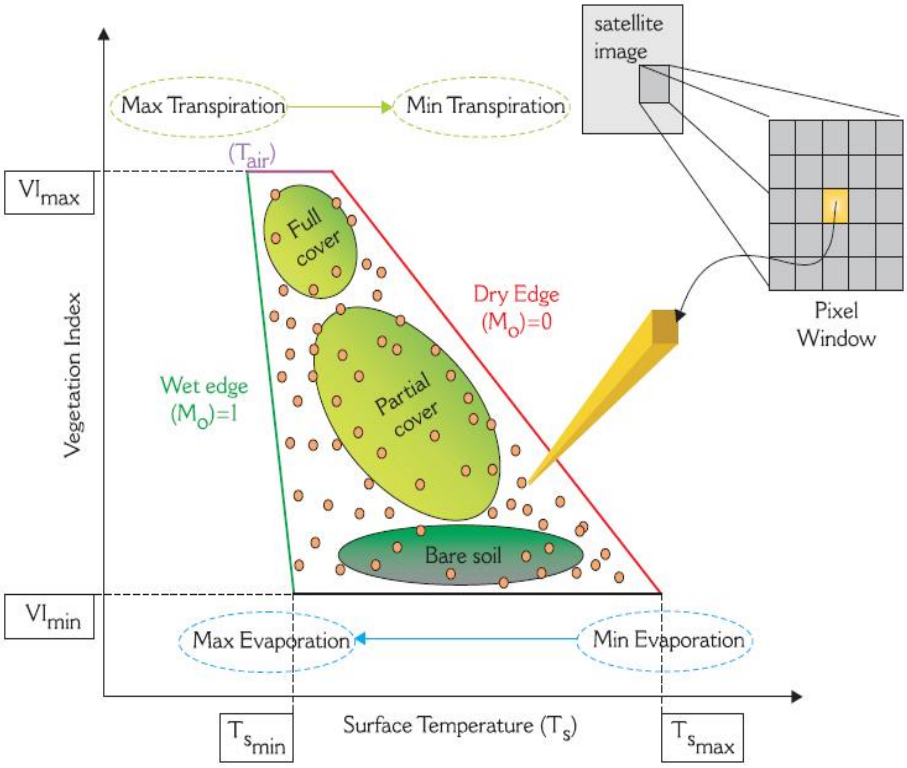

Figure 3. Summary of the key descriptors and physical interpretations of the Ts/VI feature space ''scatterplot'' (adapted from Petropoulos et al., 2009)

The investigations about T_s/VI feature space started from 1981. Carlson et al. (1981) were the first to underline the potential relationship between latent fluxes, Fractional Vegetation Cover (FVC) and SM. Goward et al. (1985) showed the potential of using the scatterplot derived rate of change of T_s with vegetation amount to determine the surface resistance to moisture fluxes based on the one-dimensional boundary layer model. Carlson and Buffum (1989) explored the T_s/VI feature space properties and found that changes in SM could be described as isopleths of SM which was plotted as a function of T_s and FVC. A triangular domain of the T_s/VI scatterplot appears as a result of the smaller sensitivity of T_s to SM over vegetated regions than over bare soil that has been confirmed by Carlson et al. (1990; 1995). Subsequently, some investigations have been focused on the boundaries of the triangular/trapezoidal shape which might be utilized by different spatial data to infer the physical restrictions for the surface SM availability (M_0) in Figure 3 (Carlson et al., 1995; Gillies et al., 1997; Gillies and Carlson, 1995; Moran et al., 1996, 1994). Moran et al. (1994) described a similar feature as a trapezoid that was further developed by some researchers (Carlson et al., 1995; Moran et al., 1997). Based on the resampled airborne remote sensing data, Carlson et al. (1995) found the T_s/VI feature space concept could be extended to regional scales with remote sensing satellites data.

Based on the T_s/VI feature space, Sandholt et al. (2002) proposed the Temperature Vegetation Dryness Index (TVDI) by linking the T_s/NDVI scatterplot to estimate SM in Figure 4. It is based on two assumptions that, first, SM is the main source of variation for T_s, second, TVDI is correlated with surface SM owning to the changes in TI and evaporative control. A dryness index has the value of 1 (TVDI=1) at the 'dry edge' with limited water availability. TVDI is 0 at the 'wet edge' with maximum evaporation and SM. TVDI can be defined (Sandholt et al., 2002):

$$TVDI = \frac{T_s - T_{s_{min}}}{a + bNDVI - T_{s_{min}}} \tag{18}$$

where $T_{s_{min}}$ is the minimum surface temperature in the triangle as defining the wet edge (TVDI=0); T_s is the observed surface temperature at a given pixel; *NDVI* is the observed normalized difference vegetation index; *a* and *b* are the parameters for the dry edge as a linear regression ($T_{s_{max}} = a + bNDVI$); $T_{s_{max}}$ is the maximum surface temperature for a given NDVI.

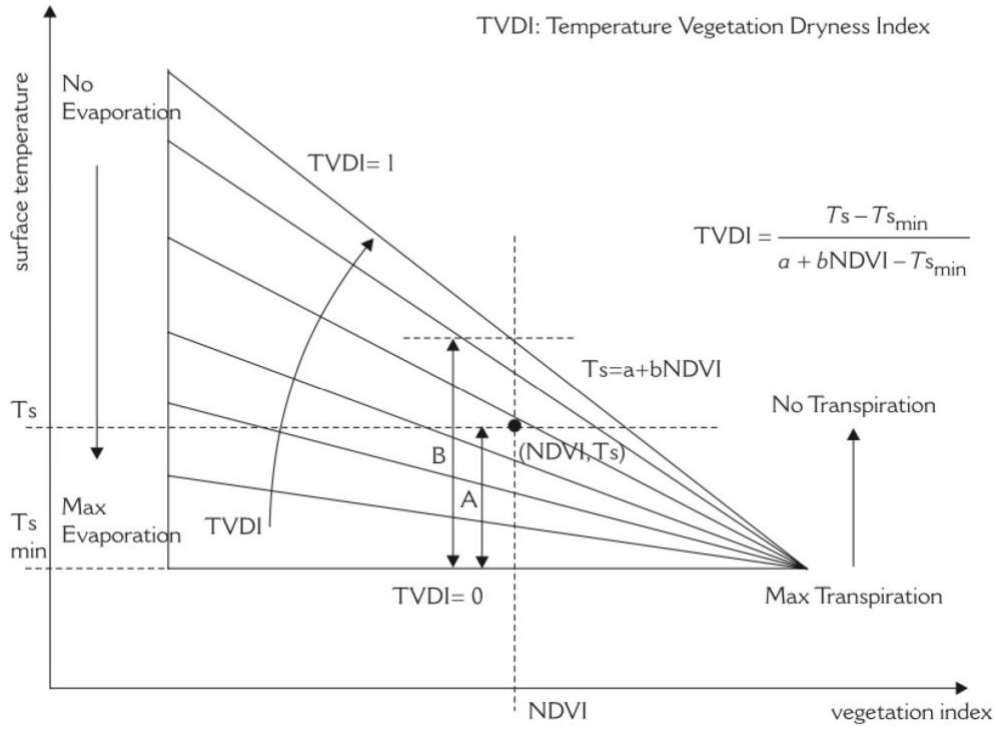

Figure 4. Computation of the Temperature Vegetation Dryness Index (TVDI) for each pixel within the NDVI/T_s feature space domain (adapted from Sandholt et al., 2002)

From a different perspective, Wan et al. (2004) proposed Vegetation Temperature Condition Index (VTCI) based on the T_s/NDVI scatterplot as shown in Figure 5. VTCI is defined as the

ratio of T_s differences among pixels with a specific NDVI value over a sufficiently large study area (Wan et al., 2004):

$$VTCI = \frac{T_{s_{max}} - T_s}{T_{s_{max}} - T_{s_{min}}} \tag{19}$$

where $T_{s_{min}}$ is the minimum surface temperature.

$$T_{s_{min}} = a' + b'NDVI \tag{20}$$

where *a'* and *b'* are the parameters for the wet edge.

Subsequently, some investigations focused on the ability of VTCI to detect drought stress (Parida, 2006; Patel et al., 2012) and downscaling the satellite coarse SM product (Peng et al., 2015a, 2015b).

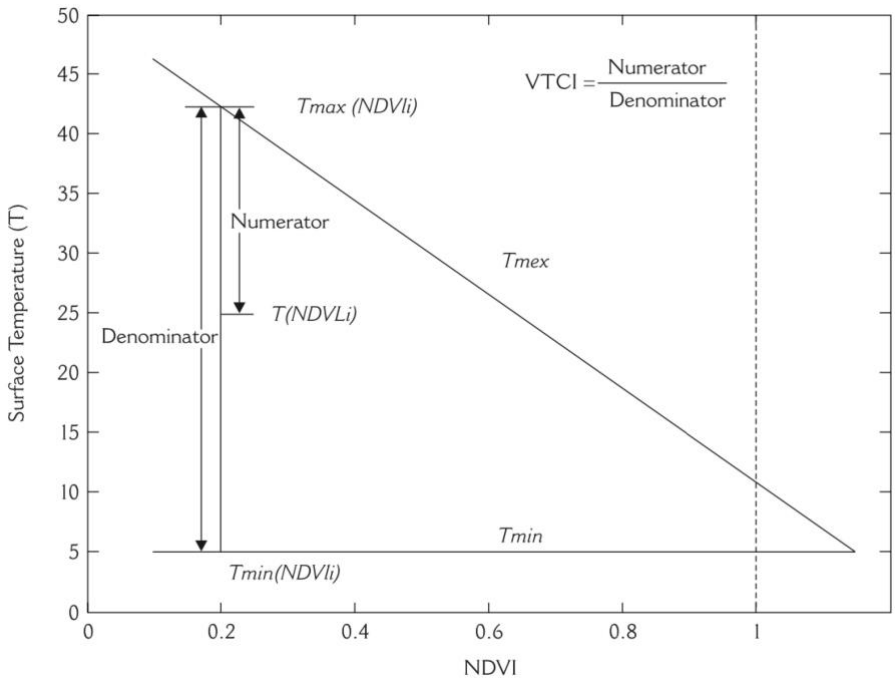

Figure 5. Illustration of the physical principles of the Vegetation Temperature Condition Index (VTCI) for each pixel within the NDVI/T_s feature space domain (adapted from Wan et al., 2004)

Additionally, except for SM retrieval from T_s/VI individually, several investigations have been focused on coupling of the T_s/VI feature space with the Soil Vegetation Atmosphere Transfer (SVAT) model. The SVAT model is a time-dependent initial value boundary layer scheme which incorporates feedback between atmosphere, plant and soil. In Figure 6, A T_s/VI feature space can be yielded based on the input (namely a full range of surface SM (θ) and FVC values) and output (e.g. latent heat flux and T_s). Slanting and nearly straight lines represent the θ at

intervals of 0.1, increasing from 0 to the right side (namely dry edge). The solution for θ can be given by a third order polynomial as (Carlson, 2007; Gillies et al., 1997; Gillies and Carlson, 1995):

$$\theta = f_\theta(\mathrm{T}_s, \mathrm{FVC}) \tag{21}$$

where $f_\theta$is a polynomial fit for θ.

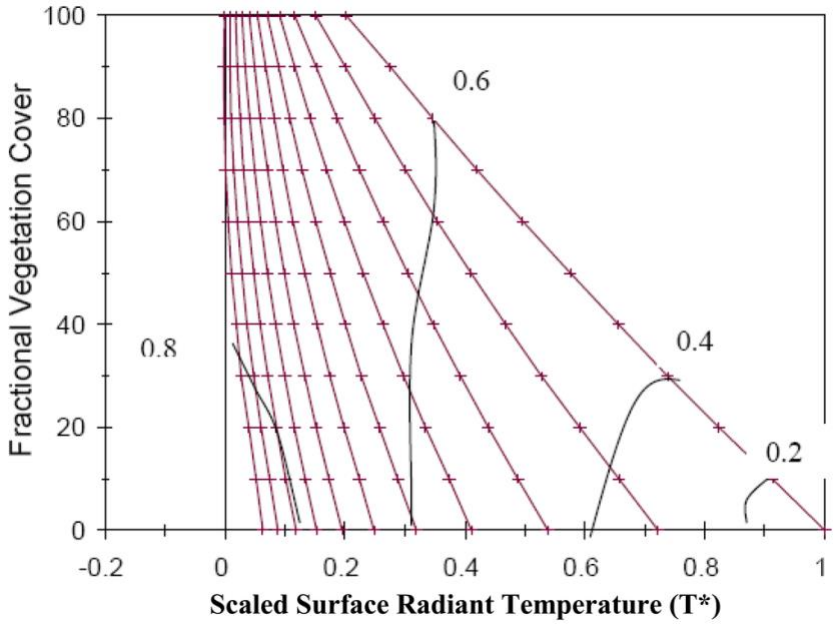

Figure 6. Soil Vegetation Atmosphere Transfer (SVAT) Model simulated triangle showing Fractional Vegetation Cover (FVC; %) versus scaled radiant surface temperature (adapted from Carlson et al., 2007)

Capehart and Carlson (1997) validated the results from this method with AVHRR data for the Mahantango region in the USA compared to SM retrieved from the soil hydrology model (Capehart and Carlson, 1994). This approach has also been widely used for other applications, including surface runoff, stormwater runoff and urbanization (Arthur-Hartranft et al., 2003; Carlson and Arthur, 2000).

Though the optical/thermal infrared methods based on T_s/VI feature space are widely used with satisfied results at finer spatial resolution, they have six limitations. First, the study area is required to be large enough to represent the entire range of SM, from dry to wet, and from bare soil to fully vegetated land surface. Second, SM is assumed to be the main source of variation for T_s which is derived from the changes in TI and evaporative control rather than changes in atmospheric conditions. Third, a large amount of ground-based SM measurements are normally required in the calibration process. Fourth, it is subjective in identifying the dense vegetation,

bare soil extremes and the warm edge. Fifth, they cannot be applied to cloudy days and night time. Last, when coupling with the SVAT model, a certain familiarity with the physics as well as their initialization and functioning on the part of the user is required, especially in regions where the knowledge of the soil and vegetation properties is patchy.

2.5.2. Active and passive microwave data fusion

Both active and passive microwave sensors have shown the potential for SM estimation for the past years. However, each sensor is more sensitive to different surface properties. A combination of passive and active sensors can provide enhanced accuracy in the retrieval of geophysical parameters (Njoku et al., 2000). Besides, the active sensor has a higher spatial resolution, while the passive one has a better temporal resolution. Therefore, some studies have been focused on the potential synergy between active and passive data for SM retrieval.

Saatchi et al. (1994) examined the synergism of radar and radiometer measurements for bare or low vegetated surface based on the SPM model. Njoku et al. (2002) estimated SM using radiometer and radar measurements from the passive and active L- and S-band airborne sensor with a RMSD accuracy of 2.3% in Oklahoma over terrain with low but variable vegetation cover. Lee and Anagnostou (2004) proposed a method synergistically using the 10.7 GHz TMI channel and 13.8 GHz precipitation radar channel observations to estimate near-surface SM and vegetation properties based on two models (i.e. the geometric optics model for bare soil and the semi-empirical WCM for vegetation). Liu et al. (2012) proposed an approach to merge SM estimates from four passive microwave products and two active microwave products into a single dataset in three steps. First, passive microwave SM retrievals from the SMMR, the SSM/I, and the TMI observations were rescaled to the AMSR-E SM product and then merged into a single passive microwave product. Second, the European Remote Sensing satellites (ERS-1/2) SCAT SM and ASCAT SM were rescaled and merged. Finally, the two passive/active merged products were rescaled against GLDAS-1Noah using the Cumulative Density Function (CDF) matching technique. Additionally, a blended microwave active and passive SM products Climate Change Initiative (CCI) SM products, including active, passive and combined active/passive SM products, have been developed by ESA (Hollmann et al., 2013). CCI combines advantages from various satellites, including AMSR-E, AMSR2, ASCAT, SMOS, SMMR, the Active Microwave Instrument Wind Scatterometer (AMI-WS) onboard the ERS-1/2, SSM/I, the TMI and the WindSat Spaceborne Polarimetric Microwave Radiometer. From the active product based on the change detection method and the passive product by the

LPRM, the combined SM has been merged and rescaled with a fixed spatial resolution of 0.25° on a daily basis. CCI SM product can be obtained from 1978 to 2019 (Dorigo et al., 2015; Gruber et al., 2019). Subsequently, with the launch of SMAP which carries both radiometer and radar instruments, several different SM products have been released using active and passive microwave data. Based on a disaggregation approach, the SMAP high-resolution radar backscatter gridded at 3 km and the radiometer brightness temperature data gridded at 36 km have been combined into a SM product at 9 km (Das et al., 2014; Entekhabi et al., 2014). Additionally, using Sentinel-1A/B C-band SAR backscatter measurements, the SMAP/Sentinel-1 L2 SM product at 3 km has been derived from the SMAP L-band brightness temperature measurements at 9 km (Das, 2019a; Das et al., 2019b). Kim et al. (2020) validated the 9 km and 3 km SMAP SM products using triple collocation analysis and CDF, which the 9 km SM product showed slightly better than the 3 km SM product. Besides, SMAP product and some other active and passive microwave SM products have been merged into a new blended microwave SM product, namely Soil Moisture Operational Product System (SMOPS). It is available from March 2017 to the present at the same spatial resolution of 0.25° as that of CCI. Compared to CCI, SMOPS has better spatial coverage at both daily and 6-hourly temporal resolutions. Overall, SMOPS and CCI combine advantages from various satellites that have finite lifetimes and different instrument characteristics with different spatial and temporal resolutions, temporal coverage and polarization.

2.5.3. Synergistic methods of microwave and optical/thermal infrared observations

Microwave and optical/thermal infrared sensors react differently to the geophysical and biophysical parameters of the land surface. Synergistic methods of microwave and optical/thermal infrared data may determine more accurate SM. Key advantage of the optical/thermal infrared data is their fine spatio-temporal resolution, which are suitable for watershed applications. The optical/thermal infrared based methods have shown promising potential in SM estimation over partially vegetated surface. Microwave data is not limited by clouds or daytime conditions. Some investigations have been focused on the contribution of microwave and optical/thermal infrared data to determine more accurate SM. However, data scaling at identical resolution and the different SM measurement depths between the instruments should be carefully taking into account when using such synergies.

A pixel-based image fusion technique was proposed by Kurucu et al. (2009) based on the Radarsat-1 fine beam mode image and Satellite Pour l'Observation de la Terre (SPOT)-2 image. It was concluded that the fusion method was useful for a partially vegetated region. Temimi et al. (2010) proposed a new Topography-based Wetness Index (TWI) based on the synergistic use of passive microwave AMSR-E 37 GHz data, MODIS Leaf Area Index (LAI) product and Digital Elevation Model (DEM) data. The results were validated over the Peace Athabasca Delta in Canada with an R near 0.7. Furthermore, some researchers used change detection approach to derived SM from microwave and optical/thermal infrared data. Gao et al. (2017) firstly tried to estimate SM from the synergetic interpretation of Sentinel-1 and Sentinel-2 data using change detection method. Foucras et al. (2020) combined numerous Sentinel-1, Sentinel-2 and MODIS data based on the change detection technique to retrieve the 500 m resolution SM at a temporal resolution of at least 6 days.

Alternative methods to high resolution SM mapping are downscaling the coarse resolution SM products using proxy observations from optical/thermal infrared data, such as LST, NDVI, FVC and surface albedo (Peng et al., 2017). Chauhan et al. (2003) proposed an approach using a Conical Scanning Microwave Imager/Sounder (CMIS) and Visible/Infrared Imager Radiometer Sensor Suite (VIIRS) data. The SM at low resolution (~ 25 km) was firstly estimated via a simplified radiative transfer model from dual-polarized microwave brightness temperature. The optical/thermal infrared parameters, including NDVI, surface albedo and LST were aggregated to the microwave resolution for building a linking model that was then used to disaggregate microwave SM into high resolution SM (Fang et al., 2013; Peng et al., 2017, 2015b). Due to the successful launch of the first L-band satellite SMOS for global measurement of the Earth's near-surface SM, some researchers focused on using optical/thermal infrared data to enhance the original SMOS spatio-temporal resolution which has a spatial resolution of 40 km and a 3-day revisit. With SMOS SM product, NDVI and LST products from MODIS, Piles et al. (2014) developed a downscaling algorithm based on a regression formula to disaggregate the SM at 1 km resolution. This approach was evaluated and proved to enhance the spatial resolution of SMOS observations over semi-arid regions (Portal et al., 2020, 2018). The model was further improved based on the LST and FVC scatterplot domain using SMOS and Meteosat Second Generation (MSG) geostationary satellite data instead of MODIS (Piles et al., 2016). Another important optical/thermal and microwave fusion method which is called Disaggregation based on Physical And Theoretical scale CHange (DISPATCH) is originally developed by Merlin et al. (2008) where the soil evaporative efficiency has been taken as SM proxy and can be estimated from the LST and FVC feature space at high resolution (Molero et al., 2016). Similar

to the DISPATCH method, a simpler downscaling method (UCLA) was proposed by Kim and Hogue (2012). It is based on a linear relationship between soil wetness index derived from the trapezoidal feature space and SM. In contrast, UCLA method and DISPATCH approach perform better than the polynomial fitting method from Chauhan et al. (2003) (Peng et al., 2017).

These simple microwave and optical/thermal fusion methods show the potential to provide fine spatio-temporal resolution SM for watershed applications. Some of them are physical and theoretical based and do not require in-situ measurements. But they are only applicable under clear-sky condition, over partially covered vegetation areas and depend on the accuracy of SM retrieved from passive microwave data. Additionally, data scaling at identical resolution, the different SM measurement depths between the instruments and different sensitivities of sensors to different surface properties should be carefully taking into account.

The above subsections describe the details of different categories of remote sensing SM retrieval methods. A brief summary of them in terms of the typical methods, advantages, and disadvantages is shown in Table 1.

Table 1. Summary of the remote sensing-based methods employed in SM retrieval

Category	Typical approaches	Advantages	Disadvantages	Example researches
Optical	Reflectance-based methods	Good spatial resolution, multiple satellites available, hyperspectral sensors promising, based on mature technology	Inapplicability in cloudy conditions and at night time, under the influence of angle of incidence and some inherent physical soil properties, for the drought status not for the quantitative SM	Idso et al. (1975), Peters et al. (2002), Gu et al. (2008), Gao et al. (2013).
Thermal infrared	TI/ATI models/ Temperature index methods	Good spatial resolution, multiple satellites available, physical basis, better accuracy by TI/ATI models over arid and semi-arid regions	Weak relationship to SM under vegetated cover, inapplicability in cloudy conditions and at night time, lack of transferability to other regions	Minacapilli et al. (2009), Sohrabinia et al. (2014), Van doninck et al. (2011).
Microwave passive	Various methods	Use not limited by clouds and/or daytime conditions, high temporal resolution and wide spatial coverage	Coarse spatial resolution, under the influence of vegetation cover, soil texture, surface roughness and RFI	Njoku and Entekhabi (1996), Moran et al., (2004)
Microwave active	Physically-based, Semi-empirical, Empirical, and Change detection approaches	Use not limited by clouds and/or daytime conditions, fine spatial resolution	Narrow spatial coverage, coarse temporal resolution, under the influence of surface roughness, vegetation cover, and water content on the backscattering coefficients	Schanda (1987), Attema and Ulaby (1978), Baghdadi et al. (2008).
Synergistic methods	Optical and thermal infrared	Good spatial resolution, multiple satellites available, have great physical significance, simple & straightforward implementation	High requirements of the study area, transferability difficult, requirement for numerous in-situ measurements, some limitations of the models basis, limited to cloud-free and daytime conditions	Carlson and Buffum (1989), Carlson et al., (1995), Petropoulos et al. (2009)
	Microwave active and passive	Improved spatio-temporal resolution and SM retrieval	Difficulties in data scaling at identical resolution, the different SM measurement depths between the instruments and different sensitivities of sensors to different surface properties	Saatchi et al. (1994)
	Microwave and optical/thermal infrared	Minimized influence of vegetation and surface roughness, fine spatio-temporal resolution, physical and theoretical based, not requiring in-situ measurements	Difficulties in data scaling at identical resolution, the different SM measurement depths between the instruments and different sensitivities of sensors to different surface properties, inapplicability in cloudy conditions and at night time	Kurucu et al. (2009)

3. Aims and structure of this thesis

3.1. Aims and goals

SM at coarse spatial resolution with long time coverage and high temporal resolution would benefit the continental or global applications. However, this spatial resolution is often too coarse for regional and local applications, including hydrology, agriculture and numerical weather prediction, which normally require a spatial resolution of 1 to 10 km (Peng et. al., 2020; Brocca et al., 2017). For instance, SMAP and optical/thermal-based SM products are used to develop irrigation physics in land surface models and improve forecasts (Lawston et al., 2017). Most optical/thermal infrared-based methods for higher resolution SM retrievals are based on the SM-related indices or proxies of SM. Either numerous in-situ SM measurements for the empirical/statistical relationships or soil field capacity and wilting point are generally required for retrieving SM at regional scales. These empirical methods naturally have many limitations, including the requirement for knowing the underlying soil texture or in-situ SM measurements, lack of transferability to other regions, low efficacy of describing physical processes or inapplicability in cloudy weather. In this thesis, a new SM retrieval model aims to overcome the drawbacks of traditional optical/thermal infrared-based approaches mentioned above. Additionally, the combination of high spatial resolution remote sensing data with low spatial resolution SM products has recently caught significant scientific attention in the context of improving the understanding of the spatial variability of SM. However, most optical/thermal infrared-based disaggregation methods can only be carried out in cloud-free days. Thus, the second purpose of the thesis is to develop a downscaling method based on temporal information. Not only can this method successfully downscale microwave SM data to avoid the failure of traditional instantaneous observations-based downscaling procedure obstructed by clouds, but it is also simpler than the first proposed method.

In the following, the relevant underlying research questions (RQ) of this thesis are presented. Additionally, the corresponding hypotheses (HY) are formulated:

Q1: Is it possible to propose an optical/thermal infrared-based SM retrieval method (or downscaling method) which can be applied to cloudy days?

HY1: High spatial resolution optical/thermal infrared data have a limited surface penetration depth and high perturbation of the signal by clouds. Since most optical/thermal infrared-based SM retrieval methods and optical/thermal infrared-based disaggregation methods rely on instantaneous optical/thermal land surface parameters, they are inapplicable in cloudy days. Geostationary satellites are capable of providing land surface parameters at much higher frequencies (48-96 times per day) than polar-orbit satellites. Therefore, the multi-observations provided by geostationary satellite data may potentially overcome the shortage that the traditional instantaneous observation from the polar-orbit satellite is not available.

Q2: Can the drawbacks of traditional optical/thermal infrared-based SM retrieval methods to estimate SM directly instead of SM-related indices be overcome by a novel retrieval approach?

HY2: Most optical/thermal infrared-based SM retrieval methods are based on a SM-related index or proxy of SM (e.g. the Temperature Vegetation Dryness Index (TVDI) and the Apparent Thermal Inertia (ATI)). However, these methods are only applicable over some specific regions. For instance, ATI method can be only applied in arid and semi-arid regions if the soil properties are known (Minacapilli et al., 2009). For the TVDI method, large research area is required so as to represent the entire range of SM, from dry to wet, and from bare soil to fully vegetated land surface. In addition, a large number of in-situ measurements are often necessary in these methods to establish the empirical relationships between ground-based SSM measurements and satellite-derived proxies of SM.

Most optical/thermal infrared-based SM retrieval studies focus on only a single daily, mid-morning or maximum measurement (Minacapilli et al., 2009; Verstraeten et al., 2006; Wetzel and Woodward, 1987; Zhao and Li, 2013). Previous studies demonstrated that TI and the diurnal change of the LST are strongly related with SM (Schmugge et al., 1978). Based on the Noah Land Surface Model (LSM) and the Gaussian emulation machine for sensitivity analysis, LST and NSSR are found to be the most sensitive parameters to SM (Zhao and Li, 2013). Diurnal cycles of LST and NSSR that provide additional information about the land surface thus have potential to improve SM retrieval. In terms of the relationship between the diurnal cycles of LST and NSSR, SM may be directly estimated instead of SM-related indices.

Q3: Among all remote sensing SM products, blended CCI and SMOPS global SM products have either better temporal or better spatial coverage than those derived from

a single sensor. Which one is more suitable for application? Can these two blended SM products synergize with each other in the application?

HY3: Although blended SMOPS and CCI SM products from most of the mainstream microwave sensors, they use different data sources, merging methods and temporal intervals to develop the final products, thus harboring different characteristics. Specifically, the SMOPS product has the same spatial resolution of 0.25° as that of CCI; however, both daily and 6 hourly temporal interval datasets are just available from SMOPS that might provide more alternatives than CCI in potential applications, such as drought/flood monitoring and land surface assimilation systems where frequent SM measurements are required. Additionally, due to more incorporated sensors, SMOPS should have better spatial coverage than CCI. However, as the enhanced quality control of the microwave SM retrievals for CCI products, CCI may have better accuracy than SMOPS. For instance, the stricter triple collocation analysis based error characterization has been used in the CCI retrievals, which has guaranteed the quality of the combined SM product (Gruber et al., 2019). The assessments will be conducted by using reanalysis SM product and in-situ measurements to indicate when and where the CCI or SMOPS has better errors statistics. Furthermore, since SMOPS has better spatial coverage, it would have potential to be an alternative when CCI is not available, which may provide SM with acceptable accuracy over the gaps remaining by CCI as well.

Q4: Currently most microwave SM products are at coarse spatial resolution of tens of kilometers. How to improve their spatial resolution to meet the criteria of the applications at the regional or local scale?

HY4: Downscaling techniques with coarse microwave SM products and some variables related to SM from optical/thermal infrared data can improve the original SM spatial resolution. Furthermore, based on temporal information rather than instantaneous optical/thermal land surface parameters, the new downscaling method may optimize downscaling process in cloudy days.

3.2. Thesis outline and scientific publications

The cumulative thesis comprises four peer-reviewed scientific publications. Three of them were published, one is currently under review. Figure 7 illustrates the connection and contribution of each paper to this thesis as well as to the scientific areas.

The thesis encompasses two different methods for obtaining high resolution SM based on geostationary satellite data. The first method is elliptical SM retrieval model, including paper I and paper II. Paper I introduced the theory and evaluation of the generalized split-window LST retrieval method. Based on the LST estimates from paper I, the elliptical SM retrieval model was developed in paper II. The potential of geostationary satellite data was further explored to overcome drawbacks of elliptical retrieval model. Therefore, the downscaling method was proposed in paper III and paper IV. Based on the evaluation of CCI and SMOPS SM products in paper III, a new downscaling approach using CCI was developed in paper IV.

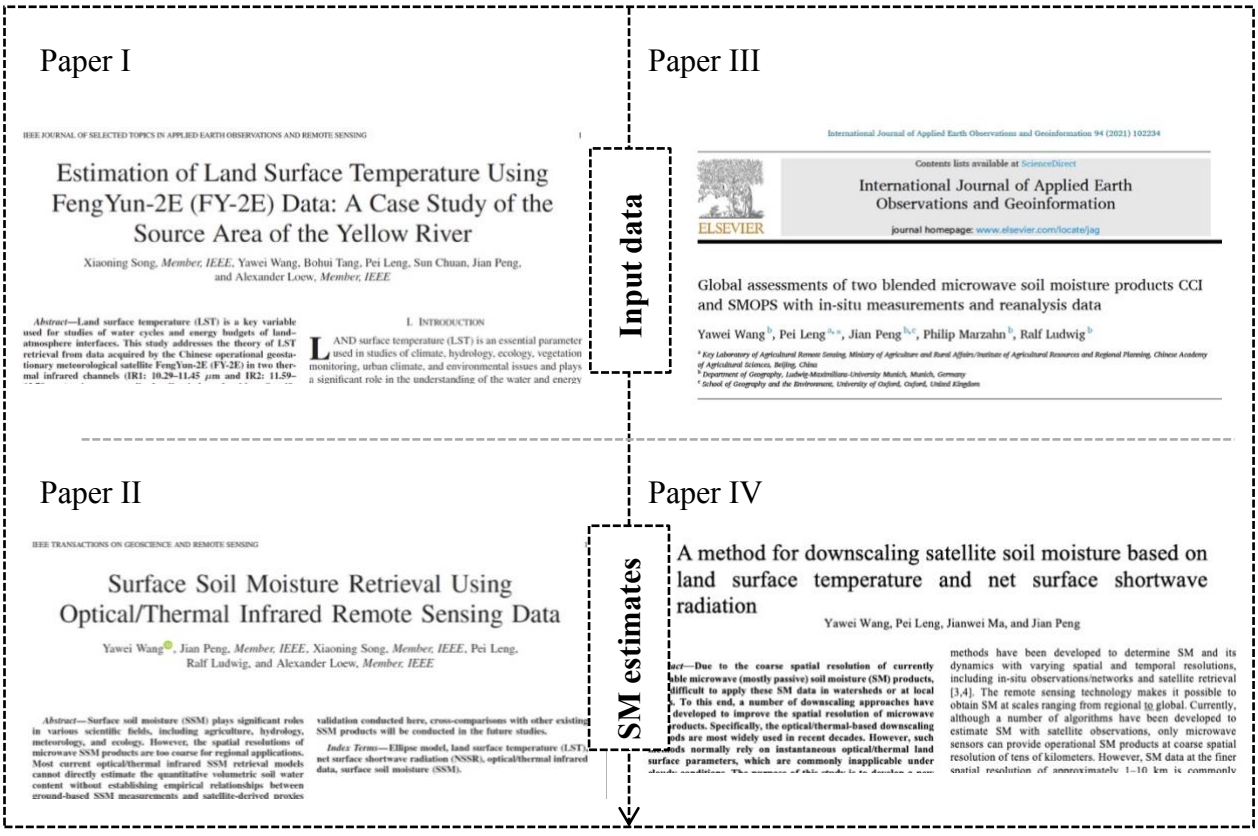

Figure 7. Position of the papers and topics they are covering within this PhD thesis

Paper I: Publication in the journal IEEE Journal of Selected Topics in Applied Earth Observations and Remote Sensing

Citation: Song, X., Wang, Y., Tang, B., Leng, P., Chuan, S., Peng, J., & Löw, A. (2017). Estimation of land surface temperature using FengYun-2E (FY-2E) data: A case study of the source area of the Yellow River. *IEEE Journal of Selected Topics in Applied Earth Observations and Remote Sensing*, 10(8), 3744-3751.

Impact Factor: 3.827

Status: published

Research outline: This study addresses the theory of LST retrieval from data acquired by a geostationary satellite (FY-2E) in two thermal infrared channels (IR1: 10.29–11.45 μm and IR2: 11.59–12.79 μm) using a generalized split-window algorithm. Specifically, land surface emissivity (LSE) in the two thermal infrared channels is estimated from the LSE in channels 31 and 32 of a polar-orbit satellite (MODIS) product. Results indicate that the LST retrieval agrees well with in-situ measurements and MODIS LST product. Therefore, the generalized split-window algorithm was demonstrated its applicability on geostationary satellite data to estimate LST and further for SM estimation in paper II.

Authors' contributions: Xiaoning Song: Conceptualization, writing - review & editing, funding acquisition, supervision. Yawei Wang: Conceptualization, methodology, analysis, interpretation, writing - original draft, review & editing. Bohui Tang: Methodology. Pei Leng: Writing - review & editing, resources. Chuan Sun: Writing - review & editing, resources. Jian Peng: Writing - review & editing, resources. Alexandar Löw: Methodology, writing - review & editing, supervision.

Paper II: Publication in the journal IEEE Transactions on Geoscience and Remote Sensing

Citation: Wang, Y., Peng, J., Song, X., Leng, P., Ludwig, R., & Loew, A. (2018). Surface soil moisture retrieval using optical / thermal infrared remote sensing data. *IEEE Transactions on Geoscience and Remote Sensing*, 56 (9), 5433-5442.

Impact Factor: 5.855

Status: published

Research outline: Based on the diurnal cycles of LST retrieval from paper I and Net Surface Shortwave Radiation (NSSR), an elliptical-new SM retrieval model has been developed. This retrieval model directly estimates the quantitative volumetric soil water content without establishing empirical relationships between ground-based SM measurements and satellite-derived proxies of SM. By considering the influence of vegetation, the model has been optimized using Fractional Vegetation Cover (FVC) data. A correlation coefficient (R) of 0.845, a RMSE of 0.064 m^3/m^3, and a bias of 0.017 m^3/m^3 have been obtained when comparing with the in-situ measurements. It is revealed that the elliptical-new SM retrieval model can obtain good SM estimates using geostationary satellite data. The article investigates the following research questions:

Q1: Is it possible to propose an optical/thermal infrared-based SM retrieval method (or downscaling method) which can be applied to cloudy days?

Q2: Can the drawbacks of traditional optical/thermal infrared-based SM retrieval methods to estimate SM directly instead of SM-related indices be overcome by a novel retrieval approach?

Authors' contributions: Yawei Wang: Conceptualization, methodology, analysis, visualization, writing - original draft, review & editing. Jian Peng: Conceptualization, writing - review & editing. Xiaoning Song: Writing - review & editing. Pei Leng: Writing - review & editing. Ralf Ludwig: Writing - review & editing, supervision, funding acquisition. Alexandar Löw: Conceptualization, methodology, writing - review & editing, supervision.

Paper III: Publication in the journal International Journal of Applied Earth Observation and Geoinformation

Citation: Wang, Y., Leng, P., Peng, J., Marzahn, P., Ludwig, R., (2021). Global assessments of two blended microwave soil moisture products CCI and SMOPS with in-situ measurements and reanalysis data. *International Journal of Applied Earth Observation and Geoinformation 94*, 102234. https://doi.org/10.1016/j.jag.2020.102234

Impact Factor: 4.650

Status: published

Research outline: Currently, only two blended microwave SM products, namely the CCI from the ESA and the SMOPS from the National Oceanic and Atmospheric Administration, are available with either better temporal or better spatial coverage than those of other SM products

derived from a single sensor. However, an assessment and especially a synchronous comparison of these two products are still lacking, making it difficult to determine a better alternative in actual applications. In the present study, a comprehensive assessment of the two blended products was conducted with reanalysis SM data from the ECMWF and in-situ measurements from the International Soil Moisture Network. The results indicated that CCI reveals overall better accuracy than that of SMOPS with both in-situ measurements and reanalysis data under different climate patterns. Further investigation also confirmed that SMOPS could be a potential alternative over the regions where CCI is not available, since SMOPS has better spatial coverage than CCI. This work provides the foundation for downscaling method development in paper IV. The article investigates the following research questions:

Q3: Among all remote sensing SM products, blended CCI and SMOPS global SM products have either better temporal or better spatial coverage than those derived from a single sensor. Which one is more suitable for application? Can these two blended SM products synergize with each other in the application?

Authors' contributions: Yawei Wang: Conceptualization, methodology, analysis, visualization, writing - original draft, review & editing. Pei Leng: Conceptualization, writing - review & editing, funding acquisition. Jian Peng: Writing - review & editing. Marzahn Philip: Writing - review & editing. Ralf Ludwig: Conceptualization, writing - review & editing, supervision, funding acquisition.

Paper IV: Submitted to the journal IEEE Geoscience and Remote Sensing Letters

Citation: Wang, Y., Leng, P., Ma, J., and Peng, J. A method for downscaling satellite soil moisture based on land surface temperature and net surface shortwave radiation. *IEEE Geoscience and Remote Sensing Letters*, doi: 10.1109/LGRS.2021.3062453.

Impact Factor: 3.833

Status: published

Research outline: Most optical/thermal-based downscaling methods normally rely on instantaneous optical/thermal land surface parameters, which are only applicable in clear days. The purpose of this study is to develop a new downscaling method based on the temporal variation of geostationary satellite derived LST, NSSR and blended microwave CCI SM product aforementioned in paper III. The proposed method is expected to improve data

availability in cloudy days, because geostationary satellites are capable of providing land surface parameters at high temporal resolution. Results indicate that the downscaled SM agrees well with in-situ measurements and has comparable accuracy with the original microwave CCI SM product. The overall RMSE with the in-situ measurements for the original microwave SM and the downscaled SM are 0.054 m^3/m^3 and 0.057 m^3/m^3, respectively. This method is not only a successful attempt to downscale microwave SM data using temporal information, but also has the potential to avoid the failure of traditional instantaneous observations-based downscaling procedure due to clouds. The paper addresses the following research questions:

Q4: Currently most microwave SM products are at coarse spatial resolution of tens of kilometers. How to improve their spatial resolution to meet the criteria of the applications at the regional or local scale?

Authors' contributions: Yawei Wang: Conceptualization, methodology, analysis, visualization, writing - original draft, review & editing. Pei Leng: Conceptualization, writing - review & editing, funding acquisition. Jianwei Ma: Writing - review & editing. Jian Peng: Conceptualization, writing - review & editing, supervision.

4. Scientific Papers

4.1 Paper I: IEEE JSTARS - Estimation of land surface temperature using FengYun-2E (FY-2E) data: A case study of the source area of the Yellow River

Estimation of Land Surface Temperature Using FengYun-2E (FY-2E) Data: A Case Study of the Source Area of the Yellow River

Xiaoning Song, *Member, IEEE*, Yawei Wang, Bohui Tang, Pei Leng, Sun Chuan, Jian Peng, and Alexander Loew, *Member, IEEE*

***Abstract*—Land surface temperature (LST) is a key variable used for studies of water cycles and energy budgets of land–atmosphere interfaces. This study addresses the theory of LST retrieval from data acquired by the Chinese operational geostationary meteorological satellite FengYun-2E (FY-2E) in two thermal infrared channels (IR1: 10.29–11.45 μm and IR2: 11.59–12.79 μm) using a generalized split-window algorithm. Specifically, land surface emissivity (LSE) in the two thermal infrared channels is estimated from the LSE in channels 31 and 32 of the moderate-resolution imaging spectroradiometer (MODIS) product. In addition, an eight-day composition MODIS LSE product (MOD11A2) and the daily MODIS LSE product (MOD11A1) are used in the algorithm to estimate FY-2E emissivities. The results indicate that the LST derived from MOD11A1 is more accurate and, therefore, more appropriate for daily cloud-free LST estimation. Finally, the estimated LST was validated using the MODIS LST product for the heterogeneous source area of the Yellow River. The results show a significant correlation between the two datasets, with a correlation coefficient (R) varying from 0.60 to 0.94 and a root mean square error ranging from 1.89 to 3.71 K. Moreover, the estimated LST agrees well with ground-measured soil temperatures, with an R of 0.98.**

***Index Terms*—FengYun-2E (FY-2E), land surface temperature (LST), moderate-resolution imaging spectroradiometer (MODIS), split-window algorithm.**

Manuscript received July 7, 2016; revised November 6, 2016, January 24, 2017, and February 27, 2017; accepted March 13, 2017. This work was supported in part by the National Nature Science Foundation of China Grant 41271379 and the Chinese Academy of Sciences (CAS) Key Research Program "Hydrological Impacts from Degrading Permafrost in the source area of the Yellow River" Grant KZZD-EW-13. *(Corresponding author: Yawei Wang.)*

X. Song and C. Sun are with the College of Resources and Environment, University of Chinese Academy of Sciences, Beijing 100049, China (e-mail: songxn@ucas.ac.cn; sunchuan14@mails.ucas.ac.cn).

Y. Wang, J. Peng, and A. Loew are with the Department of Geography, the Ludwig Maximilian University of Munich (LMU), Munich 80337, Germany (e-mail: yawei.wang1@gmail.com; jian.peng@mpimet.mpg.de; alexander.loew@lmu.de).

B. Tang is with the Institute of Geographic Sciences and Natural Resources Research, Chinese Academy of Sciences, Beijing 100864, China (e-mail: tangbh@igsnrr.ac.cn).

P. Leng is with the Key Laboratory of Agri-Informatics, Ministry of Agriculture/Institute of Agricultural Resources and Regional Planning, Chinese Academy of Agricultural Sciences, Beijing 100081, China (e-mail: lengpei09@mails.ucas.ac.cn).

Color versions of one or more of the figures in this paper are available online at http://ieeexplore.ieee.org.

Digital Object Identifier 10.1109/JSTARS.2017.2682961

I. Introduction

LAND surface temperature (LST) is an essential parameter used in studies of climate, hydrology, ecology, vegetation monitoring, urban climate, and environmental issues and plays a significant role in the understanding of the water and energy balance of the Earth's surface [1]–[9]. With the rapid development of the remote sensing technologies, a series of methods and algorithms has been developed to retrieve LST from satellite data [10]–[18]. Algorithms can roughly be grouped into three categories: single-channel methods [19]–[23], split-window algorithms, and multiangle methods [24], [25].

McMillin [26] initially proposed a split-window algorithm to express LST as a simple linear combination of the two brightness temperatures measured in the two thermal infrared (TIR) channels. A variety of split-window algorithms were subsequently developed and modified to successfully estimate sea surface temperatures [27]–[29]. Because of the homogeneous nature of sea surfaces, emissivity under these conditions can usually be regarded as stable and close to one. A split-window algorithm was shown to be suitable for sea surface temperature retrieval in a study by Niclòs *et al.* [30], with an error as low as 0.3 K. Due to the success of sea surface temperature retrieval, split-window algorithms were also used to estimate LST [31]. However, because natural land surfaces are more complicated than sea surfaces, the aforementioned split-window technique may not be suitable for land applications. As a result, numerous researchers have developed different split-window techniques to estimate LSTs for different land surface conditions [32]–[34]. Becker [35] evaluated the effects of reflectance difference between the two thermal infrared channels of advanced very high-resolution radiometer data on LST retrieval and showed that using a split-window algorithm for estimating LST was practical in theory. Vidal [36] subsequently demonstrated that LST could be estimated from National Oceanic and Atmospheric Administration data with an error of 3 K. Similar to the equation developed by Becker and Li [32], Wan and Dozier [33] proposed a generalized split-window (GSW) algorithm to estimate LST from the moderate resolution imaging spectroradiometer (MODIS) TIR channels 31 and 32. The MODIS LST product has been widely verified and used in various applications all over the world.

Compared with commonly used polar-orbit satellites, geostationary satellites are capable of providing 48–96 images per day

with a fixed observation angle for a given pixel, which is beneficial for understanding energy budgets. In recent years, LST estimation based on European or Chinese geostationary meteorological satellite data have drawn widespread attention. Based on the Meteosat Second Generation (MSG) data in Europe, Qian et al. [37] shows the MSG LST products are consistent with MODIS LST products and have the same trend over the two study areas during both the daytime and the night-time. Atitar and Sobrino [38] also derived LST from MSG data, and found root mean square errors (RMSE) of 1.9 K and 1.5 K relative to measured data and MODIS products, respectively. In a recent study, Gao et al. [39] addressed three significant improvements to the algorithm based on day/night temperature-independent spectral indices (TISIs) for estimating Land Surface Emissivity (LSE) from MSG data. The results demonstrated that more than 70% of the differences are within 2.5 K and that the LST differences tend to be lower at night than in the day.

Several researchers in China have studied LST retrieval using China's geostationary data. Tang [34] initially estimated LST from China's FengYun-2C (FY-2C) geostationary satellite data using the GSW algorithm originally proposed by Wan and Dozier [33]. The simulated results indicated that the GSW algorithm could be successfully applied to LST retrievals using FY-2C data. However, persuasive validation was lacking during a further study of FY-2C observations. Zhang and Wang [40] subsequently obtained LST from FY-2D based on a split-window algorithm and a diurnal evolution cycle of LST, preliminarily assessing the accuracy for a single cloud-free day over a small area. As a result, a correlation coefficient (R) of 0.5 and an RMSE of 4.4 K were found between the retrieval and the MODIS product. Quan [41] estimated LST with a diurnal linear hybrid model and used FY-2C data to evaluate the model. The mean absolute differences for October 7 and March 28, 2005 in Beijing were 1.64 K and 2.48 K, respectively. In summary, although LST estimation using FY data has been proven feasible, actual applications and validations are relatively deficient, particularly over heterogeneous regions. The primary objective of this study is to derive LST data from one of the newly operational geostationary meteorological satellites, FengYun-2E (FY-2E). For the heterogeneous source area of the Yellow River, FY-2E-derived LST is verified with the MODIS LST product and compared with the ground-measured soil temperature.

II. Study Area and Data

A. Description of the Study Area

The source region of the Yellow River (SAYR, 95°50′E–103°30′E and 32°20′N–36°10′N) covers an area of 121 972 km^2 on the northeastern Qinghai-Tibet Plateau (see Fig. 1). The elevation of the area ranges from 2500 to 6200 m above sea level and exhibits heterogeneous features with various landscapes, including alpine meadows, steppes, lakes, and even permafrost. According to a previous study, the mean annual air temperature in the study area varies between −4 °C and +2 °C from the northwest to the southeast and the mean annual precipitation is approximately 530 mm [42]. The south and southeast regions of the study area are characterized by cold and semihumid climate, while the northern and western regions present a cold and arid to semiarid climate pattern. Moreover, the Cold and Arid Regions Environmental and Engineering Research Institute (CARRERI) and the Faculty of Geo-Information Science and Earth Observation of the University of Twente (ITC) have installed an extensive soil temperature monitoring network in the eastern part of the SAYR, as shown in Fig. 1. The network consists of 20 stations that monitor the soil temperature at a depth of 5 cm every 15 min and can serve as a surface temperature proxy for the evaluation of estimated LST.

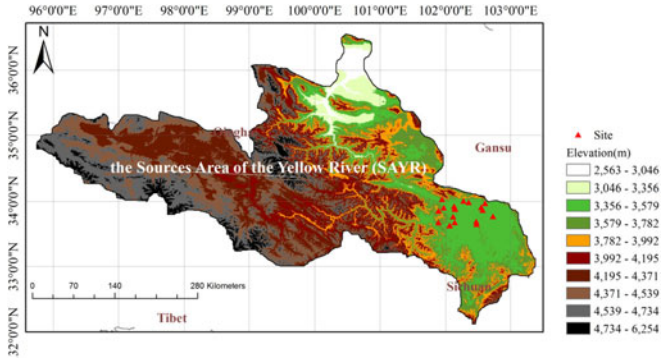

Fig. 1. Digital elevation model of the source area of the Yellow River (SAYR).

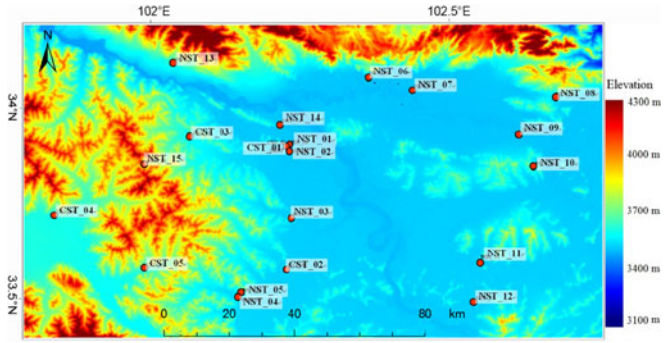

Fig. 2. DEM of the 20 soil temperature sites.

B. FY-2E Data

China announced the FY-2 series project in 2001, which includes five geostationary meteorological satellites, namely, FY-2C/2D/2E/2F/2G. In particular, FY-2E was launched at the end of 2008 to replace FY-2C. Satellite data collected by FY-2E can better meet the validation requirements of ground soil temperature measurements than FY-2C [43]. Thus, FY-2E observations were selected to estimate LST in the study area. The optical imaging radiometer onboard the FY-2E satellite is a stretched-visible and infrared spin-scan radiometer (S-VISSR) that includes one visible channel and four infrared thermal channels. Instrument characteristics are shown in Table I. The FY-2E can obtain one full disc image covering the Earth's surface from 60 °N to 60 °S latitude and from 45 °E to 165 °E longitude every 90 min. The adjustments of FY-2E spectral response functions can increase the brightness temperature differences between FY-2E's two split-window channels within all dynamic ranges relative to that of the

TABLE I
MAIN TECHNICAL SPECIFICATIONS OF THE RADIOMETER

Channel	Spectral range (μm)	Spatial resolution (km)	$\mathrm{NE\Delta T}_{300\mathrm{K}}$
VIS	0.510–0.905	1.25	–
IR1	10.29–11.45	5	0.19 K
IR2	11.59–12.79	5	0.26 K
IR3	3.59–4.09	5	0.30 K
IR4	6.32–7.55	5	0.19 K

*NEΔT is the noise equivalent temperature difference.

FY-2C [43]. This improves the inversion ability of FY-2E's split-window channels. In this study, the FY-2E data are obtained from the National Satellite Meteorological Center (NSMC) (*http://www.nsmc.cma.gov.cn/NSMC/Home/Index.html*) and are used as the data sources to estimate LST in the study area.

C. MODIS Data

MODIS is an instrument aboard the Terra and Aqua satellites. It covers the globe every one to two days, providing data at moderate spatial resolution (250 m at nadir) with a large spectral range (36 channels). The MOD11B1, MOD11A1, and MOD11A2 products are used in this study to estimate and verify the derived LST. Product MOD11B1, which provides LST at 6-km spatial resolution, is obtained using the day/night LST algorithm [44] and GSW algorithm [33] in seven MODIS bands (bands 20, 22, 23, 29, 31, 32, and 33). The MOD11A1 product has a tile of daily LSE at 1-km spatial resolution with emissivities of bands 31 and 32, which are retrieved by a classification-based emissivity method according to land-cover types [45]. The MOD11A2 product at 1-km spatial resolution is an eight-day composition LST dataset that is derived by averaging MOD11A1 data. The LAADS provides the MODIS data (http://ladsweb.nascom.nasa.gov/data/search.html).

D. Ground Soil Temperature Measurements

The soil temperature monitoring network operated by CARRERI and ITC in fig. 2 from report "Continuous *in situ* soil moisture measurements at Maqu site" in CEOP-AEGIS by L.Dente, Z. Vekerdy, Z. Su and J. Wen provided is located in the south of Maqu City, in SAYR. The soil temperature monitoring network operated by CARRERI and ITC is located in the south of Maqu City, in SAYR. The *in situ* soil temperature measurements indicate soil temperature at about 5-cm depth, which is most closely related to LST [47]. Soil temperature measurements from the 20 soil temperature sites are used as the surface temperature proxy for evaluation of the FY-2E derived LST.

III. METHODOLOGY

A. GSW Algorithm for LST Estimation

Based on the GSW algorithm proposed by Wan and Dozier [33], the LST can be expressed as

$$T_S = a_0 + \left(a_1 + a_2\frac{1-\varepsilon}{\varepsilon} + a_3\frac{\delta\varepsilon}{\varepsilon^2}\right)\frac{T_{IR1}+T_{IR2}}{2} + \left(a_4 + a_5\frac{1-\varepsilon}{\varepsilon} + a_6\frac{\delta\varepsilon}{\varepsilon^2}\right)\frac{T_{IR1}-T_{IR2}}{2} \quad (1)$$

where T_{IR1} and T_{IR2} are the TOA brightness temperatures measured in channels IR1 and IR2, ε is the averaged emissivity of channels IR1 and IR2, $\delta\varepsilon$ is the emissivity difference between the two thermal infrared channels IR1 and IR2, and $a_0 - a_6$ are unknown coefficients that can be derived from simulated data through statistical regression methods for each viewing zenith angle (VZA) and each subrange.

Because FY-2E replaces FY-2C, the setting of each parameter depends on the simulation of FY-2C data [34]. In the MODTRAN simulation, six different VZAs (0°, 33.56°, 44.42°, 51.32°, 56.25°, 60°) are used. Six subranges of water vapor content (WVC) (0, 1.5), (1.0, 2.5), (2.0, 3.5), (3.0, 4.5), (4.0, 5.5), and (5.0, 6.5) g cm^{-2} are also used in the model. The LSTs are divided into five subranges: $T_s \leq 280$ K, 275 $K \leq T_s \leq 295$ K, 290 K $\leq T_s \leq 310$ K, 305 K $\leq T_s \leq 325$ K, and $T_s \geq 320$ K. The averaged emissivity ε varies from 0.90 to 1.0 with a step of 0.02 and the emissivity difference $\delta\varepsilon$ ranges from -0.025 to 0.015 with a step of 0.005. According to the study by Tang *et al.* (2008), the accuracy of LST retrieval can decrease by 3% for $\mathrm{NE\Delta T} = +0.1$ K, by 16% for $\mathrm{NE\Delta T} = 0.2$ K, and by 81% for $\mathrm{NE\Delta T} = 0.5$ K. Using coefficients corresponding to the two subranges *WVC* $\in$ [0, 1.5] and *WVC* $\in$ [1.0, 2.5], the RMSEs for LST are 0.18 K and 0.43 K, respectively. As FY-2E service better compared to FY-2C, the sensitivity to instrumental noise will be acceptable.

In the GSW algorithm for LST estimation, WVC and LSE are two key input parameters; therefore, the determination of these two parameters is further described in the following sections.

B. Determination of Atmospheric WVC

According to Li et al. [52] and Tang et al. [46], atmospheric WVC can be derived from the transmittance ratio of the split-window channels. The relationship between the transmittance ratio and WVC is determined by synthetic regression on the simulated data:

$$\mathrm{WVC} = C_1 + C_2 \times \frac{\tau_{IR2}}{\tau_{IR1}} \quad (2)$$

where C_1 and C_2 are unknown coefficients that can be derived by the MODTRAN simulation, and τ_{IR1} and τ_{IR2} are the atmospheric transmittances in the split-window channels. The ratio of τ_{IR1} to τ_{IR2} can be calculated as follows:

$$\frac{\tau_{IR2}}{\tau_{IR1}} = \frac{\varepsilon_{IR1}}{\varepsilon_{IR2}}R \quad (3)$$

where ε_{IR1} and ε_{IR2} are the emissivities of the two thermal infrared channels IR1 and IR2 and *R* is an unknown coefficient that can be calculated as follows:

$$R = \frac{\sum_{K=1}^{N}(T_{IR1,k} - \overline{T}_{IR1})(T_{IR2,k} - \overline{T}_{IR2})}{\sum_{K=1}^{N}(T_{IR1,k} - \overline{T}_{IR1})^2} \quad (4)$$

where the subscript *k* denotes pixel *k*, $T_{IR1,k}$ and $T_{IR2,k}$ are the TOA brightness temperatures measured in channels IR1 and IR2 of the *k* pixel, and $\overline{T}_{IR1}$ and $\overline{T}_{IR2}$ are the TOA mean channel

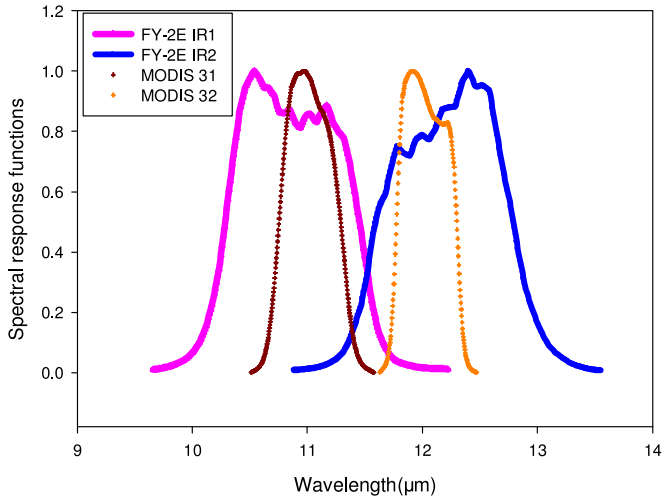

Fig. 3. Spectral response functions of IR1 and IR2 channels of FY-2E and those of channels 31 and 32 in MODIS.

brightness temperatures of the N neighboring pixels of channels IR1 and IR2, respectively.

C. Determination of LSEs

The LSEs in channels IR1 and IR2 of FY-2E can be estimated from the LSEs in channels 31 and 32 of MODIS provided by the MODIS LST product MOD11A1. The relationships of spectral response functions between IR1 of FY-2E and channel 31 of MODIS, IR2 of FY-2E and channel 32 of MODIS can be determinate. Therefore, the emissivities in the two split-window channels of MODIS and FY-2E can be calculated using the integrals of the spectral emissivity with the channel response functions, as shown in Fig. 3, over the spectral range of the channels. The emissivities of MODIS provided by MOD11A1 are applied to estimate the LSEs in channels IR1 and IR2 of FY-2E. The University of California Santa Barbara spectral database (http://www.icess.ucsb.edu/modis/EMIS/html/em.html) was used to determine the emissivity relationship between the S-VISSR channels and the MODIS 31 and 32 channels. Considering the particular situation of the study area, the emissivities of all categories of materials were included, except for manmade materials. The statistical relationships of (5) and (6) between MODIS channels and FY-2E channels are established by a linear regression analysis as shown in Fig. 4

$$\varepsilon_{IR1} = 1.1113\varepsilon_{31} - 0.1099 \quad (5)$$

$$\varepsilon_{IR2} = 0.9412\varepsilon_{32} + 0.0406. \quad (6)$$

IV. Results and Discussion

A. LST Retrieval using FY-2E Data

Based on the method described earlier, Fig. 5 presents an example of LST derived from FY-2E measurements on 14 September 2010 at 11:00 Beijing time over SAYR. Symbol A in Fig. 5 represents the areas of Lake Zhaling and Lake Eling, whereas symbol B refers to a sand area. It is evident from Fig. 5 that the

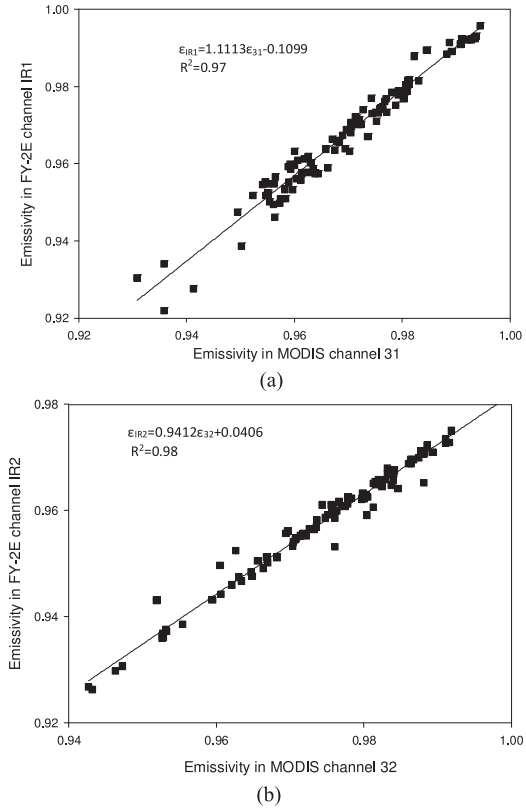

Fig. 4. Statistical relationship of the emissivities between the FY-2E channels IR1 and IR2 and the MODIS channels 31 (a) and 32 (b), respectively.

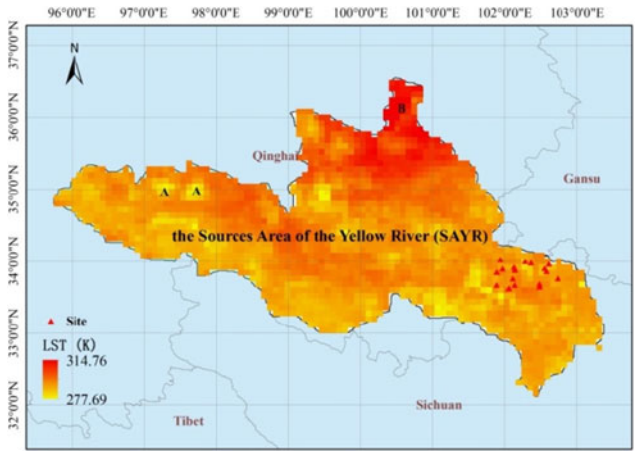

Fig. 5. LST retrieval at 11:00 Beijing time for September 14, 2010.

lakes exhibit relatively low temperatures, while high temperature occurs throughout the sand area, which is in accordance with the actual situation on the ground.

B. Validation with MODIS Products

The soil temperature measurements in SAYR operated by CARRERI and ITC are only available for August, September, and October 2010. Four days were randomly selected within this period (August 28, September 14, September 15, and October 8, 2010), from which data provided more than 2000

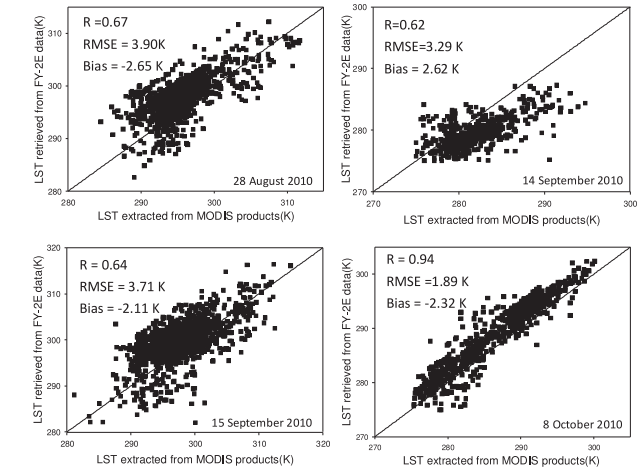

(a)

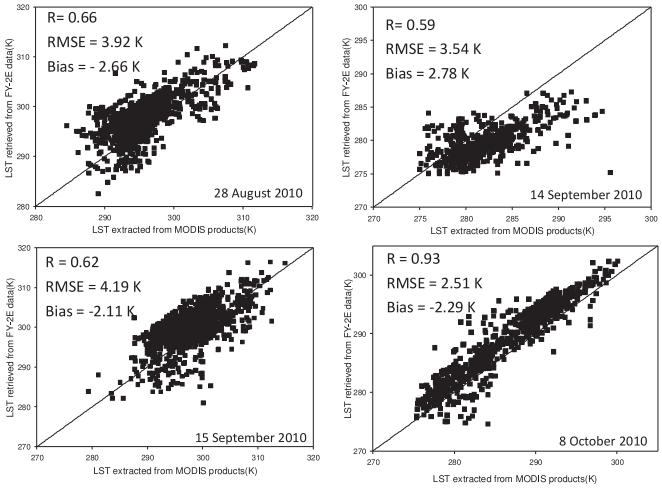

(b)

Fig. 6. Comparison of MODIS LST product and FY-2E-derived LST with LSE obtained from (a) MOD11A1 and (b) MOD11A2 over SAYR.

valid pixels. The MODIS product (MOD11B1) was chosen to verify the LST derived from MOD11A1 and MOD11A2 in the study area during those four cloud-free days. MOD11A2 was selected because the corresponding LSE product was first derived by Tang *et al*. [46] to estimate the LST calculated from FY-2C satellite data. However, MOD11A1, being a daily LSE product, is probably more suitable than an eight-day composition product for deriving LST for a given cloud-free day. In Fig. 6, eight scatter diagrams illustrate the relationship between the MODIS product and LST retrieval in SAYR, except for permafrost/frozen areas, which were plotted separately for MOD11A1 and MOD11A2. MOD11A1 shows a better correlation between the MODIS LST products and FY-2E-derived LST when compared with that of MOD11A2. Specifically, the correlation coefficients for MOD11A1 range from 0.62 to 0.94, while those for MOD11A2 range from 0.59 to 0.93 within selected cloud-free days. Moreover, the RMSEs range from 1.89 to 3.71 K (MOD11A1) and 2.51 to 4.19 K (MOD11A2), respectively, which further indicates that the FY-2E-derived LST of the daily LSE product is more suitable for daily cloud-free LST estimation.

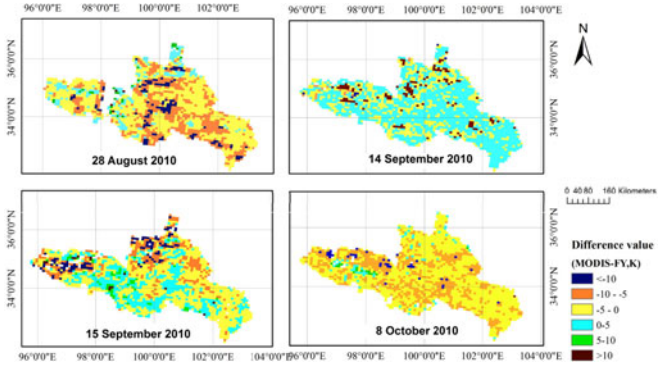

Fig. 7. Differences between FY-2E-derived LST and MODIS LST product for SAYR.

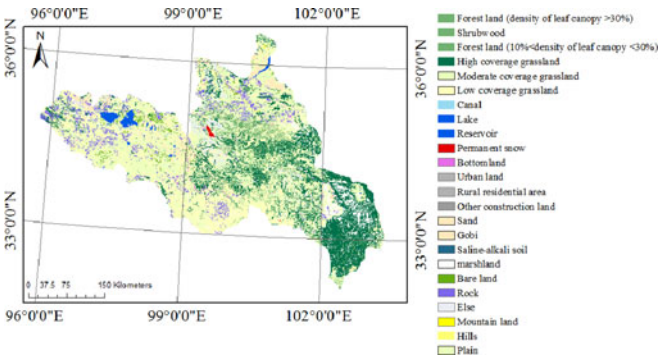

Fig. 8. Land use and land cover in the study area.

Using the MODIS LST product as the reference dataset, the differences between FY-2E-derived LST and MODIS LST for the entire study area are shown in Fig. 7. The errors have been grouped into six classes based on the differences between FY-2E-derived LST and MODIS LST product and are shown in different colors from blue to brown: more than −10 K, −5 K to −10 K, −5 K to 0 K, 0 K to 5 K, 5 K to 10 K, and over 10 K.

Different types of surface features are present within the study area such as woodlands, predominately grasslands, water, sand, permafrost, and 24 other surface characteristics, which are shown in Fig. 8. The eastern part of the study area is homogeneous grassland at an altitude of about 3500 m. The retrieval is therefore accurate in the east. In contrast, in the central part of the study area, near 99.5 °E and 35 °N, a large elevation difference and the presence of permanent snow cover result in an error, which partly explains why the absolute error between FY-2E-derived LST and MODIS LST product is higher than 10 K in this area (see Fig. 7). Additionally, errors are more likely to occur in the heterogeneous areas. For instance, a number of outliers occur near the white areas in the western part of SAYR on September 15 and August 28, 2010. For the entire SAYR, LST estimation in the eastern part of SAYR is generally more accurate than LST retrieval in the western region, which is due to the large surface heterogeneity in the western area compared to the eastern part of the region.

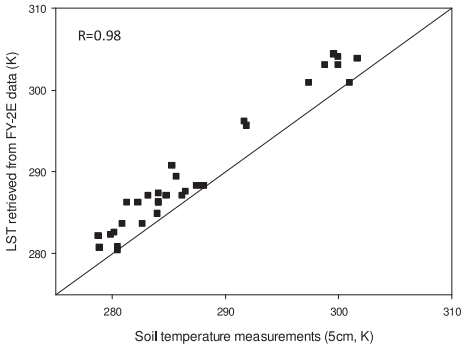

Fig. 9. Relationship between ground-measured soil temperature and FY-2E-derived LST.

C. Relationship Between FY-2E-Derived LST and Ground-Measured Soil Temperature

In this study, ground-truthing temperature data were collected at 5 cm below the land surface, whereas LST retrieval shows the ground surface temperature. Due to the lack of actual ground surface temperature measurements, the correlation coefficient (R) is used as a measure of comparison between LST retrieval and *in situ* measurements in previous studies. For example, Hachem [49] compared LST and soil temperature measurements (3–5 cm) from 2000 to 2008 at herbaceous and shrub tundra sites located in Canada, demonstrating an R ranging from 0.84 to 0.97. Wen [50] noted that the estimated LST corresponded well ($R = 0.80$) with measured soil temperature (0.04–2.0 m) at GAME/Tibet field campaign sites. Therefore, in this study, the ground soil temperature at 5 cm was used as a proxy of LST for comparison to the FY-2E-derived LST. Fig. 9 shows a scatter plot for FY-2E-derived LST and soil temperature measurements from the soil temperature monitoring network. The high R-value of 0.98 implies that the estimated LST agrees well with measured soil temperature. The general trend of LST overestimation using FY-2E-derived temperatures might be due to lower soil temperatures at a depth of 5 cm compared to the surface temperature. A more comprehensive validation of FY-2E-derived LSTs will be carried out using ground-measured LSTs for different surface conditions in future studies.

D. Discussion and Analysis

In general, the proposed method can be use to retrieve LST and achieve better accuracy compared to previous studies [40], [48], [51]. In this section, possible reasons for the observed discrepancies between FY-2E-derived LST and MODIS LST products are analyzed. First, heterogeneous surfaces may lead to the errors as discussed in Section IV-B. Altitudes in the western part of the study area are more than 6200 m, while the altitude in the eastern part is as low as 2500 m; even in some of the 5 km $\times$ 5 km pixels, the difference between the highest and lowest altitude is over 2000 m. Furthermore, the presence of more than two types of surface features in each 5 km $\times$ 5 km pixel may also result in errors. In addition, when using MODIS LST data as counterpart to FY-2E-derived LST, an observation time of 11:00 is assumed for both, although some pixels of the MODIS LST product were in fact observed from 10:00 to 11:30. These different observation times could be another error source. Finally, the low signal-to-noise ratio of the FY-2E data could also cause significant discrepancies between FY-2E-derived and MODIS LSTs.

V. Summary and Conclusion

This study investigated LST retrieval from two thermal infrared channels of the Chinese operational geostationary meteorological satellite FY-2E using a GSW algorithm. Atmospheric WVC was derived using the transmittance ratio of IR1 and IR2 according to Li [46]. The LSEs in channels IR1 and IR2 of FY-2E were estimated from the LSEs in channels 31 and 32 of MODIS provided by the MODIS product. The MOD11A1 product is generally more accurate than MOD11A2 in obtaining the LSE of FY-2E for LST estimation for individual cloud-free days.

To confirm the feasibility of this method, comparison with MODIS products was conducted for the study area. The results reveal a significant correlation between LST retrieval and the MODIS product, with R ranging from 0.60 to 0.94 and RMSE ranging from 1.89 to 3.71 K. The high R-value of 0.98 between retrieved LST and ground-measured soil temperature further proves the feasibility of using FY-2E to retrieve LST. Nevertheless, future studies will conduct a comprehensive validation of the proposed method using ground-measured LSTs for various surface and climate conditions.

Acknowledgment

The authors would like to thank LAADS for providing the MODIS data (http://ladsweb.nascom.nasa.gov/data/search.html) and NSMC for supplying the FY data (http://www.nsmc.cma.gov.cn/NSMC/Home/Index.htm).

References

[1] A. J. Arnfield, "Two decades of urban climate research: A review of turbulence, exchanges of energy and water, and the urban heat island," *Int. J. Climatol.*, vol. 23, pp. 1–26, 2003.

[2] J. A. Voogt and T. R. Oke, "Thermal remote sensing of urban climates," *Remote Sensing Environ.*, vol. 86, pp. 370–384, 2003.

[3] J. Peng, Y., Liu, X. Zhao, and A. Loew, "Estimation of evapotranspiration from TOA radiances in the Poyang lake basin, China," *Hydrol. Earth Syst. Sci.*, vol. 17, pp. 1431–1444, 2013.

[4] A. Loew, "Impact of surface heterogeneity on surface soil moisture retrievals from passive microwave data," *Remote Sens. Environ.*, vol. 112, pp. 231–248, 2008.

[5] J. Peng, J. Niesel, and A. Loew, "Evaluation of soil moisture downscaling using a simple thermal based proxy—The Remedhus network (Spain) example," *Hydrol. Earth Syst. Sci.*, vol. 19, pp. 4765–4782, 2015.

[6] J. Peng, A. Loew, S. Zhang, and J. Wang, "Spatial downscaling of satellite soil moisture data using a vegetation temperature condition index," *IEEE Trans. Geosci. Remote Sens.*, vol. 54, no. 1, pp. 1–9, Jan. 2016.

[7] Y. W. Wang *et al.*, "Estimation of surface soil moisture using FengYun-2E (FY-2E) data: A case study over the source area of the Yellow River," in *Proc. IEEE Int. Geosci. Remote Sens. Symp.*, 2016, pp. 4327–4330.

[8] P. Leng, X. Song, S. B. Duan, and Z. L. Li, "A practical algorithm for estimating surface soil moisture using combined optical and thermal infrared data," *Int. J. Appl. Earth Observation Geoinform*, vol. 52, pp. 338–348, 2016.

[9] Q. Weng, D. Lu, and J. Schubring, "Estimation of land surface temperature vegetation abundance relationship for urban heat island studies," *Remote Sens. Environ.*, vol. 89, pp. 467–483, 2004.

[10] Z. L. Li and F. Becker, "Properties and comparison of temperature-independent thermal infrared spectral indices with NDVI for HAPEX data," *Remote Sens. Environ.*, vol. 33, pp. 165–182, 1990.
[11] Z. L. Li and F. Becker, "Feasibility of land surface temperature and emissivity determination from AVHRR data," *Remote Sens. Environ.*, vol. 43, pp. 67–85, 1993.
[12] Z. L. Li *et al.*, "On the separate retrieval of soil and vegetation temperatures from ATSR data," *Sci. China Series D: Earth Sci.*, vol. 44, pp. 97–111, 2001.
[13] Z. L. Li *et al.*, "Land surface emissivity retrieval from satellite data," *Int. J. Remote Sens.*, vol. 34, pp. 3084–3127, 2013.
[14] Z. L. Li *et al.*, "Satellite-derived land surface temperature: Current status and perspectives," *Remote Sens. Environ.*, vol. 131, pp. 14–37, 2013.
[15] S. B. Duan and Z.-L. Li, "Intercomparison of operational land surface temperature products derived from MSG-SEVIRI and Terra/Aqua-MODIS Data," *IEEE J. Sel. Topics Appl. Earth Observ. Remote Sens.*, vol. 8, pp. 1–8, 2015.
[16] J. Peng, Y. Liu, and A. Loew, "Uncertainties in estimating normalized difference temperature index from TOA radiances," *IEEE Trans. Geosci. Remote Sens.*, vol. 51, no. 5, pp. 2487–2497, May 2013.
[17] S. B. Duan *et al*., "Estimation of diurnal cycle of land surface temperature at high temporal and spatial resolution from clear-sky MODIS Data," *Remote Sens.*, vol. 6, pp. 3247–3262, 2014.
[18] S. B. Duan, Z. L. Li, W. Ning, W. Hua, and B. H. Tang, "Evaluation of six land-surface diurnal temperature cycle models using clear-sky in situ and satellite data," *Remote Sens. Environ.*, vol. 124, pp. 15–25, 2012.
[19] Z. Qin and A. Karnieli², "Progress in remote sensing of land surface temperature and ground using NOAA-AVHRR data," *Int. J. Remote Sens.*, vol. 20, pp. 2367–2393, 1999.
[20] J. C. Jiménez-Muñoz and J. A. Sobrino, "A generalized single-channel method for retrieving land surface temperature from remote sensing data," *J. Geophys. Res.*, vol. 108, pp. 2015–2023, 2003.
[21] J. C. Jimenez-Munoz, J. Cristobal, J. A. Sobrino, and G. Soria, "Revision of the single-channel algorithm for land surface temperature retrieval from landsat thermal-infrared data," *IEEE Trans. Geosci. Remote Sens.*, vol. 47, no. 1, pp. 339–349, Jan. 2009.
[22] J. C. Jimenez-Munoz and J. A. Sobrino, "A single-channel algorithm for land-surface temperature retrieval from ASTER data," *IEEE Geosci. Remote Sens. Lett.*, vol. 7, no. 1, pp. 176–179, Jan. 2010.
[23] J. A. Sobrino *et al*., "Single-channel and two-channel methods for land surface temperature retrieval from DAIS data and its application to the Barrax site," *Int. J. Remote Sens.*, vol. 25, pp. 215–230(16), 2004.
[24] Z. Wan and Z. L. Li, "A physics-based algorithm for retrieving land-surface emissivity and temperature from EOS/MODIS data," *IEEE Trans. Geosci. Remote Sens.*, vol. 35, no. 4, pp. 980–996, Jul. 1997.
[25] X. L. Ma *et al*., "Retrieval of geophysical parameters from moderate resolution imaging spectroradiometer thermal infrared data: Evaluation of a two-step physical algorithm," *Appl. Opt.*, vol. 39, pp. 3537–50, 2000.
[26] L. M. Mcmillin, "Estimation of sea surface temperatures from two infrared window measurements with different absorption," *J. Geophys. Res. Atmospheres*, vol. 80, pp. 5113–5117, 1975.
[27] P. Y. Deschamps and T. Phulpin, "Atmospheric correction of infrared measurements of sea surface temperature using channels at 3.7, 11 and 12 Mm," *Boundary-Layer Meteorol.*, vol. 18, pp. 131–143, 1980.
[28] E. P. Mcclain, W. G. Pichel, and C. C. Walton, "Comparative performance of AVHRR-based multichannel sea surface temperatures," *J. Geophys. Res. Oceans*, vol. 90, pp. 11587–11601, 1985.
[29] G. B. França and W. S. Carvalho, "Sea surface temperature GOES-8 estimation approach for the Brazilian coast," *Int. J. Remote Sens.*, vol. 25, pp. 3439–3450, 2004.
[30] R. Niclòs, V. Caselles, C. Coll, and E. Valor, "Determination of sea surface temperature at large observation angles using an angular and emissivity-dependent split-window equation," *Remote Sens. Environ.*, vol. 111, pp. 107–121, 2007.
[31] J. C. Price, "Land surface temperature measurements from the split window channels of the NOAA 7 advanced very high resolution radiometer," *J. Geophys. Res. Atmospheres*, vol. 89, pp. 7231–7237, 1984.
[32] F. Becker and Z. Li, "Towards a local split window method over land surfaces," *Int. J. Remote Sens.*, vol. 11, pp. 369–393, 2007.
[33] Z. Wan and J. Dozier, "A generalized split-window algorithm for retrieving land-surface temperature from space," *IEEE Trans. Geosci. Remote Sens.*, vol. 34, no. 4, pp. 892–905, Jul. 1996.
[34] B. Tang, Y. Bi, Z. L. Li, and J. Xia, "Generalized split-window algorithm for estimate of land surface temperature from Chinese geostationary Fengyun meteorological satellite (FY-2C) Data," *Sensors*, vol. 8, pp. 933–951, 2008.
[35] F. Becker, "The impact of spectral emissivity on the measurement of land surface temperature from a satellite," *Int. J. Remote Sens.*, vol. 10, pp. 1509–1522, 1987.
[36] A. Vidal, "Atmospheric and emissivity correction of land surface temperature measured from satellite using ground measurements or satellite data," *Int. J. Remote Sens.*, vol. 12, pp. 2449–2460, 2007.
[37] Y. G. Qian, Z. L. Li, and F. Nerry, "Evaluation of land surface temperature and emissivities retrieved from MSG/SEVIRI data with MODIS land surface temperature and emissivity products," *Int. J. Remote Sens.*, Vol. 34, pp. 3140–3152, 2006.
[38] M. Atitar and J. A. Sobrino, "A split-window algorithm for estimating LST from Meteosat 9 Data: Test and comparison with in situ data and MODIS LSTs," *IEEE Geosci. Remote Sens. Lett.*, vol. 6, no. 1, pp. 122–126, Jan. 2009.
[39] C. Gao *et al*., "An improved algorithm for retrieving land surface emissivity and temperature from MSG-2/SEVIRI data," *IEEE Trans. Geosci. Remote Sens.*, vol. 52, no. 6, pp. 3175–3191, Jun. 2014.
[40] X. Zhang and J. Wang, "Estimation of land surface temperature using geostationary meteorological satellite data," *Remote Sens. Technol. Appl.*, vol. 28, pp. 12–17, 2013.
[41] J. Quan *et al*., "A hybrid method combining neighborhood information from satellite data with modeled diurnal temperature cycles over consecutive days," *Remote Sens. Environ.*, vol. 155, pp. 257–274, 2014.
[42] Y. C. Tian *et al*., "Evidence for a recent warming and wetting in the source area of the Yellow River (SAYR) and its hydrological impacts," *J. Geographical Sci.*, vol. 25, pp. 643–668, 2015.
[43] Y. Zhao, Y. Li, and Z. G. Rong, "Comparisons and analysis of the spectral response functions' difference between FY-2E's and FY2C's split window channels," *Spectroscopy Spectral Anal.*, vol. 30, pp. 1634–1637, 2010.
[44] Z. Wan and Z. L. Li, "A physics-based algorithm for retrieving land-surface emissivity and temperature from EOS/MODIS data," *IEEE Trans. Geosci. Remote Sens.*, vol. 35, no. 4, pp. 980–996, Jul. 1997.
[45] W. C. Snyder, Z. Wan, Y. Zhang, and Y. Z. Feng, "Classification-based emissivity for land surface temperature measurement from space," *Int. J. Remote Sens.*, vol. 19, pp. 2753–2774, 1998.
[46] Z. Li, L. Jia, Z. Su, Z. Wan, and R. Zhang, "A new approach for retrieving precipitable water from ATSR2 split-window channel data over land area," *Int. J. Remote Sens.*, vol. 24, pp. 5095–5117(23), 2010.
[47] Y. Xia *et al.*, "Validation of Noah-simulated soil temperature in the north American land data assimilation system phase 2," *J. Appl. Meteorol. Climatol.*, vol. 52, pp. 455–471, 2012.
[48] A. C. Gao *et al.*, "Comparison of land surface temperatures from MSG-2/SEVIRI and Terra/MODIS," *J. Appl. Remote Sens.*, vol. 6, pp. 245–249, 2012.
[49] S. Hachem, C. R. Duguay, and M. Allard, "Comparison of modis-derived land surface temperatures with ground surface and air temperature measurements in continuous permafrost terrain," *Cryosphere*, vol. 6, pp. 51–69, 2012.
[50] J. Wen, Z. Su, and Y. Ma, "Determination of land surface temperature and soil moisture from tropical rainfall measuring mission/microwave imager remote sensing data," *J. Geophys. Res.*, vol. 108, pp. ACL 2-1.ACL 2-10, Oct. 2, 2003.
[51] M. Akhoondzadeh and M. R. Saradjian, "Comparison of land surface temperature mapping using MODIS and ASTER images in semi-arid area," in *XXI ISPRS Congr.*, pp. 873–876, 2008.
[52] Z.-L Li *et al.*, "A new approach for retrieving precipitable water from ATSR2 split-window channel data over land area," in *Int. J. Remote Sensing*, vol. 24, pp. 5095–5117, 2003.

Xiaoning Song (M'04) received the Ph.D. in geographic information system from Institute of Remote Sensing Applications, Chinese Academy of Sciences in 2004. She works in University of Chinese Academy of Sciences from 2004. Her research interests include parameters inversion of land surface temperature, surface emissivity, surface albedo, leaf area index, NPP, evapotranspiration and soil moisture.

Yawei Wang was born in Hubei, China, in 1991. She received the B.S. in geographic information system from Sichuan Normal University, Chengdu, in 2013 and the M.S. degree in geographic information system from University of Chinese Academy of Sciences, Beijing, in 2016. She is currently pursuing the Ph.D. degree in Ludwig Maximilian University of Munich (LMU), Munich, Germany. Her research interests include moisture and energy fluxes from remote sensing data.

Bohui Tang received the B.S. degree in geographic information system from Wuhan University, Wuhan, China, in 1999 and the M.S. and Ph.D. degrees in geographic information system from the Chinese Academy of Sciences, Beijing, China, in 2004 and 2007, respectively.

He is currently in the Institute of Geographic Sciences and Natural Resources Research, Chinese Academy of Sciences, Beijing. His research interest includes the moisture and energy fluxes from remote sensing data.

Pei Leng received the Ph.D. degree in geographic information system from the University of Chinese Academy of Sciences, Beijing, China, in 2015.

He is currently in the Key Laboratory of Agri-Informatics, Ministry of Agriculture/Institute of Agricultural Resources and Regional Planning, Chinese Academy of Agricultural Sciences, Beijing. His research interest includes the moisture and energy fluxes from remote sensing data.

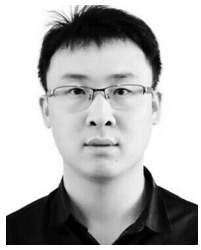

Sun Chuan was born in Shandong, China, in 1990. He received the B.S. degree in geographic information system from Shandong university of science and technology, Qingdao, China, in 2014. He is currently working toward the M.S. degree in geographic information system in University of Chinese Academy of Sciences. His research interests are retrieving the land surface temperature from passive microwave remote sensing data, by considering the atmosphere and cloud.

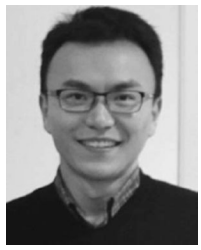

Jian Peng received the Ph.D. degree in Earth sciences from the Max Planck Institute for Meteorology/University of Hamburg, Hamburg, Germany, in 2013.

He is currently a Postdoctoral Scientist in the Land Department, Max Planck Institute for Meteorology, Hamburg, and a Guest Scientist at the University of Munich, Munich, Germany. His research interests include quantitative retrieval of land surface parameters from Earth observations, with a special emphasis on evapotranspiration and soil moisture, and the development of downscaling schemes, as well as the application of remote sensing products in hydrological and meteorological studies.

Alexander Loew (M'04) received the M.S. degree in geography and the Ph.D. degree in physical geography from the Ludwig Maximilian University of Munich (LMU), Munich, Germany, in 2001 and 2004, respectively. He is currently a Full Professor of physical geography and microwave remote sensing with the University of Munich (LMU), Munich, Germany. His research interests include the derivation of quantitative land surface parameters from remote sensing data, the assimilation of remote sensing data into climate and land surface process models, and the evaluation of climate models using observational data.

4.2 Paper II: IEEE TGRS - Surface soil moisture retrieval using optical / thermal infrared remote sensing data

Surface Soil Moisture Retrieval Using Optical/Thermal Infrared Remote Sensing Data

Yawei Wang, Jian Peng, *Member, IEEE*, Xiaoning Song, *Member, IEEE*, Pei Leng, Ralf Ludwig, and Alexander Loew, *Member, IEEE*

***Abstract*— Surface soil moisture (SSM) plays significant roles in various scientific fields, including agriculture, hydrology, meteorology, and ecology. However, the spatial resolutions of microwave SSM products are too coarse for regional applications. Most current optical/thermal infrared SSM retrieval models cannot directly estimate the quantitative volumetric soil water content without establishing empirical relationships between ground-based SSM measurements and satellite-derived proxies of SSM. Therefore, in this paper, SSM is estimated directly from 5-km-resolution Chinese Geostationary Meteorological Satellite FY-2E data based on an elliptical-new SSM retrieval model developed from the synergistic use of diurnal cycles of land surface temperature (LST) and net surface shortwave radiation (NSSR). The elliptical-original model was constructed for bare soil and did not consider the impacts of different fractional vegetation cover (FVC) conditions. To optimize the elliptical-original model for regional-scale SSM estimates, it is improved in this paper by considering the influence of FVC, which is based on a dimidiate pixel model and a Moderate Resolution Imaging Spectroradiometer normalized difference vegetation index product. A preliminary validation of the model is conducted based on ground measurements from the counties of Maqu, Luqu, and Ruoergai in the source area of the Yellow River. A correlation coefficient (R) of 0.620, a root-mean-square error (RMSE) of 0.146 m^3/m^3, and a bias of 0.038 m^3/m^3 were obtained when comparing the in situ measurements with the FY-2E-derived SSM using the elliptical-original model. In contrast, the FY-2E-derived SSM using the elliptical-new model exhibited greater consistency with the ground measurements, as evidenced by an R of 0.845, an RMSE of 0.064 m^3/m^3, and a bias of 0.017 m^3/m^3. To provide accurate SSM estimates, high-accuracy FVC, LST, and NSSR data are required. To complement the point-scale validation conducted here, cross-comparisons with other existing SSM products will be conducted in the future studies.**

***Index Terms*— Ellipse model, land surface temperature (LST), net surface shortwave radiation (NSSR), optical/thermal infrared data, surface soil moisture (SSM).**

I. Introduction

SURFACE soil moisture (SSM), which is represented by water that is retained in the top few centimeters (approximately 0 to 5 cm) of the soil, represents an important connection between the land surface and the atmosphere [1]–[6]. Real-time, accurate SSM monitoring plays critical roles in guiding agricultural irrigation and production forecasts for agricultural applications [7]. As a significant component of the hydrological cycle, SSM effectively regulates the partitioning of rainfall into infiltration and runoff. Furthermore, soil moisture was listed as an essential climate variable by the World Meteorological Organization in 2010 due to its impacts on climate change over a temporal range of hours to years. In addition, SSM is closely associated with various fundamental areas of research and many scientific disciplines [8]–[12].

Both regional- and global-scale quantitative estimates of SSM are essential. However, due to the combined effects of weather and surface conditions, SSM displays broad heterogeneity at both temporal and spatial scales [13], [14]. Therefore, it is particularly difficult to acquire quantitative estimates of SSM at the regional scale. Numerous investigations have focused on obtaining regional-scale SSM estimates [15]–[20]. Although microwave remote sensing of SSM has various deficiencies including a lack of soil roughness information and problems arising from sun-glint contamination at the L-band, microwave band has all-day observation capability [21]. Some SSM products have been produced based on the Advanced Microwave Scanning Radiometer—Earth Observing System instrument, the Soil Moisture Ocean Salinity mission, the climate change initiative, and the Soil Moisture Active Passive [22]–[28]. However, the spatial resolutions of microwave SSM products are overly coarse (approximately 25–50 km) for regional applications. Optical/thermal infrared data have the advantage of a high spatial resolution, and thus, the estimation of SSM from optical/thermal infrared data has been attempted in several studies [29]–[31]. However, most existing methods cannot quantitatively estimate the volumetric soil water content directly without establishing empirical

Manuscript received August 23, 2017; revised December 22, 2017 and March 12, 2018; accepted March 14, 2018. This work was supported in part by the National Natural Science Foundation of China under Grant 41601397 and in part by the Scientific Exploitation of Operational Missions Program of the European Space Agency through the project "Exploitation of S-1 for Surface Soil Moisture Retrieval at High Resolution" under Contract 4000118762/16/I-NB (https://exploit-s-1.ba.issia.cnr.it). The work of Y. Wang was supported by China Scholarship Council. *(Corresponding author: Yawei Wang.)*

Y. Wang, R. Ludwig, and A. Loew is with the Geography Department, Ludwig Maximilian University of Munich, 80337 Munich, Germany (e-mail: yawei.wang1@gmail.com).

J. Peng is with the School of Geography and the Environment, University of Oxford, Oxford OX1 3QY, U.K., with the Geography Department, Ludwig Maximilian University of Munich, 80337 Munich, Germany, and also with the Max Planck Institute for Meteorology, 20146 Hamburg, Germany.

X. Song is with the College of Resources and Environment, University of Chinese Academy of Sciences, Beijing 100049, China.

P. Leng is with the Key Laboratory of Agri-Informatics, Ministry of Agriculture/Institute of Agricultural Resources and Regional Planning, Chinese Academy of Agricultural Sciences, Beijing 100081, China.

Color versions of one or more of the figures in this paper are available online at http://ieeexplore.ieee.org.

Digital Object Identifier 10.1109/TGRS.2018.2817370

relationships between SSM measurements and satellite-derived proxies of SSM.

The increasing number of geostationary satellites is facilitating the development of more practical SSM retrieval methods with higher spatial and temporal resolutions [31]–[36]. Geostationary satellites have a higher frequency of observations than do polar orbiting satellites and can produce 48 to 96 images per day with a fixed observation angle for a given pixel, substantially enriching our understanding of terrestrial water and energy budgets. A novel SSM retrieval model was proposed by Leng *et al.* [32], [33] to directly estimate SSM without ground soil moisture data for calibration. This model is based on the synergistic use of diurnal cycles of land surface temperature (LST) and net surface shortwave radiation (NSSR) data obtained from geostationary satellite data. This innovative ellipse model exhibits some advantages over other methods that utilize optical/thermal infrared data. First, the ellipse model is capable of directly estimating SSM without establishing empirical relationships between field-scale soil moisture measurements and remotely sensed parameters. Field-scale soil moisture measurements are essential for many SSM retrieval models but are difficult to obtain. Consequently, the ellipse model is less labor intensive and more convenient. Second, the ellipse model can estimate SSM via a great number of approaches than can other methods. Polar orbiting satellites can only observe one target once every 12 h. If it is cloudy during the satellite pass, the retrieval method will provide no information. However, the ellipse model requires only five of 48/96 images, offering a greater probability of estimating the SSM. Following the approaches of previous investigations, this paper aims to analyze the effects of fractional vegetation cover (FVC) and to optimize the elliptical-original model over different vegetation cover types. A preliminary validation of the model is conducted using ground measurements for the counties of Maqu, Luqu, and Ruoergai.

II. Study Area and Data

A. Description of the Study Area

The study area, which includes the counties of Maqu, Luqu, and Ruoergai (33.05° N–34.81° N, 100.76° E–103.61° E), is located to the east of the source area of the Yellow River (SAYR), the catchment of which lies above the Tangnag Hydrological Station in the Northeastern Qinghai–Tibet Plateau [37]. The area encompasses a large river valley and surrounding hills, wetlands, grassland, and bare areas. The climate is wet and cold with dry winters and rainy summers due to the monsoon season. The mass and energy fluxes between the land surface and the atmosphere in the Qinghai–Tibet Plateau have substantial effects on regional and global climates. Thus, studying the SSM over the study area in the Qinghai–Tibet Plateau is of great significance.

B. FY-2E Data

The FY-2 series of satellites, which were launched by China beginning in 2001, consists of five geostationary meteorological satellites FY-2C/2D/2E/2F/2G. The FY-2E satellite was launched at the end of 2008 to replace FY-2C. The optical imaging radiometer onboard the FY-2E satellite is a stretched-visible and infrared spin-scan radiometer (S-VISSR) that includes one visible channel and four infrared thermal channels (Table I) [38]. FY-2E can obtain one full disc image per hour or every 30 min that covers the earth's surface over latitudes from 60° N to 60° S and longitudes from 45° E to 165° E during the flooding season. FY-2E data are obtained from the National Satellite Meteorological Center (http://www.nsmc.cma.gov.cn/NSMC/Home/Index.html).

TABLE I
Main Technical Specifications of the Radiometer

Channel	Spectral range (μm)	Spatial resolution (km)	NEΔT300K
VIS	0.510-0.905	1.25	-
IR1	10.29-11.45	5	0.19K
IR2	11.59-12.79	5	0.26K
IR3	3.59-4.09	5	0.30K
IR4	6.32-7.55	5	0.19K

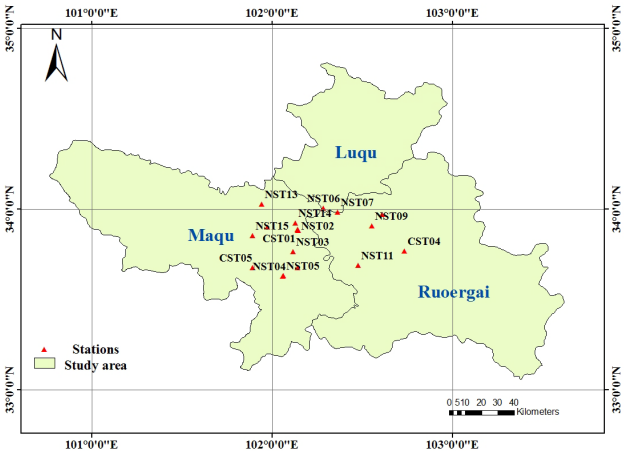

Fig. 1. Map of the study area, which includes the counties of Maqu, Luqu, and Ruoergai.

C. Ground Soil Temperature Measurements

The soil moisture monitoring network used in this paper was installed by the Cold and Arid Regions Environmental and Engineering Research Institute and the Faculty of Geo-Information Science and Earth Observation of the University of Twente, Enschede, The Netherlands; the stations are shown in Fig. 1. Table II displays information on the soil moisture monitoring stations, which was derived from the coordinated Asia–European long-term observing system of Qinghai–Tibet Plateau hydrometeorological processes and the Asian-monsoon system with ground satellite image data and numerical simulations report "continuous *in situ* soil moisture measurements at Maqu site" by L. Dente, Z. Vekerdy, Z. Su, and J. Wen. The ground measurements represent the soil moisture at a depth of approximately 5 cm, which is most closely related to the SSM estimates retrieved from satellite data in this paper.

TABLE II
NETWORK STATION INFORMATION

Station ID	Latitude/Longitude	Elevation (m)	Topography	Land cover	Station ID	Latitude/Longitude	Elevation(m)	Topography	Land cover
CST_01	33°53'14.16" 102°08'25.62"	3431	River valley	Grass	NST_06	34°00'29.70" 102°16'53.58"	3428	River valley	Grass
CST_02	33°40'42.60" 102°08'18.66"	3449	River valley	Grass	NST_07	33°59'13.74" 102°21'37.20"	3430	River valley	Grass
CST_03	33°54'17.82" 101°58'15.66"	3507	Hill valley	Grass	NST_08	33°58'19.44" 102°36'31.08"	3473	valley	Grass
CST_04	33°46'12.84" 101°43'52.98"	3504	Hill valley	Grass	NST_09	33°54'38.64" 102°33'00.78"	3434	River valley	Grass
CST_05	33°40'46.50" 101°53'21.78"	3542	Hill valley	Grass	NST_10	33°51'07.74" 102°34'25.44"	3512	Hill slope	Grass
NST_01	33°53'22.68" 102°08'27.48"	3431	River valley	Grass	NST_11	33°41'33.18" 102°28'36.12"	3442	River valley	Wetland grass
NST_02	33°53'04.74" 102°08'32.28"	3434	River valley	Grass	NST_12	33°37'16.02" 102°28'00.36"	3441	River valley	Grass
NST_03	33°46'00.54" 102°08'50.52"	3513	Hill slope	Grass	NST_13	34°01'53.70" 101°56'31.44"	3519	valley	Grass
NST_04	33°37'52.14" 102°03'25.56"	3448	River valley	Wetland grass	NST_14	33°55'35.64" 102°07'42.78"	3432	River valley	Grass
NST_05	33°38'05.10" 102°03'34.68"	3476	Hill slope	Grass	NST_15	33°51'26.10" 101°53'28.08"	3752	Hill slope	Grass

D. Simulated Data

Simulated data from the common land model (CoLM) are used to improve the elliptical-original SSM retrieval model [39]. Various studies show that the CoLM provides reasonable simulations of the land surface state in Northwestern China and the Tibetan Plateau, including at Maqu station, which is located in the current study area [40]. The CoLM can adequately represent basic features of the land surface energy balance at daily time scales in China [41].

The CoLM primarily represents physical, hydrological, and biological processes and exhibits high accuracy in the simulation of multiple parameters, including snow cover, soil moisture, sensible heat flux, and latent heat flux. Atmospheric forcing data that are employed for driving the CoLM primarily encompass the downward solar radiation, downward longwave radiation, wind speed, wind direction, precipitation, air temperature at a reference height, atmospheric pressure at the surface, and relative humidity at a reference height.

III. METHODOLOGY

A. Elliptical-Original SSM Retrieval Model

The diurnal LST cycle can be described as a sine or cosine function. The daytime part of the diurnal temperature cycle model can be expressed as follows [42]:

$$T_{\text{day}}(t) = T_0 + T_a \cos[\beta(t - t_m)] \tag{1}$$

where $T_{\text{day}}(t)$ is the LST (K) at time t (hours), T_0 is the residual temperature at sunrise, T_a is the temperature amplitude, β is the width of the half-period of the cosine term, and t_m is the time at which the temperature reaches its maximum.

A similar cosine function can be used to express the diurnal NSSR cycle

$$S_{\text{day}}(t) = S_0 + S_a \cos[\alpha(t - t_r)] \tag{2}$$

where $S_{\text{day}}(t)$ is the NSSR (W/m^2) at time t (hours), S_0 is the residual NSSR at sunrise, S_a is the NSSR amplitude, α is the width of the half-period of the cosine term, and t_r is the time (hours) of the maximum NSSR.

To facilitate investigating the relationship between the diurnal cycles of LST and NSSR and simplify the expression, LST and NSSR can be made dimensionless as follows:

$$x = \frac{T_{\text{day}}(t) - s}{r - s} = p_1 \cos[\beta(t - t_m)] + q_1 \tag{3}$$

$$y = \frac{S_{\text{day}}(t) - j}{k - j} = p_2 \cos[\alpha(t - t_r)] + q_2 \tag{4}$$

where x and y are the dimensionless LST and NSSR, respectively, r and s are set as 325 and 275 K, respectively, and k and j are set as 1200 and 0 W/m^2, respectively. p_1, q_1, p_2, and q_2 are parameters of the diurnal LST and NSSR cycles.

For a day of clear skies, it is assumed that β in (1) is equal to α in (2). The difference between maximum LST time t_m and maximum NSSR time t_r is calculated as follows:

$$\Delta t = t_m - t_r. \tag{5}$$

An elliptical relationship exists between LST and NSSR during the daytime on fully cloud-free days, which can be expressed as follows [33]:

$$p_2^2(x-q_1)^2 - 2p_1p_2[\cos(\beta \cdot \Delta t)](x-q_1)(y-q_2) + p_1^2(y-q_2)^2 = [p_1p_2\sin(\beta \cdot \Delta t)]^2. \tag{6}$$

For a given atmospheric condition, p_1, q_1, p_2, q_2, β, and Δt are constants for a particular soil type and soil moisture content. The ellipse parameters, including the center horizontal coordinate (x_0), the center vertical coordinate (y_0), the semimajor axis (a), the semiminor axis (b), and the rotation angle (θ), can be calculated as follows:

$$\begin{cases} x_0 = q_1 \\ y_0 = q_2 \\ \theta = \dfrac{1}{2}\cot^{-1}\left[\dfrac{p_1^2 - p_2^2}{2p_1p_2\cos(\beta \cdot \Delta t)}\right] \\ a = p_1\sin(\beta \cdot \Delta t) \\ b = p_2\sin(\beta \cdot \Delta t). \end{cases} \tag{7}$$

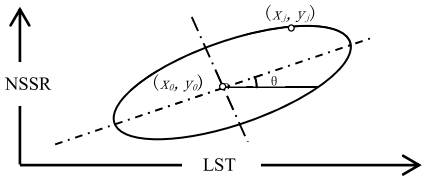

Fig. 2. Diagram of the elliptical relationship between the diurnal cycles of the LST and NSSR. x_0, y_0, a, and θ represent the horizontal and vertical coordinates of the ellipse center, the semimajor axis, and the rotation angle, respectively. (x_j, y_j) represent the LST and NSSR at time j ($j = 1, 2, 3, 4, 5$).

The elliptical relationship varies with different soil types and soil moisture contents under a given atmospheric condition. Furthermore, there is an elliptical relationship between the diurnal LST and NSSR cycles, as shown in Fig. 2. A stepwise regression method is used to determine the parameters for SSM retrieval. With the simulated data, it is found that the four ellipse parameters (x_0, y_0, a, and θ) are the most significant for the estimation of SSM. However, the center horizontal coordinate x_0 and the rotation angle θ have a strong linear relationship [38].

Therefore, the newly developed SSM retrieval model can be written as follows [33], [38]:

$$\mathrm{SSM} = n_1 \times y_0 + n_2 \times a + n_3 \times \ln\theta + n_0 \tag{8}$$

where SSM is the daily-averaged SSM (m^3/m^3), y_0, a, and θ, which, respectively, represent the vertical coordinates of the ellipse center, the semimajor axis and the rotation angle, are the ellipse parameters for the elliptical relationship between the diurnal LST and NSSR cycles, and n_i ($i = 0, 1, 2, 3$) is the model coefficients (m^3/m^3) that can be simulated from the CoLM. It should be noticed that elliptical parameters and model coefficients will change with different days.

B. Determination of LST

The diurnal cycles of LST and NSSR are prerequisite information for the elliptical SSM retrieval model. As determined in [43] and [44], LST can be expressed as follows based on the split-window algorithm [45]:

$$T_s = a_0 + \left(a_1 + a_2\frac{1-\varepsilon}{\varepsilon} + a_3\frac{\delta\varepsilon}{\varepsilon^2}\right)\frac{T_{\mathrm{IR1}} + T_{\mathrm{IR2}}}{2} + \left(a_4 + a_5\frac{1-\varepsilon}{\varepsilon}a_6\frac{\delta\varepsilon}{\varepsilon^2}\right)\frac{T_{\mathrm{IR1}}T_{\mathrm{IR2}}}{2} \tag{9}$$

where T_{IR1} and T_{IR2} are the top-of-atmosphere (TOA) brightness temperatures (K) measured in channels IR1 and IR2; ε is the averaged emissivity from channels IR1 and IR2 of FY-2E which can be estimated from the LSEs in channels 31 and 32 of Moderate Resolution Imaging Spectroradiometer (MODIS) provided by the MODIS LST product MOD11A1; $\delta\varepsilon$ is the emissivity difference between the two thermal infrared channels IR1 and IR2; and a_0–a_6 are unknown coefficients that can be derived from the simulated data through statistical regression methods for each viewing zenith angle and subrange. The University of California Santa Barbara, Santa Barbara, CA, USA, spectral database was used to determine the emissivity relationship between the S-VISSR channels and the MODIS 31 and 32 channels [44].

C. Determination of NSSR

NSSR is mainly calculated using downward surface shortwave radiation (DSSR), upward surface shortwave radiation (USSR), and land surface albedo as follows [46], [47]:

$$S_n = R_s^{\downarrow} - R_s^{\uparrow} = (1-r)R_s^{\downarrow} \tag{10}$$

$$R_s^{\downarrow} = G \times \cos(\mathrm{SZA}) \times d_r \times \tau \tag{11}$$

$$d_r = 1.00011 + 0.034221\cos(\alpha) + 0.00128\sin(\alpha) + 0.000719\cos(2\alpha) + 0.000077\sin(2\alpha). \tag{12}$$

According to Tang *et al.*[43] and Li *et al.*[48], the atmospheric water vapor content (WVC) can be derived from the transmittance ratio of the split-window channels. The relationship between the transmittance ratio and WVC is determined by synthetic regression on the simulated data from MODTRAN with aerosol model (VIS = 23 km, rural model)

$$\mathrm{WVC} = C_1 + C_2 \times \frac{\tau_{\mathrm{IR2}}}{\tau_{\mathrm{IR1}}} \tag{13}$$

$$\frac{\tau_{\mathrm{IR2}}}{\tau_{\mathrm{IR1}}} = \frac{\varepsilon_{\mathrm{IR1}}}{\varepsilon_{\mathrm{IR2}}} \times \frac{\sum_{k=1}^{N}(T_{\mathrm{IR1},k} - \overline{T_{\mathrm{IR1}}})(T_{\mathrm{IR2},k} - \overline{T_{\mathrm{IR2}}})}{\sum_{k=1}^{N}(T_{\mathrm{IR1},k} - \overline{T_{\mathrm{IR1}}})^2} \tag{14}$$

$$C_1 = 28.104 - \frac{14.996}{\cos(\mathrm{VZA})} + \frac{3.211}{\cos^2(\mathrm{VZA})} \tag{15}$$

$$C_2 = -28.056 + \frac{14.954}{\cos(\mathrm{VZA})} - \frac{3.206}{\cos^2(\mathrm{VZA})} \tag{16}$$

$$\alpha = \frac{2\pi(\mathrm{DOY} - 1)}{365} \tag{17}$$

where S_n is the NSSR (W/m^2); $R_S^{\downarrow}$ and $R_S^{\uparrow}$ represent the DSSR (W/m^2) and USSR (W/m^2), respectively; r is the land surface albedo; G is the solar constant (1367 W/m^2); SZA is the solar zenith angle; d_r is the earth–sun distance factor; τ is the atmospheric transmissivity; DOY denotes the day of year; WVC is the water vapor content (g/cm^2); τ_{IR1} and τ_{IR2} are the atmospheric transmittances in channels IR1 and IR2; $\varepsilon_{\mathrm{IR1}}$ and $\varepsilon_{\mathrm{IR2}}$ are the emissivities in channels IR1 and IR2; and $\overline{T}_{\mathrm{IR1}}$ and $\overline{T}_{\mathrm{IR2}}$ are the TOA mean channel brightness temperatures (K) of the N neighboring pixels in channels IR1 and IR2, respectively.

D. Elliptical-New SSM Retrieval Model

1) Improvement With FVC: The elliptical-original model was constructed for bare soil conditions with coefficients that do not reflect conditions with varying FVC. The coefficients for bare soil are used for SSM estimates under conditions where the FVC is less than 0.7. However, the FVC is temporally variable, and thus, using the same set of coefficients to derive the SSM under different vegetation conditions can produce errors. Accordingly, it is necessary to account for FVC

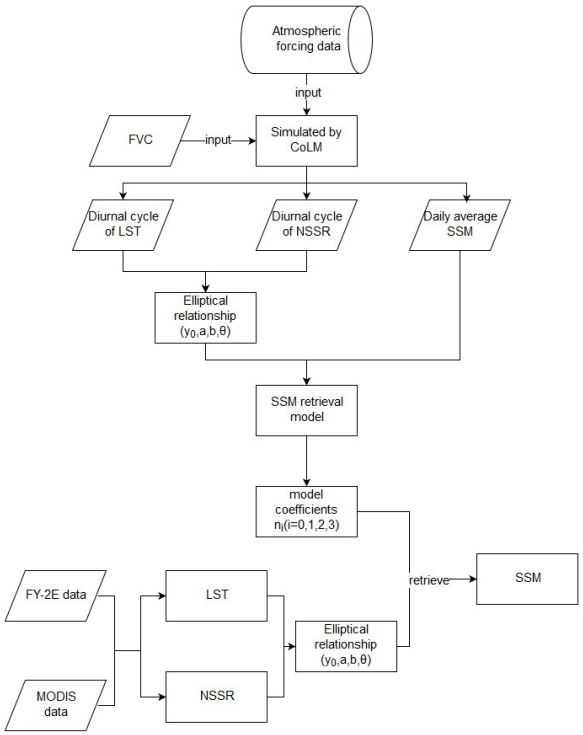

Fig. 3. Flowchart of the development of the daily-averaged SSM retrieval model.

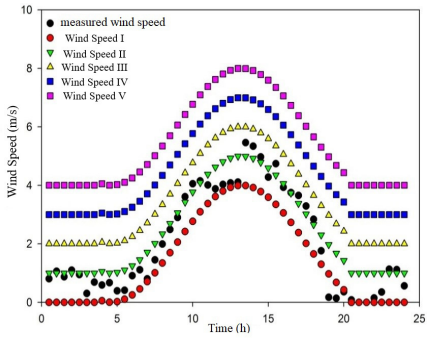

Fig. 4. Measured wind speed and five sets of simulated wind speeds.

TABLE III
VALIDATION SSM RETRIEVALS WITH DIFFERENT WIND SPEEDS

Wind Speed	R^2	RMSE (m^3m^{-3})
I	0.912	0.024
II	0.919	0.022
III	0.866	0.029
IV	0.726	0.044
V	0.608	0.057

to optimize the elliptical-original model for use at temporal and spatial scales.

The FVC can be derived from a widely used dimidiate pixel model, a linear pixel unmixing model, and a MODIS normalized difference vegetation index (NDVI) product (16-day MOD13Q1) [49], [50]. This derivation assumes that each pixel can be decomposed into a linear combination of bare soil (NDVIsoil) and full vegetation (NDVIveg) as follows:

$$\mathrm{FVC} = (\mathrm{NDVI} - \mathrm{NDVIsoil})/(\mathrm{NDVIveg} - \mathrm{NDVIsoil}) \quad (18)$$

where FVC is the fractional vegetation cover, NDVI is the normalized difference vegetation index, NDVIsoil is the NDVI of the bare soil, and NDVIveg is the NDVI of the vegetation. Due to inevitable noise, cumulative probabilities of 0.5% and 99.5% are taken for NDVIsoil and NDVIveg, respectively, in this paper.

2) Experimental Procedure: Fig. 3 depicts the process of using the elliptical-new SSM retrieval model with geostationary satellite data in detail. The data for CoLM simulation are similar to those used in [22] and [51]. The initializations of soil textures about the soil texture classification scheme of the Food and Agriculture Organization are computed from Bonan [52]. Besides, the land cover is initialized according to the United States Geological Survey vegetation categories and FVC, which is set at 0–0.7 for the study area. Atmospheric forcing data are used to drive the CoLM, as mentioned earlier in the reference to the simulated data. As indicated in the flowchart, FVC is input into the CoLM along with atmospheric forcing data to directly produce simulated data, including the diurnal cycle of LST, the diurnal cycle of NSSR, and the daily-averaged SSM, to construct the database. The model coefficients are then calculated from the simulated daily-averaged SSM and diurnal cycles of LST and NSSR. Similarly, based on the geostationary satellite data, elliptical relationships are built with the ellipse parameters. The SSM can be successfully produced with the model coefficients and ellipse parameters.

IV. RESULTS AND ANALYSIS

A. Effect of Atmospheric Forcing Data on the Elliptical-New SSM Model

The model coefficients simulated from the CoLM are based on atmospheric forcing data. However, atmospheric forcing varies temporally and spatially. Therefore, atmospheric forcing data will affect SSM retrieval. Wind speed, air temperature, and relative humidity are the atmospheric forcing variables, most likely to affect the accuracy of the elliptical-new SSM retrieval model. In this paper, the model errors from wind speed, air temperature, and relative humidity are analyzed.

1) Effect of Wind Speed on the Elliptical-New SSM Retrieval Model: Wind speed has a strong diurnal cycle, with a peak in the afternoon (2 PM) over most land areas [53], [54]. While controlling other atmospheric forcing variables, diurnal LST, diurnal NSSR, and daily SSM are simulated under different wind speeds based on the CoLM. Taking the atmospheric forcing data on DOY 217 in 2010 as an example, different diurnal wind speeds are set based on measured wind speed, as shown in Fig. 4.

After calculating the model coefficients with different wind speeds, the SSM retrievals are validated with *in situ* measurements, as shown in Table III. The accuracy of the wind speed data affects SSM retrieval. If the uncertainty of wind speed is less than 1 m/s, the accuracy of the result might not be significantly affected. As the uncertainty of wind

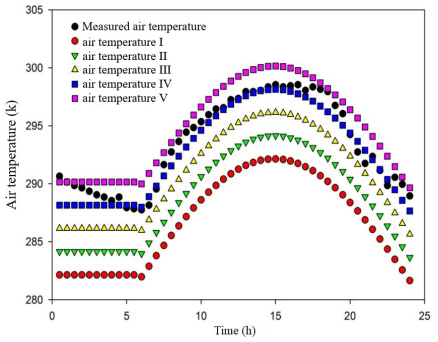

Fig. 5. Measured air temperature and five sets of simulated air temperature.

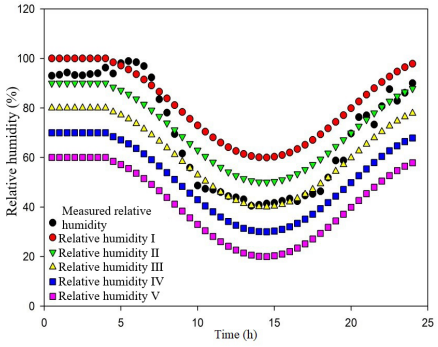

Fig. 6. Measured relative humidity and five sets of simulated relative humidity.

TABLE IV
VALIDATION SSM RETRIEVALS WITH DIFFERENT AIR TEMPERATURES

Air temperature	R^2	RMSE (m^3/m^3)
I	0.808	0.045
II	0.804	0.043
III	0.749	0.044
IV	0.842	0.031
V	0.867	0.028

TABLE V
VALIDATION SSM RETRIEVALS WITH DIFFERENT RELATIVE HUMIDITIES

Relative humidity	R^2	RMSE (m^3m^{-3})
I	0.852	0.040
II	0.903	0.026
III	0.920	0.022
IV	0.920	0.023
V	0.911	0.026

speed increases, the SSM retrievals will become increasingly inaccurate, with large uncertainties at wind speed uncertainties in excess of 3 m/s.

2) Effect of Air Temperature on the Elliptical-New SSM Retrieval Model: Air temperature has a strong diurnal cycle, with a peak in the afternoon over most land areas. Taking the DOY 217 in 2010 as an example, simulated data are produced based on the CoLM with different diurnal air temperatures, as shown in Fig. 5. The SSM retrievals are validated with *in situ* measurements, as shown in Table IV. As the uncertainty of air temperature increases, the retrievals display larger errors. As the uncertainty of air temperature reaches a threshold, the error of SSM retrieval tends to be stable within 0.02 m^3/m^3. Therefore, the retrievals are less sensitive to uncertainties in air temperature than they are to those in wind speed.

3) Effect of Relative Humidity on the Elliptical-New SSM Retrieval Model: As with wind speed and air temperature, relative humidity has a strong diurnal cycle, but with minimum value in the afternoon. Setting relative humidity III as the simulated series that is closest to the measured relative humidity, the relative humidity I and V series are the series with the greatest error in this paper, as shown in Fig. 6. The greater the uncertainty of relative humidity, the larger is the error of the SSM retrievals. As the uncertainty exceeds 20%, the accuracy of the elliptical-new SSM retrieval model is minimized. However, a relative humidity value that is higher than the true value will cause more error than one that is lower than the true value. Thus, the SSM retrievals obtained from relative humidity I are less accurate than those obtained from relative humidity V. From relative humidities I to III, the error of SSM retrieval increases by 0.018 m^3/m^3 as shown in Table V. Overall, the retrievals are less sensitive to error in relative humidity than to error in air temperature or wind speed.

B. Analysis of Model Sensitivity to LST and NSSR

To evaluate the impacts of uncertainties in LST and NSSR on SSM retrieval, a sensitivity analysis of LST and NSSR is performed in this paper. Gaussian randomly distributed errors of 1, 2, and 3 K [$\text{error}_{\text{LST}} \sim N(0, 1^2)$, $\text{error}_{\text{LST}} \sim N(0, 2^2)$, and $\text{error}_{\text{LST}} \sim N(0, 3^2)$] are systematically added to the LST. Then, SSM is estimated by using the elliptical-new SSM retrieval model with the noised LST data. Compared with the actual SSM, the root-mean-square error (RMSE) is 0.03 m^3/m^3 for $\text{error}_{\text{LST}} \sim N(0, 1^2)$, 0.04 m^3/m^3 for $\text{error}_{\text{LST}} \sim N(0, 2^2)$, and 0.06 m^3/m^3 for $\text{error}_{\text{LST}} \sim N(0, 3^2)$. As shown in Fig. 7(a), the correlation coefficient (R) is 0.91 for $\text{error}_{\text{LST}} \sim N(0, 1^2)$, 0.81 for $\text{error}_{\text{LST}} \sim N(0, 2^2)$, and 0.60 for $\text{error}_{\text{LST}} \sim N(0, 3^2)$. Similarly, we add Gaussian randomly distributed errors of 10, 20, and 30 W/m^2 to the NSSR [$\text{error}_{\text{NSSR}} \sim N(0, 10^2)$, $\text{error}_{\text{NSSR}} \sim N(0, 20^2)$, and $\text{error}_{\text{NSSR}} \sim N(0, 30^2)$]. Fig. 7(b) reveals that the RMSE is 0.02 m^3/m^3 and that the R value is 0.92 for $\text{error}_{\text{NSSR}} \sim N(0, 10^2)$. For $\text{error}_{\text{NSSR}} \sim N(0, 20^2)$, the RMSE is 0.03 m^3/m^3 and R is 0.81. For $\text{error}_{\text{NSSR}} \sim N(0, 30^2)$, the RMSE is 0.05 m^3/m^3 and R is 0.67. Errors from a Gaussian random distribution are added to the diurnal LST and NSSR for all vegetation conditions and land cover types, and therefore, the results will display the largest possible sensitivity.

C. Validation and Analysis With In Situ Measurements

To compare the elliptical-original model and the elliptical-new model and validate their feasibilities,

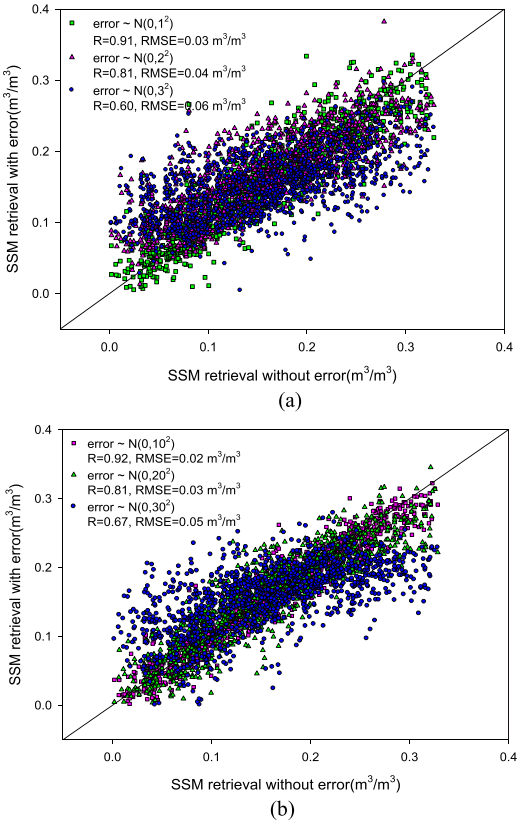

Fig. 7. Validation of the estimated SSM after adding Gaussian randomly distributed error. (a) Added error to the LST. (b) Added error to the NSSR.

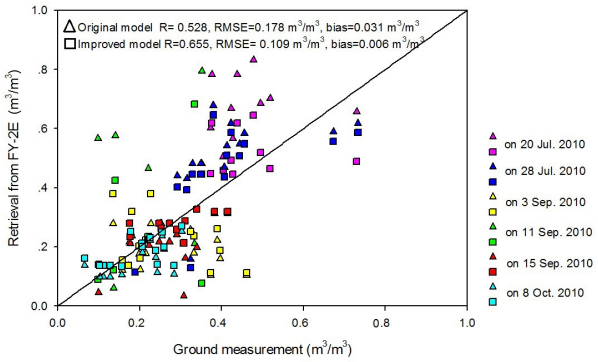

Fig. 8. Validation data for the elliptical-original (triangle) and elliptical-new (rectangle) models with *in situ* measurements.

TABLE VI
RETRIEVAL RESULTS AND GROUND MEASUREMENT AT NST_15

Date	LST at 11 a.m. (K)			Daily average SSM (m^3/m^3)		
	Retrieval	Ground measurement	BIAS*	Retrieval	Ground measurement	BIAS*
20 Jul.	293.14	286.25	6.89	0.657	0.730	-0.073
28 Jul.	299.49	289.45	10.04	0.557	0.673	-0.116
3 Sep.	295.83	281.85	13.98	0.241	0.507	-0.266
15 Sep.	297.01	283.55	13.46	0.202	0.503	-0.301

*BIAS: in situ measurement - the retrieved measurement

in situ daily-averaged SSM measurements are regarded as references for an evaluation of cloud-free days between July and October in 2010. In this model, SSM is estimated from the elliptical relationship between the diurnal cycle of LST and NSSR. For the elliptical relationship between diurnal LST and NSSR cycles, there should be one diurnal LST-NSSR ellipse for each given location for a cloud-free day. When the weather changes (e.g., clouds occur or last for a while or even rains) during the daytime, LST-NSSR and SSM can also be affected. In this case, the LST-NSSR relationship may not be elliptical, probably leading to the inapplicability of the proposed model. Otherwise, if the LST-NSSR relationship is still ellipse with weather variation, the ellipse model would be applicable. In this case, the model is based on fully cloud-free days to avoid intermittent cloudy or rainy conditions. However, more in depth investigation should be conducted to further explore the effects of clouds or rain events on the estimation of SSM with the proposed model. In addition, under situation of one diurnal LST-NSSR ellipse for each given location for a cloud-free day, the SSM retrieval should be daily averaged. *In situ* daily-averaged SSM can reflect to some extent the diurnal variation of soil moisture content. Hence, it is feasible to evaluate the model outputted SSM with daily-averaged *in situ* measurements.

When comparing the SSM retrieval from the elliptical-original model with the *in situ* measurements, an R value of 0.528, an RMSE of 0.178 m^3/m^3, and a bias of 0.031 m^3/m^3 are obtained. The elliptical-new model possesses better accuracy, with an R value of 0.655, an RMSE of 0.109 m^3/m^3, and a bias of 0.006 (m^3/m^3). The results in Fig. 8 reveal a good correlation between the retrieved and ground measurements. The satellite SSM retrievals in July are higher than the ground measurements, potentially due to atmospheric data affecting the model when SSM is high. The atmospheric forcing data, including wind speed, used to drive the CoLM might affect the model coefficients causing the SSM retrievals to be higher than the ground measurements.

1) Analysis of the Error: Station NST_04 is situated in marshland. Station NST_13 is located in high vegetation-cover conditions. The FVC at NST_13 can sometimes exceed 70%, which is too high to obtain an accurate SSM retrieval result [51].

Station NST_15 is situated along a hill slope with a large elevation difference. Heterogeneous surfaces might cause errors in the estimation of LST and NSSR. The elliptical SSM retrieval model is based on the synergistic use of diurnal cycles of LST and NSSR, and thus, errors in the LST and NSSR estimates will influence the SSM estimation. Table VI reveals that the SSM estimation will contain larger error as the LST estimate becomes less accurate. For example, the SSM estimate is more accurate on 20 July than on any other day because of the high accuracy of the LST retrieval on this day. Furthermore, if the LST retrieval is higher than the true value, the smaller ellipse rotation angle will reduce the SSM retrieval value relative to the *in situ* measurement, as is evidenced

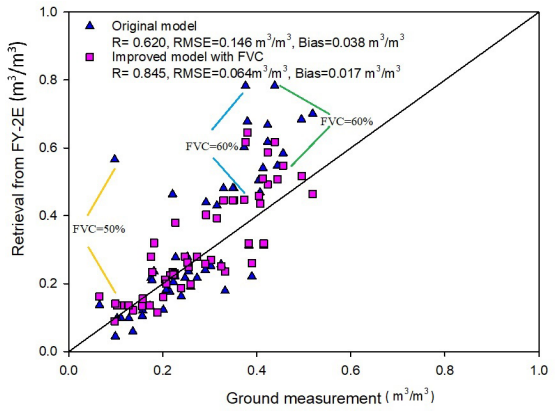

Fig. 9. Validation using the *in situ* measurements.

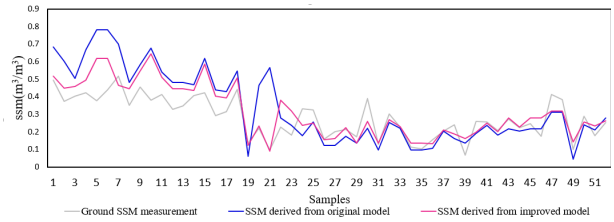

Fig. 10. SSM trends in comparison with *in situ* measurements.

in Table VI. Thus, the ellipse-new model is not suitable for station NST_15.

Due to the high uncertainties from LST, the ellipse-new model is not suitable for stations NST_04, NST_13, and NST_15. Therefore, a subset of ground-based stations will be used for validation.

2) Validation With Subset of Ground-Based Stations: Excluding the stations NST_04, NST_13, and NST_15, the *in situ* measurements are used for the validation process. As shown in Fig. 9, the results are much more effective when considering FVC, as evidenced by an R of 0.845, an RMSE of 0.064 m^3/m^3, and a bias of 0.017 m^3/m^3. These results demonstrate that using the elliptical-original model to derive the SSM with the same set of coefficients for bare soil will enlarge the error and generate an R of 0.620, an RMSE of 0.146 m^3/m^3, and a bias of 0.038 m^3/m^3. From Fig. 9, it can be seen that the discrepancies between original model and *in situ* measurements get smaller when the FVC is accounted in the new retrieval model. In particular, we label the samples that has large bias with original model, while has better agreement with *in situ* measurements when the FVC is accounted in the new retrieval model. To further compare the elliptical-original and elliptical-new models, the SSM trends and the field-scaled SSM measurements are shown in Fig. 10. Regardless of whether SSM is derived from the original- or elliptical-new model, it exhibits the same trend as the ground SSM measurements. In addition, it is evident that the SSM retrievals using the elliptical-new model (red line) are much more similar to the field-scaled SSM measurements (blue line) than are the retrievals based on the original model. Therefore, to precisely derive SSM, different vegetation conditions must be considered to optimize the applicability of the model at temporal and spatial scales.

V. Summary and Conclusion

SSM, which plays important roles in agricultural applications, environmental and climate systems, and weather forecasting and carbon/nitrogen cycling, is a key land surface variable in the earth system. Due to the capability of geostationary satellites to acquire observations more frequently relative to polar orbiting satellites, methods of greater practicality and precision can be developed. In this paper, we generate an improved and novel SSM retrieval model based on the synergistic use of diurnal cycles of LST and NSSR. Previous investigations have demonstrated the feasibility of the elliptical-original SSM retrieval model for bare soils in sparsely vegetated areas where the FVC varies from 0 to 0.7. However, the coefficients of the elliptical-original model are incapable of distinguishing different vegetation conditions. In this paper, the elliptical-new model is optimized by accounting for the influences of different FVC values. First, the diurnal cycles of LST, which are estimated using the generalized split-window algorithm [43]–[45], and of NSSR [46] are calculated. Second, FVC is calculated based on a dimidiate pixel model and a MODIS NDVI product to optimize the model for the estimation of SSM at the regional scale. Subsequently, SSM retrieval is estimated using the elliptical-new model while considering the impacts of different FVC values. Finally, a preliminary validation is conducted by employing *in situ* ground measurements for the counties of Maqu, Luqu, and Ruoergai, which are located to the east of the SAYR. When comparing the original- and elliptical-new model, stronger relationship between the ground measurements and the FY-2E-derived SSM using the elliptical-new model is reported, with an R of 0.845, an RMSE of 0.064 m^3/m^3, and a bias of 0.017 m^3/m^3. The SSM retrieval results using the elliptical-new model are more similar to the field-scaled SSM measurements than are those obtained using the original model. The FY-2E-derived SSM based on the elliptical-new model exhibits less error than does the SSM estimated from the elliptical-original model. Therefore, the preliminary validation using *in situ* measurements confirms that it is necessary to consider the impacts of FVC for improved SSM retrieval.

The sensitivity of the model to atmospheric forcing is investigated. The retrievals have larger biases when the wind speed, air temperature, or humidity has large uncertainties. The ellipse model is most sensitive to wind speed, which indicates a requirement for high-accuracy wind speed measurements to estimate soil moisture with the proposed model.

In the future studies, we will obtain LST and NSSR by employing high-quality geostationary satellite data. Furthermore, due to the observation of several errors observed during FVC estimation, including errors in the determination of the angle and some bidirectional reflectance distribution function effects from $\pm 55°$ of the MODIS threshold, the accuracy of FVC retrieval will be improved and validated. Along with a point-scale validation, cross-comparisons with other existing SSM products will be conducted in the future studies.

ACKNOWLEDGMENT

The authors would like to thank the Faculty of Geo-Information Science and Earth Observation, University of Twente (ITC), Enschede, The Netherlands, Chinese Academy of Science–Cold and Arid Regions Environmental and Engineering Research Institute (CAS-CAREERI), Lanzhou, China, International Soil Moisture Network, Vienna, Austria, and National Satellite Meteorological Center China Meteorological Administration (NSMC), Beijing, China, for providing the soil moisture measurements data, meteorological data, and FY-2E data.

REFERENCES

[1] M. H. Cosh, T. J. Jackson, R. Bindlish, and J. H. Prueger, "Watershed scale temporal and spatial stability of soil moisture and its role in validating satellite estimates," *Remote Sens. Environ.*, vol. 92, no. 4, pp. 427–435, 2004.

[2] W. A. Dorigo *et al.*, "Evaluation of the ESA CCI soil moisture product using ground-based observations," *Remote Sens. Environ.*, vol. 162, pp. 380–395, Jun. 2015.

[3] D. R. Legates *et al.*, "Soil moisture: A central and unifying theme in physical geography," *Prog. Phys. Geogr.*, vol. 35, no. 1, pp. 65–86, 2011.

[4] J. Peng, A. Loew, O. Merlin, and N. E. C. Verhoest, "A review of spatial downscaling of satellite remotely sensed soil moisture," *Rev. Geophys.*, vol. 55, no. 2, pp. 341–366, 2017.

[5] Z.-L. Li *et al.*, "A review of current methodologies for regional evapotranspiration estimation from remotely sensed data," *Sensors*, vol. 9, no. 5, pp. 3801–3853, 2009.

[6] R. Zhang, J. Tian, H. Su, X. Sun, S. Chen, and J. Xia, "Two improvements of an operational two-layer model for terrestrial surface heat flux retrieval," *Sensors*, vol. 8, no. 10, pp. 6165–6187, 2008.

[7] L. He, J. M. Chen, J. Liu, S. Bélair, and X. Luo, "Assessment of SMAP soil moisture for global simulation of gross primary production," *J. Geophys. Res. Biogeosci.*, vol. 122, no. 7, pp. 1549–1563, 2017.

[8] W. B. Anderson *et al.*, "Towards an integrated soil moisture drought monitor for East Africa," *Hydrol. Earth Syst. Sci.*, vol. 16, pp. 2893–2913, Aug. 2012.

[9] E. Meyles, A. Williams, L. Ternan, and J. Dowd, "Runoff generation in relation to soil moisture patterns in a small Dartmoor catchment, Southwest England," *Hydrol. Process.*, vol. 17, no. 2, pp. 251–264, 2003.

[10] J. Peng, A. Loew, S. Zhang, J. Wang, and J. Niesel, "Spatial downscaling of satellite soil moisture data using a vegetation temperature condition index," *IEEE Trans. Geosci. Remote Sens.*, vol. 54, no. 1, pp. 558–566, Jan. 2016.

[11] G. P. Petropoulos, G. Ireland, and B. Barrett, "Surface soil moisture retrievals from remote sensing: Current status, products & future trends," *Phys. Chem. Earth, A/B/C*, vols. 83–84, pp. 36–56, Mar. 2015.

[12] N. Sánchez, J. Martínez-Fernández, and A. González-Zamora, "A combined approach with SMOS and modis to monitor agricultural drought," *Int. Arch. Photogramm. Remote Sens. Spatial Inf. Sci.*, vol. XLI-B8, pp. 393–398, Jul. 2016.

[13] L. Brocca, F. Melone, T. Moramarco, and R. Morbidelli, "Spatial-temporal variability of soil moisture and its estimation across scales," *Water Resour. Res.*, vol. 46, no. 2, p. W02516, 2010.

[14] J. Peng, J. Niesel, A. Loew, S. Zhang, and J. Wang, "Evaluation of satellite and reanalysis soil moisture products over Southwest China using ground-based measurements," *Remote Sens.*, vol. 7, no. 11, pp. 15729–15747, 2015.

[15] J. Peng and A. Loew, "Recent advances in soil moisture estimation from remote sensing," *Water*, vol. 9, no. 7, p. 530, 2017.

[16] T. Jagdhuber, I. Hajnsek, A. Bronstert, and K. P. Papathanassiou, "Soil moisture estimation under low vegetation cover using a multi-angular polarimetric decomposition," *IEEE Trans. Geosci. Remote Sens.*, vol. 51, no. 4, pp. 2201–2215, Apr. 2013.

[17] T. Jagdhuber, I. Hajnsek, and K. P. Papathanassiou, "An iterative generalized hybrid decomposition for soil moisture retrieval under vegetation cover using fully polarimetric SAR," *IEEE J. Sel. Topics Appl. Earth Observ. Remote Sens.*, vol. 8, no. 8, pp. 3911–3922, Aug. 2015.

[18] F. Mattia, G. Satalino, V. R. N. Pauwels, and A. Loew, "Soil moisture retrieval through a merging of multi-temporal L-band SAR data and hydrologic modelling," *Hydrol. Earth Syst. Sci.*, vol. 13, no. 3, pp. 343–356, 2009.

[19] P. Leng, Z.-L. Li, S.-B. Duan, M.-F. Gao, and H.-Y. Huo, "A practical approach for deriving all-weather soil moisture content using combined satellite and meteorological data," *ISPRS J. Photogramm. Remote Sens.*, vol. 131, pp. 40–51, Sep. 2017.

[20] W. Zhao, A. Li, and T. Zhao, "Potential of estimating surface soil moisture with the triangle-based empirical relationship model," *IEEE Trans. Geosci. Remote Sens.*, vol. 55, no. 11, pp. 6494–6504, Nov. 2017.

[21] L. He, J. M. Chen, and K. S. Chen, "Simulation and SMAP observation of sun-glint over the land surface at the L-band," *IEEE Trans. Geosci. Remote Sens.*, vol. 55, no. 5, pp. 2589–2604, May 2017.

[22] L. Brocca *et al.*, "Soil moisture estimation through ASCAT and AMSR-E sensors: An intercomparison and validation study across Europe," *Remote Sens. Environ.*, vol. 115, no. 12, pp. 3390–3408, 2011.

[23] A. Loew and F. Schlenz, "A dynamic approach for evaluating coarse scale satellite soil moisture products," *Hydrol. Earth Syst. Sci.*, vol. 15, pp. 75–90, Jan. 2011.

[24] C.-H. Su, D. Ryu, R. I. Young, A. W. Western, and W. Wagner, "Inter-comparison of microwave satellite soil moisture retrievals over the Murrumbidgee Basin, southeast Australia," *Remote Sens. Environ.*, vol. 134, pp. 1–11, Jul. 2013.

[25] N. Wanders *et al.*, "Observation uncertainty of satellite soil moisture products determined with physically-based modeling," *Remote Sens. Environ.*, vol. 127, pp. 341–356, Dec. 2012.

[26] W. Zhao and A. Li, "A comparison study on empirical microwave soil moisture downscaling methods based on the integration of microwave-optical/IR data on the Tibetan Plateau," *Int. J. Remote Sens.*, vol. 36, nos. 19–20, pp. 4986–5002, 2015.

[27] D. Entekhabi *et al.*, "The soil moisture active passive (SMAP) mission," *Proc. IEEE*, vol. 98, no. 5, pp. 704–716, May 2010.

[28] A. Colliander *et al.*, "Validation and scaling of soil moisture in a semi-arid environment: SMAP validation experiment 2015 (SMAPVEX15)," *Remote Sens. Environ.*, vol. 196, pp. 101–112, Jul. 2017.

[29] D. Zhang and G. Zhou, "Estimation of soil moisture from optical and thermal remote sensing: A review," *Sensors*, vol. 16, no. 8, p. 1308, 2016.

[30] D. Zhang, R. Tang, B.-H. Tang, H. Wu, and Z.-L. Li, "A simple method for soil moisture determination from LST–VI feature space using nonlinear interpolation based on thermal infrared remotely sensed data," *IEEE J. Sel. Topics Appl. Earth Observ. Remote Sens.*, vol. 8, no. 2, pp. 638–648, Feb. 2015.

[31] D. Zhang *et al.*, "Validation of a practical normalized soil moisture model with *in situ* measurements in humid and semi-arid regions," *Int. J. Remote Sens.*, vol. 36, nos. 19–20, pp. 5015–5030, 2015.

[32] P. Leng, X. Song, S.-B. Duan, and Z.-L. Li, "A practical algorithm for estimating surface soil moisture using combined optical and thermal infrared data," *Int. J. Appl. Earth Observ. Geoinf.*, vol. 52, pp. 338–348, Oct. 2016.

[33] P. Leng, X. Song, Z.-L. Li, J. Ma, F. Zhou, and S. Li, "Bare surface soil moisture retrieval from the synergistic use of optical and thermal infrared data," *Int. J. Remote Sens.*, vol. 35, no. 3, pp. 988–1003, 2014.

[34] P. J. Wetzel, D. Atlas, and R. H. Woodward, "Determining soil moisture from geosynchronous satellite infrared data: A feasibility study," *J. Climate Appl. Meteorol.*, vol. 23, no. 3, pp. 375–391, 1984.

[35] W. Zhao *et al.*, "Determination of bare surface soil moisture from combined temporal evolution of land surface temperature and net surface shortwave radiation," *Hydrol. Process.*, vol. 27, no. 19, pp. 2825–2833, 2013.

[36] P. Leng, X. Song, S.-B. Duan, and Z.-L. Li, "Generation of continuous surface soil moisture dataset using combined optical and thermal infrared images," *Hydrol. Process.*, vol. 31, no. 6, pp. 1398–1407, 2017.

[37] H. Tian *et al.*, "Evidence for a recent warming and wetting in the source area of the Yellow River (SAYR) and its hydrological impacts," *J. Geogr. Sci.*, vol. 25, no. 6, pp. 643–668, 2015.

[38] Y. Wang, X. Song, P. Leng, C. Sun, and X. Liu, "Estimation of surface soil moisture using FengYun-2E (FY-2E) data: A case study over the source area of the Yellow River," in *Proc. IEEE Int. Geosci. Remote Sens. Symp. (IGARSS)*, Jul. 2016, pp. 4327–4330.

[39] D. Ji and Y. Dai, "The common land model (CoLM) technical guide," College Global Change Earth Syst. Sci., Beijing Normal Univ., Beijing, China, Tech. Rep., 2010. [Online]. Available: http://globalchange.bnu.edu.cn/download/doc/CoLM/CoLM_Technical_Guide.pdf

[40] S. Luo, S. Lü, and Y. Zhang, "Development and validation of the frozen soil parameterization scheme in Common Land Model," *Cold Regions Sci. Technol.*, vol. 55, no. 1, pp. 130–140, 2009.

[41] Y.-M. Song, W.-D. Guo, and Y.-C. Zhang, "Simulation of latent heat flux exchange between land surface and atmosphere in temperate mixed forest and subtropical artificial coniferous forest sites in China by CoLM," *Plateau Meteorol.*, vol. 8, no. 5, pp. E60429–E60433, 2008.

[42] G.-M. Jiang, Z.-L. Li, and F. Nerry, "Land surface emissivity retrieval from combined mid-infrared and thermal infrared data of MSG-SEVIRI," *Remote Sens. Environ.*, vol. 105, no. 4, pp. 326–340, 2006.
[43] B.-H. Tang *et al.*, "Generalized split-window algorithm for estimate of land surface temperature from Chinese geostationary FengYun meteorological satellite (FY-2C) Data," *Sensors*, vol. 8, pp. 933–951, Sep. 2008.
[44] X. Song *et al.*, "Estimation of land surface temperature using FengYun-2E (FY-2E) data: A case study of the source area of the Yellow River," *IEEE J. Sel. Topics Appl. Earth Observ. Remote Sens.*, vol. 10, no. 8, pp. 3744–3751, Aug. 2017.
[45] Z. Wan and J. Dozier, "A generalized split-window algorithm for retrieving land-surface temperature from space," *IEEE Trans. Geosci. Remote Sens.*, vol. 34, no. 4, pp. 892–905, Jul. 1996.
[46] Y. Wang, X. Song, and R. Wang, "Estimation of net surface shortwave radiation using FengYun-2E (FY-2E) data on cloud-free days," *J. Univ. Chin. Acad. Sci.*, vol. 33, no. 6, pp. 769–774, 2016.
[47] R. Liu, "Evapotranspiration estimated by using Geostationary Meteorological Satellite data over the source water region of the Yellow River," Ph.D. dissertation, Cold Arid Regions Environ. Eng. Res. Inst., Univ. Chinese Acad. Sci., Gansu, China, 2011.
[48] Z.-L. Li, L. Jia, Z. Su, Z. Wan, and R. Zhang, "A new approach for retrieving precipitable water from ATSR2 split-window channel data over land area," *Int. J. Remote Sens.*, vol. 24, no. 24, pp. 5095–5117, 2003.
[49] Y. Ding *et al.*, "Quantifying the impact of NDVIsoil determination methods and NDVIsoil variability on the estimation of fractional vegetation cover in Northeast China," *Remote Sens.*, vol. 8, no. 1, p. 29, 2016.
[50] G. Gutman and A. Ignatov, "The derivation of the green vegetation fraction from NOAA/AVHRR data for use in numerical weather prediction models," *Int. J. Remote Sens.*, vol. 19, no. 8, pp. 1533–1543, 1998.
[51] P. Leng, X. Song, Z. L. Li, Y. Wang, and D. Wang, "Effects of vegetation and soil texture on surface soil moisture retrieval using multi-temporal optical and thermal infrared observations," *Int. J. Remote Sens.*, vol. 36, nos. 19–20, pp. 4972–4985, 2015.
[52] G. B. Bonan, "A land surface model (LSM version 1.0) for ecological, hydrological, and atmospheric studies: Technical description and user's guide," Nat. Center Atmospheric Res., Boulder, CO, USA, Tech. Rep. NCAR/TN-417+STR, 1996.
[53] A. M. Hasson, N. I. Al-Hamadani, and A. A. Al-Karaghouli, "Comparison between measured and calculated diurnal variations of wind speeds in northeast Baghdad," *Solar Wind Technol.*, vol. 7, no. 4, pp. 481–487, 1990.
[54] A. Dai and C. Deser, "Diurnal and semidiurnal variations in global surface wind and divergence fields," *J. Geophys. Res. Atmos.*, vol. 104, no. D24, pp. 31109–31125, 1999.

Yawei Wang received the B.S. degree in geographic information system from Sichuan Normal University, Chengdu, China, in 2013, and the M.S. degree in geographic information system from University of Chinese Academy of Sciences, Beijing, China, in 2016. She is currently pursuing the Ph.D. degree from the Ludwig Maximilian University of Munich, Munich, Germany.

Her research interests include moisture and energy fluxes from remote sensing data.

Jian Peng (M'12) received the Ph.D. degree in earth science from the Max Planck Institute for Meteorology (MPI-M), Hamburg, Germany.

He was a Research Scientist at the University of Munich, Munich, Germany, and a Post-Doctoral Researcher at MPI-M. He is currently a Senior Researcher with the School of Geography and the Environment, University of Oxford, Oxford, U.K. His research interests include the quantitative retrieval of land surface parameters from remote sensing data, understanding land-atmosphere interactions using earth system models and observational data, development of downscaling schemes, quantification of climate change impact on water resources, estimation of high-resolution land surface water and energy fluxes from satellite observations, and the investigation of hydrological and climatic extremes and their impacts on vegetation.

Xiaoning Song (M'04) received the Ph.D. degree in geographic information system from the Institute of Remote Sensing Applications, Chinese Academy of Sciences, Beijing, China, in 2004.

She is currently a Professor with the University of Chinese Academy of Sciences, Beijing. Her research interests include parameters inversion of land surface temperature, surface emissivity, surface albedo, leaf area index, net primary production, evapotranspiration, and soil moisture.

Pei Leng received the Ph.D. degree in geographic information system from the University of Chinese Academy of Sciences, Beijing, China, in 2015.

He is currently with the Key Laboratory of Agri-Informatics, Ministry of Agriculture/Institute of Agricultural Resources and Regional Planning, Chinese Academy of Agricultural Sciences, Beijing. His research interests include the moisture and energy fluxes from remote sensing data.

Ralf Ludwig received the Diploma and Ph.D. degrees in physical geography, remote sensing geology and geophysics from the Geography Department, Ludwig Maximilian University of Munich (LMU), Munich, Germany, in 1993 and 1999, respectively.

He is the Dean of the Faculty of Geosciences and a Professor of applied physical geography and environmental modeling with Department of Geography, LMU. His research interests include process-based and spatially distributed hydrological modeling at the catchment scale, data assimilation and model integration for water resources, land use and climate change impact assessment from Mediterranean to subarctic environments, and the energy–environment interface.

Dr. Ludwig is a Steering Committee Member of the Helmholtz Research School MICMoR and the Spokesperson of the Albertan-Bavarian Energy-Environment Research Network ABBY-Net. He is the member of the European Geosciences Union, the German Society for Photogrammetry, Remote Sensing and Geoinformation, and the German Society for Canadian Studies.

Alexander Loew (M'04) received the M.S. degree in geography and the Ph.D. degree in physical geography from the Ludwig Maximilian University of Munich (LMU), Munich, Germany, in 2001 and 2004, respectively.

He is currently a Full Professor of physical geography and microwave remote sensing with the LMU. His research interests include the derivation of quantitative land surface parameters from remote sensing data, the assimilation of remote sensing data into climate and land surface process models, and the evaluation of climate models using observational data.

4.3 Paper III: JAG - Global assessments of two blended microwave soil moisture products CCI and SMOPS with in-situ measurements and reanalysis data

International Journal of Applied Earth Observations and Geoinformation 94 (2021) 102234

Contents lists available at ScienceDirect

International Journal of Applied Earth Observations and Geoinformation

journal homepage: www.elsevier.com/locate/jag

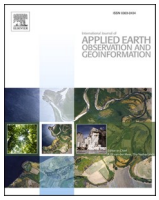

Global assessments of two blended microwave soil moisture products CCI and SMOPS with in-situ measurements and reanalysis data

Yawei Wang [b], Pei Leng [a,*], Jian Peng [b,c], Philip Marzahn [b], Ralf Ludwig [b]

[a] Key Laboratory of Agricultural Remote Sensing, Ministry of Agriculture and Rural Affairs/Institute of Agricultural Resources and Regional Planning, Chinese Academy of Agricultural Sciences, Beijing, China
[b] Department of Geography, Ludwig-Maximilians-University Munich, Munich, Germany
[c] School of Geography and the Environment, University of Oxford, Oxford, United Kingdom

ARTICLE INFO

Keywords:
Blended microwave soil moisture
CCI
SMOPS
In-situ measurements
Reanalysis data

ABSTRACT

Multiple soil moisture (SM) products have been produced based on observations from microwave satellite sensors nowadays, allowing for the acquisition of global SM dynamics in a timely manner. Currently, only two blended microwave SM products, namely the Climate Change Initiative (CCI) from the European Space Agency and the Soil Moisture Operational Product System (SMOPS) from the National Oceanic and Atmospheric Administration, are available with either better temporal or better spatial coverage than those of other SM products derived from a single sensor. However, an assessment and especially a synchronous comparison of these two products are still lacking, making it difficult to determine a better alternative in actual applications. In the present study, a comprehensive assessment of the two blended products was conducted with reanalysis SM data from the European Centre for Medium-Range Weather Forecasts and in-situ measurements from the International Soil Moisture Network. The scaling strategy of cumulative distribution function matching was used to remove the systematic differences in spatial mismatch between the satellite pixels and ground in-situ observations. The results indicated that CCI reveals overall better accuracy than that of SMOPS with both in-situ measurements and reanalysis data under different climate patterns. Specifically, the overall root mean square error (RMSE) with the in-situ measurements were 0.042 m^3/m^3 and 0.046 m^3/m^3 for CCI and SMOPS, respectively. Further investigation also confirmed that SMOPS could be a potential alternative over the regions where CCI is not available, since SMOPS has better spatial coverage than CCI.

1. Introduction

Soil moisture (SM) is an essential variable in global climate change studies, hydrology and water resources, digital agriculture and other relevant domains (Hawley et al., 1983; Legates et al., 2011; Roberts, 1983; Seneviratne et al., 2010). Currently, a number of approaches, including in-situ observations/networks, land surface/hydrological modeling and assimilation, and satellite retrievals, are frequently used to obtain SM and its dynamics with varying spatial and temporal resolutions. Among these methods, in-situ measurements can provide the most accurate SM; however, in-situ measurements are expensive, time consuming, labor intensive and limited in terms of spatial extent (Dorigo et al., 2011), making it more suitable to validate SM data derived from satellite retrievals or modeling/assimilation systems, rather than direct applications in various investigations. Based on land surface/hydrological modeling and assimilation, several global SM products with continuous spatial coverages and temporal intervals have been produced through operational forecast systems. Some typical SM products include the Global Land Data Assimilation System (GLDAS), the Global Land Evaporation Amsterdam Model (GLEAM), the Modern-Era Retrospective analysis for Research and Applications (MERRA) and the fifth generation of the European Centre for Medium-Range Weather Forecasts Atmospheric Reanalysis (ERA5) (Albergel et al., 2018; Martens et al., 2017; Rodell et al., 2004). In recent decades, with the development of remote sensing technologies, a number of regional/global SM products have been released primarily based on microwave observations. These most widely used SM products include the Advanced Microwave Scanning Radiometer-Earth Observing System (AMSR-E) and successive AMSR2, the Advanced SCATterometer (ASCAT), the Soil Moisture and Ocean Salinity Mission (SMOS) and the

* Corresponding author.
E-mail address: lengpei@caas.cn (P. Leng).

https://doi.org/10.1016/j.jag.2020.102234
Received 29 March 2020; Received in revised form 1 September 2020; Accepted 2 September 2020
Available online 21 September 2020

Soil Moisture Active Passive (SMAP) (Entekhabi et al., 2010; Kerr et al., 2012; Njoku et al., 2003; Wagner et al., 2013). Specifically, a variety of validation or intercomparision activities have been conducted to compare the performance of satellite-derived SM products with that of in-situ measurements, reanalysis data and land surface/hydrological modeling and data assimilation systems (Colliander et al., 2017; Leng et al., 2016; Wang et al., 2018; Zhang et al., 2019; Zhao et al., 2020). Moreover, nearly all previous investigations have confirmed that satellite-derived SM products can generally capture SM dynamics well across most regions under different climate patterns and landscapes all over the world, and satellite SM products generally reveal higher accuracy than those derived from land surface/hydrological modeling and assimilation systems following previous studies (Wen et al., 2014; Stillman et al., 2016). As a result, to date, satellite-derived SM products have been widely used in a series of applications, such as weather forecasting, drought monitoring and water cycling (Entekhabi et al., 2009; Kawanishi et al., 2003; Martínez-Fernández et al., 2016; Zhang et al., 2015).

Except for the aforementioned single-sensor-based SM products, blended SM products acquired from multi-sensor observations have received considerable attention in a recent decade. A number of studies have highlighted that blended SM products not only reveal improved accuracy compared with that of products derived from a single microwave sensor, but also have better performances for the simulation of land surface processes (Cheng et al., 2019; Dorigo et al., 2015; Nair and Indu, 2016; Yin et al., 2019). Currently, two globally blended microwave SM products, namely the Climate Change Initiative (CCI) from the European Space Agency (ESA) and the Soil Moisture Operational Product System (SMOPS) from the National Oceanic and Atmospheric Administration (NOAA), are available for various applications. As blended SM products, SMOPS and CCI are produced from most of the mainstream microwave sensors available but with different data sources, merging methods and temporal intervals to develop the final products. Specifically, CCI combines advantages from various satellites that have finite lifetimes and different instrument characteristics with different spatial and temporal resolutions, temporal coverage and polarization to form SM products with a fixed spatial resolution of 0.25° on a daily basis (Dorigo et al., 2015, 2017; Gruber et al., 2019). These satellite sensors not only include most of the aforementioned ones, such as AMSR-E, AMSR2, ASCAT and SMOS, but also contain other microwave missions, such as the Scanning Multichannel Microwave Radiometer (SMMR), the Active Microwave Instrument Wind Scatterometer (AMI-WS) onboard the European Remote-Sensing Satellite (ERS), the Special Sensor Microwave/Imager (SSM/I), the Tropical Rainfall Monitoring Mission (TRMM) Microwave Imager (TMI), and the WindSat Spaceborne Polarimetric Microwave Radiometer. The latest version of the CCI v4.5 dataset covers a period of over 40 years from 1978 to 2018, making it the longest record of satellite SM as so far. As a consequence, the CCI product has been widely used by over 6000 users worldwide to date (Dorigo et al., 2017; Gruber et al., 2019). Compared to CCI, SMOPS have received less attention. SMOPS has been operationally running at NOAA since 2012, aiming at increasing spatial and temporal coverage of the satellite SM observations and providing blended analysis from all the individual satellite microwave SM products for operational use (Leng et al., 2019). Specifically, SMOPS imports SM retrievals from satellite sensors and merges them with the output from the single channel (SC) algorithm using GLDAS modeled data (Jackson, 1993). Several mainstream satellite sensors, including SMAP, ASCAT, SMOS, AMSR2, WindSat, and the Microwave Imager onboard the Global Precipitation Measurement (GPM) satellite, have been used to produce the SMOPS products. It notes that the latest version of SMOPS SM v3.0 covering the period from March 2017 to the present is currently available to be obtained from the NOAA Comprehensive Large Array-data Stewardship System website. Specifically, the SMOPS product has the same spatial resolution of 0.25° as that of CCI; however, both daily and 6 -hly temporal interval datasets are available for SMOPS, which might provide more alternatives than CCI in potential applications such as drought/-flood monitoring and land surface assimilation systems where frequent SM measurements are required (Liu et al., 2016; Nair and Indu, 2016; Yin et al., 2014, 2019).

Although blended microwave SM products (especially CCI) have been extensively evaluated and applied in a recent decade, no further investigation has been dedicated to synchronously assessing the two blended SM products. Hence, the present study is motivated by two main points: (1) compared to the intensive evaluations and applications of CCI, SMOPS has received much less attention. Hence, it is necessary to evaluate SMOPS across the world and especially to synchronously assess the two SM products to provide useful recommendations for practical applications, given that the two blended products reveal significant differences in data sources, merging methods, temporal intervals and spatial coverages. (2) A main advantage of SMOPS over CCI is that the former has nearly full spatial coverage, which can fill almost all the gaps remaining by CCI; therefore, it is of great importance to investigate the accuracy of SMOPS under different climate patterns and especially over the regions where CCI is not available. In the present study, except for the available in-situ SM measurements, a frequently used SM dataset with the same spatial resolution of 0.25° as that of CCI and SMOPS, namely, the reanalysis product of ERA5, is also implemented to assess the two blended SM products. The present study is organized as follows: Section 2 presents the materials and methods. The results and discussion are presented in Section 3 and Section 4, respectively. Section 5 presents the conclusions.

2. Materials and methods

2.1. Satellite SM product

2.1.1. SMOPS

SMOPS was developed to make effective use of all available microwave-based observations to obtain a blended SM product with increased spatial and temporal coverage. SMOPS has been operational running since 2012, which can not only provide global SM data products from individual sensors, but also provides a blended analysis from all SM product produced by the individual sensors. The basic retrieval strategy of SMOPS is first to obtain SM from a baseline satellite sensor and then to potentially extend the spatial and temporal coverage using SM retrievals from other satellite sensors. Specifically, the retrievals from multiple sensors are finally regridded to a spatial resolution of 0.25° with the cumulative distribution function (CDF) matching method in daily and 6 -hly intervals (Liu et al., 2016; Yin et al., 2019; Zheng et al., 2018). It notes that the previous version 1.0 and 2.0 of SMOPS take the WindSat and AMSR2 as baseline satellite sensor, respectively. Currently, the latest version 3.0 of the SMOPS uses the more reliable SMAP as baseline emission, and is capable of providing a seamless SM product over global land with both daily and 6 -hly intervals from March 2017 to present. In this study, SMOPS v3.0 daily SM data stored as the NetCDF file format during the study period from August 2017 to December 2018 is obtained from the NOAA website (https://www.avl.class.noaa.gov/saa/products/welcome). It notes that a significant advantage of SMOPS v3.0 is that the data have almost full land coverage, which can well fill the gaps remaining by most of the currently available satellite SM products. However, the overall full coverage is probably not realistic in SMOPS potentially highlighting SM retrieval over likely frozen ground/ice and over regions with dense vegetation.

2.1.2. CCI

The CCI products were developed under the framework of the ESA Soil Moisture Climate Change Initiative and Water Cycle Multi-Mission Observation Strategy (Hollmann et al., 2013). The CCI SM has a spatial resolution of 0.25° and a daily time stamp. Moreover, for each version of CCI, three products including active, passive and combined active/-passive, are available at the official website (https://www.esa-

soilmoisture-cci.org/node/145). Specifically, the active product was derived based on the change detection method, whereas the passive product was generated following the land parameter retrieval method (LPRM). Moreover, the CDF matching method was used to rescale all the active and passive microwave datasets to the climatology of GLDAS output, which is similar to that in the procedure of producing the SMOPS product. Finally, the combined product was generated by merging the rescaled active and passive datasets (Gruber et al., 2017, 2019; Liu et al., 2012; Wagner et al., 2012). It notes that errors in the individual active and passive products are characterized by means of a stricter triple collocation (TC) analysis to reduce possible uncertainties in the latest version (v4.5) of CCI. These errors are used both for estimating the merging parameters and for characterizing the errors of the merged product, which is different from previous versions of CCI products. Because the latest version (v4.5) of CCI extends the three global SM products covering a long period from 1978 to 2018, the combined product stored as NetCDF classic format during the study period is obtained for further investigation.

2.2. SM reanalysis data

ERA5 is the fifth global reanalysis produced by the European Centre for Medium-Range Weather Forecasts (ECMWF). As the successive dataset for the widely used ERA-Interim reanalysis that stopped at the end of August 2019, ERA5 inherits the framework of model physics, data assimilation and core dynamics from the previous version and combines vast amounts of historical observations into global estimates using advanced modeling and data assimilation systems, which generally reveals better accuracy than that of its previous version (Dee et al., 2011; Albergel et al., 2018). The SM product of ERA5 includes data from four different depths at 0.25°×0.25° (the original SM data is with a spatial resolution of 0.28°×0.28°, however has been processed with current form in the official website for users) with hourly temporal resolution. Currently, EAR5 data stored as GRIB and NetCDF formats are available from 1979 to present (https://cds.climate.copernicus.eu/cdsapp#!/dataset/reanalysis-era5-single-levels?tab = overview). In this study, hourly SM data in the first layer (0−7 cm) with the classic NetCDF format are obtained from the website and are subsequently averaged to daily values for the study period from August 2017 to December 2018. It notes that ERA5 combines vast amounts of historical observations into global estimates using advanced modelling and data assimilation systems. Specifically, the number of observations assimilated in ERA5 has increased from approximately 0.75 million per day on average in 1979 to around 21 million per day by July 2018 (Hersbach et al., 2018). In general, the observations primarily include satellite data and in-situ data. For an example, the satellite data contains a variety of sensors for observing the atmospheric motions vectors, radiances, radio occulation, scatterometer, ozone and SM. Specifically, as for satellite SM, only ASCAT based SM is directly assimilated into ERA5. Moreover, the in-situ data assimilated in ERA5 primarily contains the essential meteorological elements (e.g. surface pressure, air temperature, wind and humidity) and snow parameters (e.g. snow depth and snow cover) collected from land stations and radiosondes. Except for these, ERA5 SM data are corrected by 2-m analysis increments of air temperature and relative humidity following an empirical approach (Drusch et al., 2009; Li et al., 2020).

2.3. In-situ SM networks

For the assessment of the two blended microwave SM products, in-situ measurements are obtained from the International Soil Moisture Network (ISMN; https://ismn.geo.tuwien.ac.at/en/) (Dorigo et al., 2011, 2013). The ISMN is a data-hosting center where globally available in-situ SM measurements are collected, harmonized and made available to users. For the study period from August 2017 to December 2018, in-situ SM measurements with a depth of 5 cm are acquired from 12 available networks, including REMEDHUS, TERENO, SMOSMANIA, FMI, OZNET, RSMN, SCAN, SNOTEL, iRON, PBO_H2O, FR_Aqui and USCRN. Fig. 1 shows the geographic distribution of the 12 SM networks across the world. Specifically, SM measurements beyond the physically possible range or under frozen conditions were excluded in advance. Finally, a total of 449 stations over the 12 networks, including 20 stations in REMEDHUS, two stations in TERENO, three stations in FR_Aqui, 22 stations in SMOSMANIA, 16 stations in FMI, 15 stations in OZNET, 17 stations in RSMN, 113 stations in SCAN, 164 stations in SNOTEL, 65 stations in USCRN, 9 stations in iRON and three stations in PBO_H2O, are used for the present investigation. Details for the 12 networks are described in the following subsections.

2.3.1. REMEDHUS (Spain)

REMEDHUS is located in the semi-arid parts of the Duero Basin in Spain, which mainly covers shrublands and croplands of a 35 km × 35 km flat area (41.1–41.5 °N, 5.1−5.7 °W) with elevations ranging from 700 to 900 m (Martínez-Fernández, 2003). The climate for the REMEDHUS region is semiarid continental Mediterranean, with dry and warm summers and cool to mild and wet winters. The average annual temperature is 12 °C, and the mean annual rainfall is 385 mm. In the present study, SM data collected at 20 stations over the REMEDHUS network are obtained from the ISMN. The REMEDHUS network was operated from March 2005 and has been widely used for various applications, such as calibration and validation of microwave SM products (Peng et al., 2015a).

2.3.2. TERENO (Germany)

The TERENO network is located in western Germany near Köln and Aachen. The elevation of the terrain over the entire Rur catchment generally rises from 30 to 680 m from north to south. The land cover types of the region are arable land (37 %), coniferous and deciduous forests (34 %), pastures (22 %), settlements (5%) and open-cast lignite mines (2%) (Bogena et al., 2018). For TERENO, in-situ SM measurements at depths of 5, 20 and 50 cm are available from December 2009. In the present study, SM measurements at 5 cm at two stations are acquired for the investigation (Zacharias et al., 2011).

2.3.3. FR_Aqui and SMOSMANIA (France)

The FR_Aqui network was set up by the National Institute of Agricultural Research in southwestern France. Trees and vineyards are the dominant vegetation types over this area (Wigneron et al., 2018). In-situ SM measurements at 0−5 cm are available from January 2012 in this network. The SMOSMANIA network is based on the automatic weather station network of Météo-France (RADOME), which observes humidity, wind speed, air temperature and precipitation in southwestern France (Albergel et al., 2008). The stations for SM monitoring are in relatively flat areas (mountainous areas are avoided as much as possible), and the station with the highest altitude is Mouthoumet at 538 m (Calvet et al., 2007). SM probes were installed at depths of 5, 10, 20 and 30 cm horizontally for each station for monitoring from January 2007.

2.3.4. FMI (Finland)

The FMI network is located in northern Finland and is characterized by a mosaic of sparse conifer-dominated forests, small lakes and open and forested bogs. SM probes were installed at depths of 2, 5, 10, 20, 40, 60 and 80 cm horizontally for each station. Ground-based observations are available from January 2007 to the present.

2.3.5. OZNET (Australia)

OZNET in southern New South Wales, Australia, gradually transforms from semiarid regions in the west to temperate regions in the east. With latitude ranging from 34.628 to 35.393 °S and longitude varying from 145.848 to 147.566 °E, the OZNET region is mainly covered by grazing and crops. Specifically, the elevation over the OZNET network varies from 113 to 327 m with little slope. Over the OZNET region,

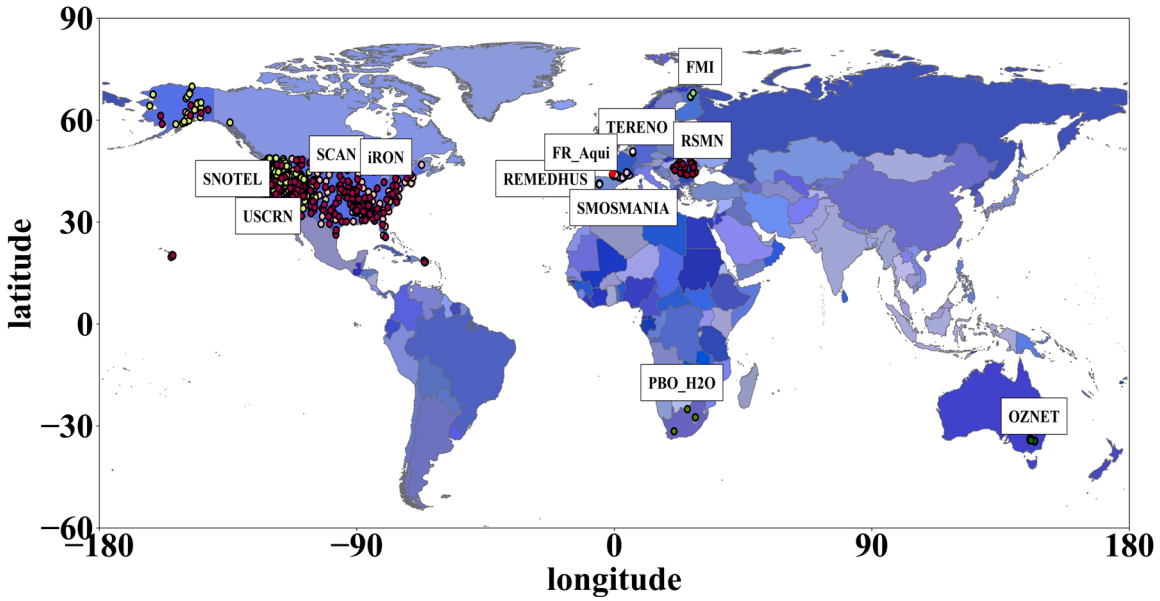

Fig. 1. Locations of the 12 soil moisture networks used in the present study.

annual precipitation ranges from 406 to 783 mm (Young et al., 2008). The SM stations are evenly distributed throughout the experimental catchment for monitoring SM at depths of 0−5 cm, 0−8 cm, 0−30 cm, 30−60 cm and 60−90 cm from September 2001 (Smith et al., 2012).

2.3.6. RSMN (Romania)

The stations of the RSMN network are mainly located along the borders of Romania, with latitudes ranging from 43.9–48.2 °N and longitudes varying from 20.6–28.3 °E, and elevations varying from nearly 300–500 m. In general, the dominant land use types over the RSMN network are minimal forest, water and localities and a small amount of argil soil. The stations have been monitoring SM at 0−5 cm depth since April 2014.

2.3.7. SCAN, SNOTEL, USCRN and iRON (USA)

The SCAN network across the conterminous USA, Alaska, and Hawaii provides a number of parameter observations, including precipitation, air temperature, wind speed and direction, solar radiation, snow depth, SM and soil temperature. The stations monitor various depths of SM from January 1996 to the present. The SNOTEL network is located in the western USA and Alaska (Schaefer and Paetzold, 2001). Most stations in the SNOTEL network provide multiple observations per day, including snow water content, precipitation, snow depth, SM and others, with approximately 30 % providing hourly data. Ground-based observations at different depths varying from 0 to 100 cm can be obtained from October 1980 to the present. The USCRN is a systematic and sustained network with sites throughout the conterminous U.S. The USCRN network offers monthly, daily, and hourly SM observations at depths of 5, 10, 20, 50, and 100 cm from November 2000 to the present (Bell et al., 2013). The interactive Roaring Fork Observation Network (iRON), which is hosted by the Aspen Global Change Institute, is a series of in-situ soil and meteorological monitoring stations (Osenga et al., 2019). Each station is equipped with one dielectric sensor at depths of 5, 20, 50 and 100 cm for SM from August 2012 to January 2019. In this study, in-situ SM measurements in these three networks at 5 cm depth are employed from August 2017 to December 2018.

2.3.8. PBO_H2O (South Africa)

The PBO_H2O network primarily contains SM stations in USA and South Africa. Because a number of stations in SCAN, SNOTEL, USCRN and iRON networks have been used in this study, three stations of the PBO_H2O network located in South Africa are selected for the present investigation (Larson et al., 2008).

2.4. Scaling strategy

The CDF matching method has been widely used to remove systematic differences between satellite imagery and site-specific observations for SM assessments (Brocca et al., 2011; Drusch et al., 2005). Based on the CDF matching procedure, the time series satellite images can be rescaled to make them better match the synchronous in-situ measurements. In this study, the CDF matching method is implemented for the assessments of SMOPS and CCI SM products with in-situ SM measurements collected at the 12 available networks across the world. Specifically, nearly 75 % of the 449 stations at the 12 networks are sparsely distributed where one given pixel of the blended microwave SM data contains only one station. In present study, after the procedure of CDF matching, the in-situ SM measurements are first averaged if more than a single station occur within a CCI or SMOPS pixel. Furthermore, the averaged SM that represent the pixel mean are used to assess the satellite SM data. It notes that the blended SM products are with a daily basis, whereas in-situ SM data are commonly with much more frequent observations (hourly). Considering the temporal variation of SM, to better match the in-situ and satellite SM in temporal dimension, the in-situ SM records are first averaged to daily values, and are subsequently used to assess the blended SM products on a daily basis.

3. Results

3.1. Spatial coverages and temporal intervals of CCI and SMOPS

Because both the daily CCI and SMOPS reveal the same spatial resolution of 0.25°, a direct comparison is first presented to investigate the spatial coverage for the two blended SM products. Take the SM data on the 15th day for the typical months of January, April, July and October 2018 as an example. Fig. 2 shows the two blended SM products for the four selected days. It is evident that SMOPS reveals much better spatial coverage than CCI on all the selected days. Specifically, SMOPS has almost full coverage over the land worldwide regardless of the season, whereas significant gaps can be found for CCI on each scenery of the selected days, especially in winter and over the regions with high latitude. This is because the dielectric properties of the water changes

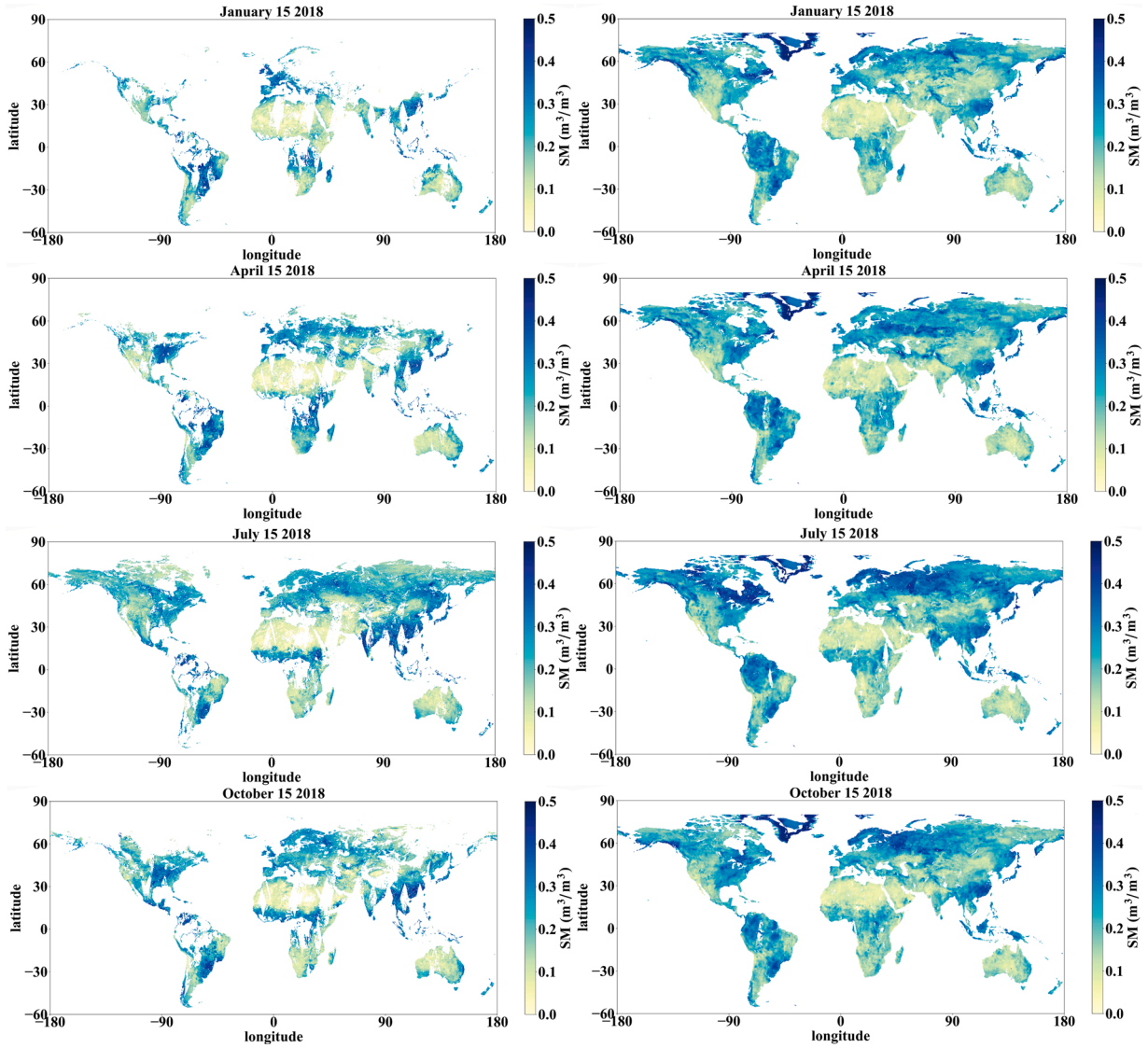

Fig. 2. Global soil moisture distribution of CCI (left column) and SMOPS (right) on the 15th day of the four typical months of January, April, July and October 2018.

dramatically under frozen snow/frozen ground, which can lead to invalid SM retrievals with microwave observations. Hence, all pixels where the land use type is frozen land/snow cover and the surface temperature is observed to be at or below 0 °C, are assigned with an appropriate data flag in the CCI products. Moreover, distinct gaps can also be found around the tropical forest regions along the equator, including regions in Africa, Southeast Asia and South America on nearly all the selected days. Because vegetation can affect the microwave emission, and under a sufficiently dense canopy the emitted soil radiation will become completely masked by the overlaying vegetation, the vegetation optical depth (VOD) data derived from microwave observations has been used to detect regions with excessive vegetation. As a consequence, the data for high VOD has been flagged in the CCI products. Except for the minimum spatial coverage in winter, the spatial coverage of CCI reveals significant seasonal variation where the maximum coverage occurs in summer (July) and medium coverage can be found in spring and autumn (April and October).

In general, the different spatial coverages of CCI and SMOPS data can be attributed to several reasons including different methods, sensors and quality controls for developing the two blended microwave SM products. To better assess the two datasets synchronously, the quality flags of CCI product are used to remove unreliable pixels (e.g. pixels with frozen land, snow cover, temperatures below 0 °C and dense vegetation) of SMOPS data. Fig. 3 shows the available number of days for each pixel of the two blended SM products at monthly interval. It is obvious that except for the masked areas, SMOPS has significantly more observations for each pixel than that of CCI in each of the selected typical month. Following the statistics, average observation days for the valid pixels of CCI are 20, 20, 25 and 21 in January, April, July and October, respectively, whereas these numbers for SMOPS are 24, 24, 30 and 25, respectively. All these results indicate that SMOPS has significantly higher observation frequency than CCI at monthly interval. More specifically, Table 1 shows the percentages of pixels with different observation frequencies at monthly interval for the two blended SM products. It is evident that for all the pixels with valid SM in monthly interval, over 20 % of the monthly CCI SM are averaged with less than 15 available daily CCI data, and approximately one third of those pixels have valid CCI observations over 26 days in the months of January, April and October. As for July, although more observation frequencies can be found compared to that for the other three months, less than two thirds of the pixels of monthly CCI have more than 26 daily observations. Compared to CCI, it is clear that the vast majority (over two thirds) of valid monthly SMOPS SM are obtained by more than 26 daily observations. All these results reveal that SMOPS has significantly more frequent observations for most of the pixels across the world at monthly interval.

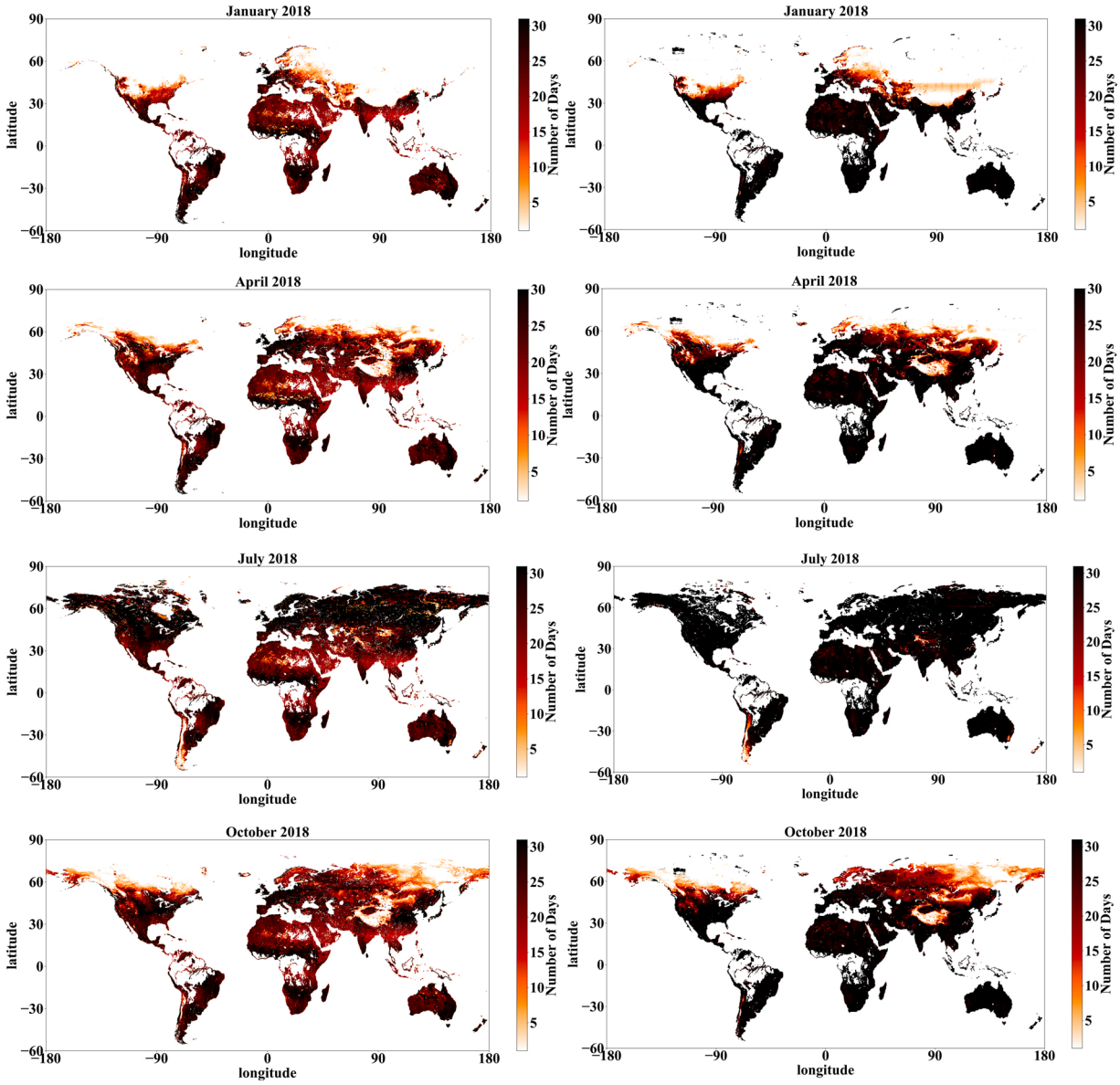

Fig. 3. Available number of days for each pixel of the CCI (left column) and SMOPS (right) in the four typical months of January, April, July and October 2018.

Table 1
Percentages of pixels with different observation frequencies at monthly interval for CCI and SMOPS in the four typical months of January, April, July and October 2018.

Percentage Month	Observation frequencies (days) for pixels with monthly CCI					
	1–5	6–10	11–15	16–20	21–25	≥26
January	10 %	6%	6%	20 %	23 %	35 %
April	10 %	6%	7%	19 %	26 %	32 %
July	3%	2%	3%	11 %	18 %	63 %
October	9%	6%	8%	17 %	23 %	37 %
Percentage Month	Observation frequencies (days) for pixels with monthly SMOPS					
	1–5	6–10	11–15	16–20	21–25	≥26
January	14 %	4%	3%	3%	5%	71 %
April	8%	5%	4%	5%	7%	71 %
July	0%	0%	0%	1%	2%	97 %
October	7%	6%	5%	7%	8%	67 %

3.2. Assessments of the blended SM products with in-situ measurements

This section assesses blended microwave SM products with in-situ measurements collected from 12 available SM networks across the world. Because scale mismatches commonly exist between satellite pixel footprints and ground in-situ observations, to better match satellite SM products and site-specific measurements in time series, the CDF matching method is used to remove the systematic errors caused by the scale mismatch between the blended SM products and in-situ measurements. Fig. 4 shows an example for the comparison between blended SM products with CDF matching and in-situ measurements collected at the Zamarron station of the REMEDHUS network in Spain. It is obvious that the two blended SM products can generally capture well the overall SM dynamic in the temporal dimension over the study period from August 2017 to December 2018. Following this result, almost all the sub-period of SM increases (e.g. from early to middle August 2017), decreases (e.g. from January to late February 2018) and fluctuation changes (e.g. from November 2017 to early January 2018) can be precisely obtained from the two blended SM products. Specifically, a rain event on March 1st, 2018 is also detected by both of the blended SM data, in which SM revels

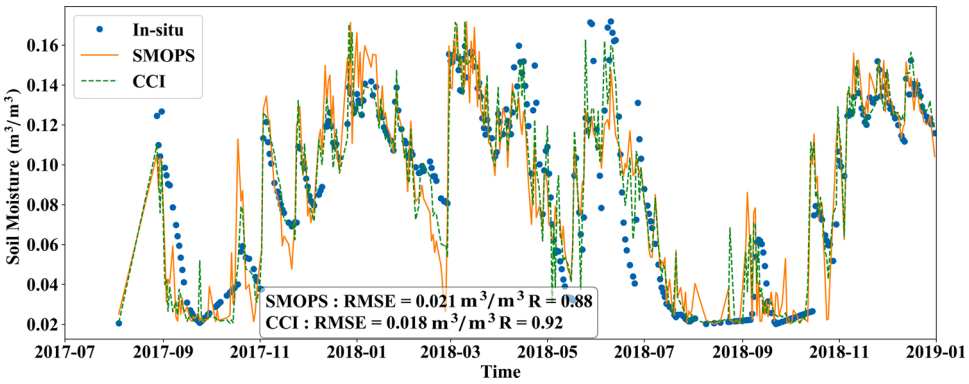

Fig. 4. Comparison between blended SM products and in-situ measurements through CDF matching at the Zamarron station of REMEDHUS.

a dramatic increase from both the satellite SM and in-situ measurements. With the in-situ SM measurements, a considerable accuracy with a correlation coefficient (R) of 0.92 and root mean square error (RMSE) of 0.018 m^3/m^3 can be obtained for the CCI data, which is slightly better than that of the SMOPS data with an R of 0.88 and RMSE of 0.021 m^3/m^3. Nevertheless, the results of the Zamarron station indicate a relatively high and comparable accuracy of the two blended microwave SM products.

To better investigate the accuracy of SMOPS and CCI, further assessments are implemented for other in-situ SM measurements at all 12 networks. Fig. 5 shows the accuracy of the two blended SM products compared to in-situ measurements for the 12 networks in detail. The RMSEs for most of the networks are within 0.050 m^3/m^3, with FR_Aqui, OZNET, PBO, REMEDHUS and RSMN having RMSEs close to 0.040 m^3/m^3. Specifically, the RMSE between SMOPS and the in-situ measurements varies from 0.035 to 0.066 m^3/m^3, whereas a comparable RMSE range of 0.031 to 0.060 m^3/m^3 can be obtained between CCI and the in-situ SM measurements. The correlation coefficient between SMOPS and the in-situ measurements varies from 0.144 to 0.764, whereas CCI shows similar correlation coefficient with a range of 0.227 to 0.792. According to the statistical results, both CCI and SMOPS perform the best in FR_Aqui and worse in FMI and iRON. Moreover, averaged RMSEs are 0.046 m^3/m^3 and 0.042 m^3/m^3 for SMOPS and CCI, respectively, indicating that both blended microwave SM data are well correlated to the in-situ measurements. These results preliminarily indicate that both blended SM products exhibit significant accuracy close to the target accuracy of 0.040 m^3/m^3 for microwave SM data dedicated by existing satellite missions. Nevertheless, the results also indicate that CCI has slightly better accuracy than that of SMOPS, with an improved RMSE from 0.001 to 0.008 m^3/m^3 for the 12 networks.

3.3. Assessments of the blended SM products under different climate classifications

To investigate the accuracy of two blended SM products under different hydrologic and vegetation conditions, comparisons of satellite SM products with referenced SM data were commonly grouped to multiple climate patterns (Cho et al., 2017; Wagner et al., 2003; Zohaib et al., 2017). Because the reanalysis SM data have the same spatial resolution of 0.25° as the blended SM products, no CDF matching is required to assess the blended SM products with reanalysis data. In this section, the Köppen-Geiger climate classification is used to divide the global land across the world into five main climate groups, with each group being divided based on seasonal precipitation and temperature patterns (Kottek et al., 2006; Rubel and Kottek, 2010). Fig. 6 shows a widely used global Köppen-Geiger climate classifications in detail.

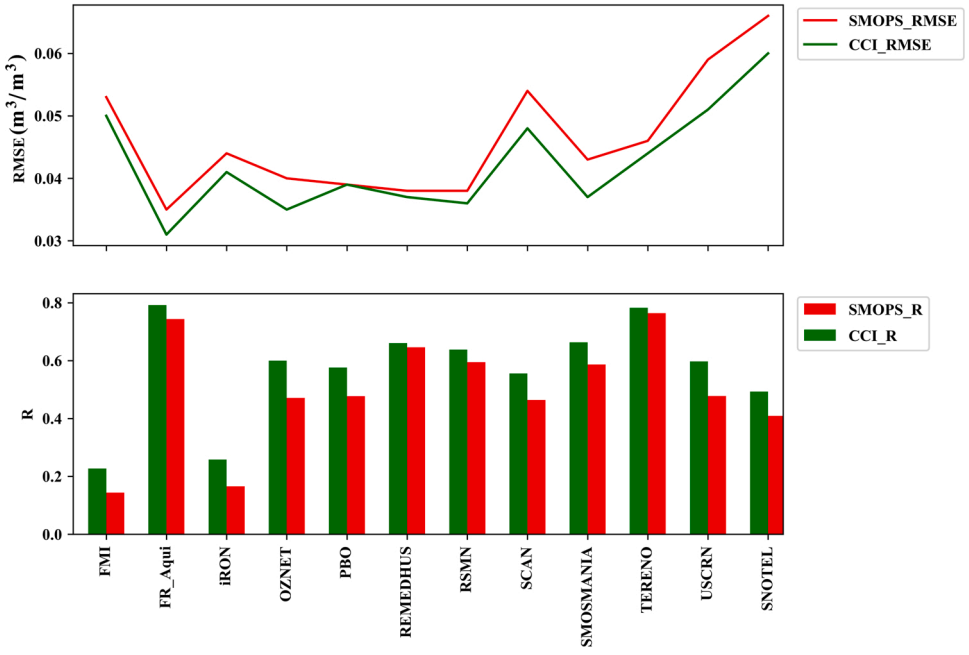

Fig. 5. RMSE and correlation coefficient (R) of the blended SM products and in-situ measurements for the 12 networks.

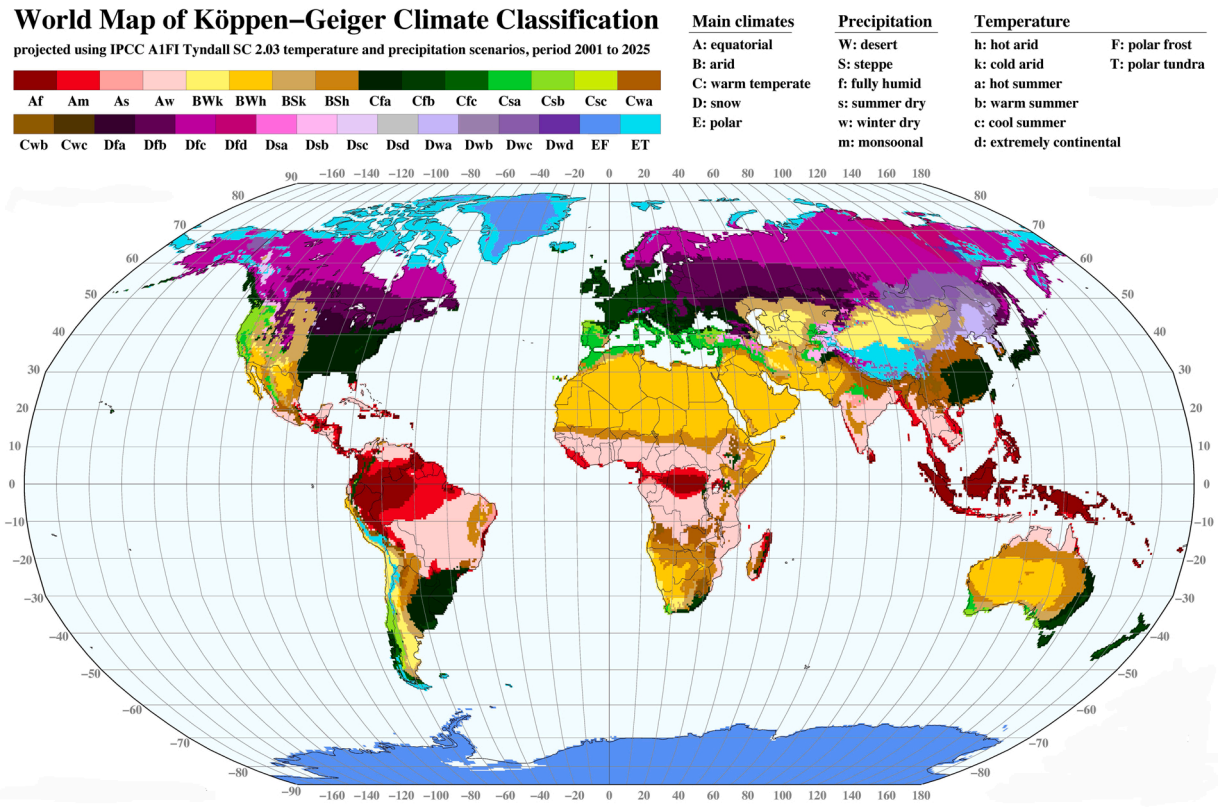

Fig. 6. Global Köppen-Geiger climate classifications (adapted from Rubel and Kottek, 2010).
(a) SMOPS (b) CCI

Except for the Polar Regions, it is clear that each of the Köppen-Geiger climate pattern is constituted by a letter from each of the main climate, precipitation and temperature, respectively.

To make it consistency when comparing the two blended products with the referenced ERA5 SM data synchronously, the regions where SMOPS is available while CCI has no valid values are first removed from the SMOPS. Fig. 7 shows the bias between the two blended microwave SM products and ERA5 across the world. It is evident that both SMOPS and CCI have similar bias distributions when comparing to ERA5 over the study period. Specifically, both SMOPS and CCI overestimate SM in arid climate such as BWk, BWh and BSk (labeled as yellow in Fig. 6), whereas underestimate SM in equatorial climate such as Am, As and Aw (labeled as red in Fig. 6).

In addition to the bias, the global distributions of the unbiased RMSE (ubRMSE) are obtained between the two blended microwave SM products and ERA5 data (Fig. 8). It is clear that an ubRMSE within 0.08 m^3/m^3 can be obtained for the two blended SM data over most areas, and the pixels with larger uncertainties are most likely to occur over high latitude regions, especially for CCI. Fig. 9 depicts the ubRMSE for each of the Köppen-Geiger climate classifications in detail. It is evident that CCI reveals significantly high accuracy in equatorial climate (Af, Am, As and Aw) and the continental climate of Dsb. For the arid climate (BSh and BWh), the major warm temperate climate (Cfa, Csa, Csb, Cwa, Cwb and Cwc) and several continental climate (Dfa and Dsa), CCI also shows slightly better accuracy than SMOPS. However, the two blended microwave SM products exhibit comparable accuracy under a few warm temperate climate (Cfc and Csc), several continental climate (Dfc, Dwa and Dwb) and polar climate (ET). Except for these, SMOPS is slightly better than CCI in several continental climate (Dfd, Dwc and Dwd). All these accuracy statistics indicate that CCI show overall significantly better or comparable accuracy than SMOPS in most of the regions worldwide.

3.4. Performances of SMOPS over the regions where CCI is unavailable

Following the previous section, it is evident that CCI reveals better or comparable accuracy than SMOPS across most regions worldwide. Nevertheless, it is essential to investigate the accuracy of SMOPS over

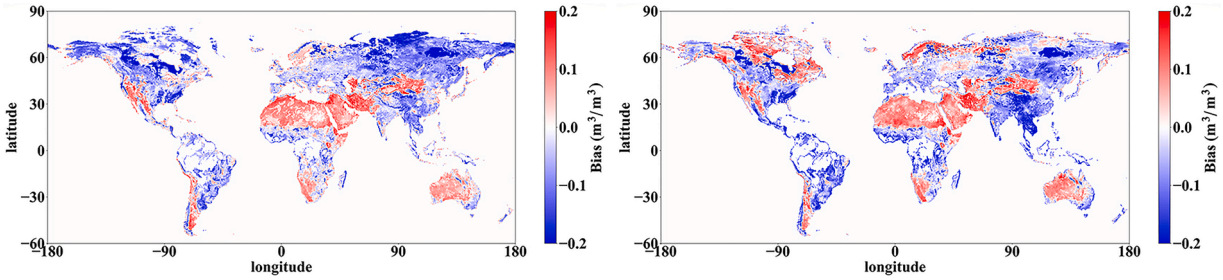

Fig. 7. Bias between SMOPS and ERA5 (a), and between CCI and ERA5 (b).
(a) SMOPS (b) CCI

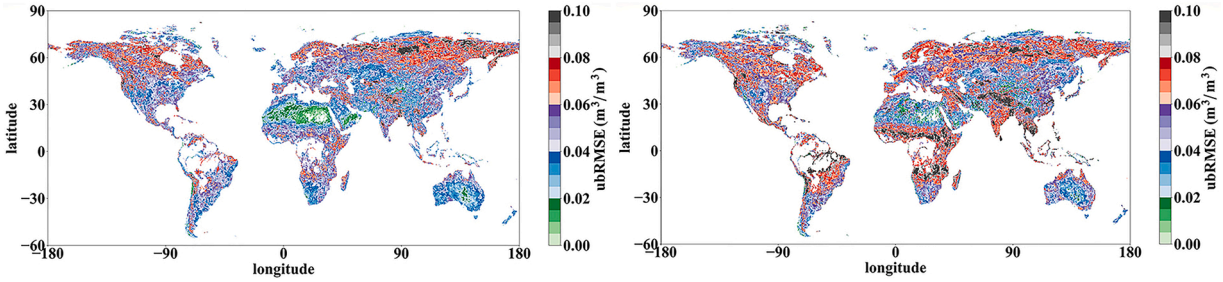

Fig. 8. Unbiased RMSE between SMOPS and ERA5 (a), and between CCI and ERA5 (b).

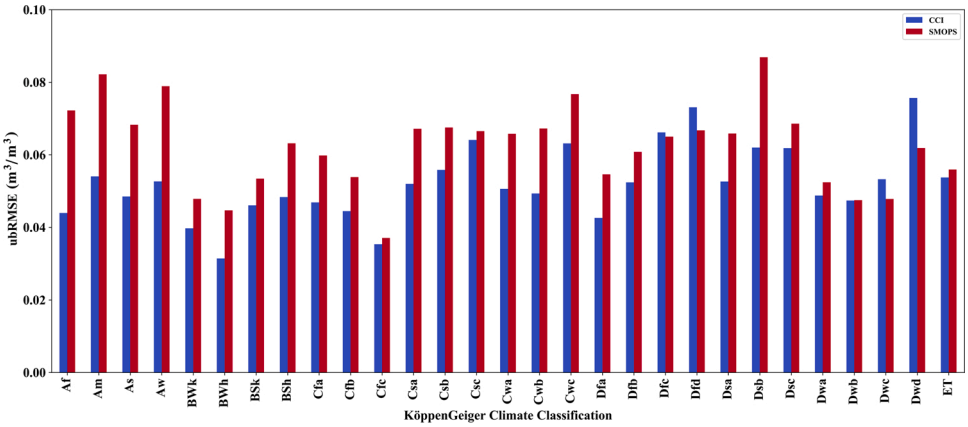

Fig. 9. Unbiased RMSE for each of the Köppen-Geiger climate classifications.

the regions where CCI is unavailable, given that the former has better spatial coverage. From this perspective, SMOPS is most likely to be a potential alternative for the gaps of CCI, only if SMOPS can provide SM estimates with acceptable accuracy. Taking the year 2018 as an example, Fig. 10 depicts the available number of days for valid CCI and available number of days for valid SMOPS while CCI is unavailable, respectively. Following the results, an average of 212 valid daily SM observations for each pixel can be obtained from the CCI in 2018. However, SMOPS can provide an average of 81 more daily SM observations for each pixel to supplement CCI in the same period, making it almost available to acquire SM measurements with a daily basis for each pixel.

Fig. 11 depicts the ubRMSE when comparing SMOPS with ERA5 for each pixel where CCI is not available in the year 2018. It is obvious that most of the ubRMSE is within 0.080 m^3/m^3. Following the statistics, the percentages of pixels for ubRMSE within 0.050 m^3/m^3 and 0.080 m^3/m^3 are 43 % and 84 %, respectively. Moreover, an averaged ubRMSE of 0.058 m^3/m^3 can be obtained for all the pixels. These results reveal that SMOPS can provide SM estimates with comparable accuracy over the gaps. Hence, it is promising that SMOPS could be a potential alternative over the regions where CCI is unavailable.

4. Discussion

4.1. On the differences between the two blended products

The two blended SM products are different in many aspects primarily including data sources, merging methods and quality controls. All these differences can probably result in different performances with respect to temporal intervals, spatial coverages and retrieval accuracy of the SM products. Specifically, during the study period (from August 2017 to December 2018), CCI merged data from ASCAT, SMOS and AMSR2 sensors, while SMOPS merged all available sensors including SMAP, ASCAT, SMOS, AMSR2 and GPM Microwave Imager. This would explain the reason for the worse temporal interval and spatial coverage of CCI than SMOPS, given that CCI takes fewer microwave satellite observations to produce the blended SM product, whereas SMOPS has much more chances to obtain SM estimates with added observations.

Following the results in previous sections, it is obvious that CCI reveals significantly better or comparable accuracy than SMOPS across most of the regions worldwide. A primary reason to the higher accuracy of CCI can be attributed to the enhanced quality control of the microwave SM retrievals for CCI products. For instance, the stricter TC

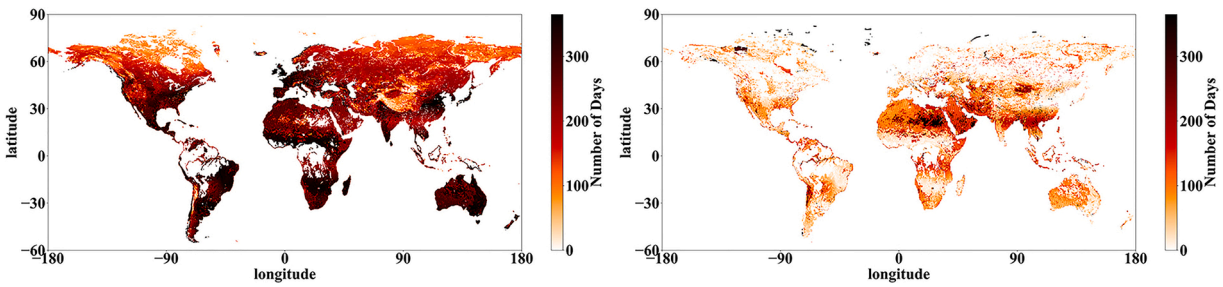

Fig. 10. Available number of days for CCI (a), SMOPS while CCI is unavailable (b) in the year 2018.

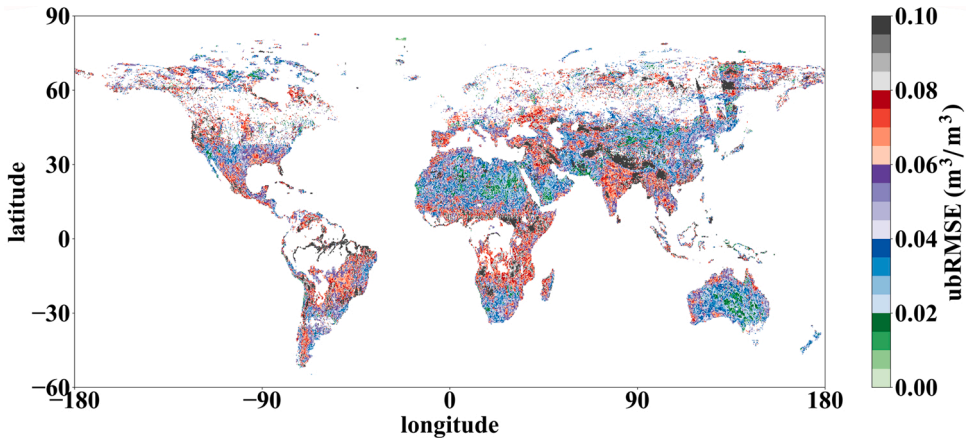

Fig. 11. Unbiased RMSE between SMOPS and ERA5 for each pixel with the data records where SMOPS is valid while CCI is unavailable in 2018.

analysis based error characterization is used in the latest version of the CCI retrievals, which has guaranteed the quality of the combined SM product. Additionally, CCI SM retrievals under specific conditions (e.g. frozen land, snow covered land, temperatures below 0 °C and dense vegetation) are directly masked out in the procedure of CCI SM products. However, it should be noted that with the development of microwave satellite observations, SMOPS has been taking more reliable baseline satellite sensor in the SC algorithm for producing blended SM product since its initial version. Currently, the SMAP is used as the baseline satellite sensor to produce the latest version (v3.0) of SMOPS product, indicating that the increasing accuracy of SMOPS data can be provided at present or near future.

4.2. Recommendations for actual applications with the two blended products

Following the results from both in-situ SM measurements and reanalysis SM data, it is obvious that CCI has better errors statistics compared to SMOPS. Specifically, CCI shows better accuracy than SMOPS for all 12 SM networks, and a number of previous studies have also indicated that CCI data can outperform other products and agree well with the spatial and temporal patterns from in-situ SM observations (Dorigo et al., 2017; Peng et al., 2015b).

In general, we would encourage the use of CCI for actual applications if both CCI and SMOPS are available, given that CCI generally reveals better or comparable accuracy than that of SMOPS across most of the regions worldwide. Specifically, CCI should be the first choice in all equatorial climate, several arid climate (BSh and Bwh), most of the warm temperate climate (Cfa, Csa, Csb, Cwa, Cwb and Cwc), and several continental climate regions (Dfa and Dsa). In contrast, SMOPS only performs better under several continental climate regions (Dfd, Dwc and Dwd). Nevertheless, a significant advantage of SMOPS over CCI is that the former has better spatial coverage. Following the results in previous sections, it was found that SMOPS can provide an average of 81 more daily SM observations with a reliable averaged ubRMSE of 0.058 m^3/m^3 for each pixel in 2018, which is an effective supplement for CCI where only an average of 212 daily SM observations is available for each pixel by CCI in the same period. Except for these, compared to the daily CCI data, SMOPS can provide both daily and 6 -hly interval data. Hence, SMOPS might meet some special needs with higher temporal resolution. However, because the SC algorithm used in SMOPS is sensitive to vegetation, the existence of vegetation would decrease the accuracy of SMOPS SM retrievals. As a consequence, SMOPS would not be suggested to be used in actual applications over the regions where the VOD is high, although it probably can provide SM estimates in these areas.

4.3. Follow-up assessments of the two blended products

In the present study, both in-situ SM measurements and reanalysis SM data are used to assess blended microwave SM products. Despite the performances of accuracy under the Köppen-Geiger climate patterns with ERA5 data across the world, it should be noted that the results based on in-situ measurements are mostly constrained in Europe, USA and Australia, due to the limited data availability for both in-situ measurements and synchronous blended SM products. Hence, assessments with ground station measurements are still lacking for a majority of the Köppen-Geiger climate classifications, especially in the continents of Asia, South America and Africa.

In present study, a total number of 449 stations are used to evaluate the two blended microwave SM products. However, most of these stations (~75 %) are sparsely distributed where one given CCI or SMOPS pixel contains only single station. As a result, the CDF method is used to eliminate the effects of scale mismatch on SM assessments. Additionally, the CDF-matched SM observations from single ground station have been widely used to represent SM associated with a satellite pixel (Brocca et al., 2011; Lacava et al., 2012). Furthermore, if several stations occur within a pixel of the blended SM data, the in-situ SM measurements are primarily CDF-matched for each station. Then, the CDF-matched SM from the stations contained in the given pixel are averaged to represent the reference pixel mean. Although the CDF matching method has been implemented to eliminate the systematic differences created by scale mismatch for the time series of satellite SM and in-situ measurements, uncertainties probably still exist to lead to unreliable assessment results, given that even the averaged SM after CDF matching within a grid cell is only a reference pixel SM rather than the truth itself, and no actual SM at pixel scale is currently available. In a recent study, Chen et al. (2019) investigated the uncertainty of reference pixel SM averages sampled at SMAP core validation sites, which has highlighted a new direction to assess coarse spatial resolution satellite SM in the cases where several stations contained within a satellite footprint scale. To this end, future assessments can focus more on the SM networks with intensive stations and enhanced spatial sampling methods to improve the upscaling functions for the better obtaining of pixel SM mean.

Furthermore, as complementary assessments, the results from the ERA5 data have been used to investigate the two blended SM products under different Köppen-Geiger climate patterns. It is noteworthy that SM derived from ASCAT and other passive microwave observations assimilated into ERA5, have also been used to produce the blended microwave SM products, which seems to make it somewhat lack of independence in the assessments. However, these observations are only a small part in the determination of the ERA5 SM data and blended SM products. Specifically, as for the ERA5, the complicated assimilation system contains a large number of inputs from satellite and in-situ

observations. Similarly, the blended SM products are obtained from several available active/passive sensors, in which ASCAT is only one of the many inputs for the blended microwave SM products. From this perspective, these commonly used observations will not play dominant role in the determination of ERA5 and blended SM estimates. Nevertheless, other SM datasets that completed independent of CCI and SMOPS are also expected to assess the two blended SM products in future investigation.

5. Conclusions

The present study has investigated the accuracy of two blended microwave SM products using both ground in-situ measurements and reanalysis data. With the available in-situ measurements collected at 12 networks across the world and the CDF procedure to eliminate scale issues, it was found that the two blended microwave SM products can provide good agreements when compared to in-situ measurements, with overall RMSEs of 0.042 m^3/m^3 and 0.046 m^3/m^3 for CCI and SMOPS, respectively. Further investigation with ERA5 also confirmed that CCI can obtain better or comparable accuracy than SMOPS across most of the regions worldwide. However, due to the significant better spatial coverage of SMOPS, it can be a potential alternative to provide SM estimates with comparable accuracy of 0.058 m^3/m^3 over the gaps remaining by CCI. Hence, it is promising that the two blended SM products might have the potential to complement each other in actual applications.

Author statement

The authors of the manuscript “Global assessments of two blended microwave soil moisture products CCI and SMOPS with in-situ measurements and reanalysis data” state that this manuscript has not been published or presented elsewhere in part or in entirety and is not under consideration by another journal. We have read and understood your journal’s policies, and we believe that neither the manuscript nor the study violates any of these. There are no conflicts of interest to declare.

Declaration of Competing Interest

The authors declare that they have no known competing financial interests or personal relationships that could have appeared to influence the work reported in this paper.

Acknowledgments

The authors appreciate ESA and NOAA for providing the blended microwave soil moisture products, ISMN for providing in-situ soil moisture measurements and ECMWF for providing reanalysis soil moisture data. Special thanks also go to the group led by Dr. Xiwu Zhan in NOAA and Dr. Xiaojing-Han in IARRP/CAAS for their kindly help with the present study. This work was supported by the National Natural Science Foundation of China under grants 41921001 and41601397, the Fundamental Research Funds for the Central Non-profit Scientific Institution under grant 1610132019012, the Postdoctoral Science Foundation of China under grant 2019M660884, and the European Union’s Horizon 2020 research and innovation program under grant 687320. Ms. Yawei Wang was supported by China Scholarship Council with the study in Ludwig-Maximilians-University Munich.

References

Albergel, C., Rüdiger, C., Pellarin, T., Calvet, J., Fritz, N., Froissard, F., Suquia, D., Petitpa, A., Piguet, B., Martin, E., 2008. From near-surface to root-zone soil moisture using an exponential filter: an assessment of the method based on in-situ observations and model simulations. Hydrol. Earth Syst. Sci. 12, 1323–1337. https://doi.org/10.5194/hess-12-1323-2008.

Albergel, C., Dutra, E., Munier, S., Calvet, J., Munoz-Sabater, J., Rosnay, P., Balsamo, G., 2018. ERA-5 and ERA-Interim driven ISBA land surface model simulations: which one performs better? Hydrol. Earth Syst. Sci. 22, 3515–3532. https://doi.org/10.5194/hess-22-3515-2018.

Bell, J., Palecki, M., Baker, C., Collins, W., Lawrimore, J., Leeper, R., Hall, M., Kochendorfer, J., Meyers, T., Wilson, T., 2013. US climate reference network soil moisture and temperature observations. J. Hydrometeorol. 14, 977–988. https://doi.org/10.1175/JHM-D-12-0146.1.

Bogena, H., Montzka, C., Huisman, J., Graf, A., Schmidt, M., Stockinger, M., von Hebel, C., Hendricks-Franssen, H., van der Kruk, J., Tappe, W., Lücke, A., Baatz, R., Bol, R., Groh, J., Pütz, T., Jakobi, J., Kunkel, R., Sorg, J., Vereecken, H., 2018. The TERENO-Rur hydrological observatory: a multiscale multi-compartment research platform for the advancement of hydrological science. Vadose Zone J. 17, 1–22. https://doi.org/10.2136/vzj2018.03.0055.

Brocca, L., Hasenauer, S., Lacava, T., Melone, F., Moramarco, T., Wagner, W., Dorigo, W., Matgen, P., Martínez-Fernández, J., Llorens, P., Latron, J., Martin, C., Bittelli, M., 2011. Soil moisture estimation through ASCAT and AMSR-E sensors: an intercomparison and validation study across Europe. Remote Sens. Environ. 115, 3390–3408. https://doi.org/10.1016/j.rse.2011.08.003.

Calvet, J., Fritz, N., Froissard, F., Suquia, D., Petitpa, A., Piguet, B., 2007. In situ soil moisture observations for the CAL/VAL of SMOS: the SMOSMANIA network. 2007 IEEE International Geoscience and Remote Sensing Symposium 1196–1199. https://doi.org/10.1109/IGARSS.2007.4423019.

Chen, F., Crow, W., Cosh, M., Colliander, A., Asanuma, J., Berg, A., Martínez-Fernández, J., 2019. Uncertainty of reference pixel soil moisture averages sampled at SMAP core validation sites. J. Hydrometeor. 20, 1553–1569. https://doi.org/10.1175/JHM-D-19-0049.1.

Cheng, M., Zhong, L., Ma, Y., Zou, M., Ge, N., Wang, X., Hu, Y., 2019. A study on the assessment of multi-source satellite soil moisture products and reanalysis data for the Tibetan plateau. Remote Sens. 11, 1196. https://doi.org/10.3390/rs11101196.

Cho, E., Su, C., Ryu, D., Kim, H., Choi, M., 2017. Does AMSR2 produce better soil moisture retrievals than AMSR-E over Australia? Remote Sens. Environ. 188, 95–105. https://doi.org/10.1016/j.rse.2016.10.050.

Colliander, A., Jackson, T., Bindlish, R., Chan, S., Das, N., Kim, B., Cosh, M., Dunbar, R., Dang, L., Pashaian, L., Asanuma, J., Aida, K., Berg, A., Rowlandson, T., Bosch, D., Caldwell, T., Caylor, K., Goodrich, D., al Jassar, H., Lopez-Baeza, E., Martinez-Fernandez, J., Gonzalez-Zamora, A., Livingston, S., McNairn, H., Pacheco, A., Moghaddam, M., Montzka, C., Notarnicola, C., Niedrist, G., Pellarin, T., Prueger, J., Pulliainen, J., Rautiainen, K., Ramos, J., Seyfried, M., Starks, P., Su, Z., Zeng can der Velde, R., Thibeault, M., Dorigo, W., Vreugdenhil, M., Walker, J., Wu, X., Monerris, A., O’Neill, P., Entekhabi, D., Njoku, E., Yueh, S., 2017. Validation of SMAP surface soil moisture products with core validation sites. Remote Sens. Environ. 191, 215–231. https://doi.org/10.1016/j.rse.2017.01.021.

Dee, D., Uppala, S., Simmons, A., Berrisford, P., Poli, P., Kobayashi, S., Andrae, U., Balmaseda, M., Balsamo, G., Bauer, P., Bechtold, P., Beljaars, A., van de Berg, L., Bidlot, J., Bormann, N., Delsol, C., Dragani, R., Fuentes, M., Geer, A., Haimberger, L., Healy, S., Hersbach, H., Hólm, E., Isaksen, L., Kållberg, P., Köhler, M., Matricardi, M., McNally, A., Monge-Sanz, B., Morcrette, J., Park, B., Peubey, C., de Rosnay, P., Tavolato, C., Thépaut, J., Vitart, F., 2011. The ERA-Interim reanalysis: configuration and performance of the data assimilation system. Q. J. R. Meteorol. Soc. 137, 553–597. https://doi.org/10.1002/qj.828.

Dorigo, W., Wagner, W., Hohensinn, R., Hahn, S., Paulik, C., Xaver, A., Gruber, A., Drusch, M., Mecklenburg, S., Oevelen, P., 2011. The International Soil Moisture Network: a data hosting facility for global in situ soil moisture measurements. Hydrol. Earth Syst. Sci. 15, 1675–1698. https://doi.org/10.5194/hess-15-1675-2011.

Dorigo, W., Xaver, A., Vreugdenhil, M., Gruber, A., Hegyiova, A., Sanchis-Dufau, A., Zamojski, D., Cordes, C., Wagner, W., Drusch, M., 2013. Global automated quality control of in situ soil moisture data from the International Soil Moisture Network. Vadose Zone J. 12 https://doi.org/10.2136/vzj2012.0097.

Dorigo, W., Gruber, A., de Jeu, R., Wagner, W., Stacke, T., Loew, A., Albergel, C., Brocca, L., Chung, D., Parinussa, R., 2015. Evaluation of the ESA CCI soil moisture product using ground-based observations. Remote Sens. Enviro. 162, 380–395. https://doi.org/10.1016/j.rse.2014.07.023.

Dorigo, W., Wagner, W., Albergel, C., Albrecht, F., Balsamo, G., Brocca, L., Chung, D., Ertl, M., Forkel, M., Gruber, A., Haas, E., Hamer, P., Hirschi, M., Ikonen, J., de Jeu, R., Kidd, R., Lahoz, W., Liu, Y., Miralles, D., Mistelbauer, T., Nicolai-Shaw, N., Parinussa, R., Pratola, C., Reimer, C., van der Schalie, R., Seneviratne, S., Smolander, T., Lecomte, P., 2017. ESA CCI soil moisture for improved earth system understanding: state-of-the art and future directions. Remote Sens. Environ. 203, 185–215. https://doi.org/10.1016/j.rse.2017.07.001.

Drusch, M., Wood, E., Gao, H., 2005. Observation operators for the direct assimilation of TRMM microwave imager retrieved soil moisture. Geophys. Res. Lett. 32, L15403 https://doi.org/10.1029/2005GL023623.

Drusch, M., Scipal, K., De Rosnay, P., Balsamo, G., Andersson, E., Bougeault, P., Viterbo, P., 2009. Towards a Kalman Filter based soil moisture analysis system for the operational ECMWF Integrated Forecast System. Geophys. Res. L. 36, L10401 https://doi.org/10.1029/2009GL037716.

Entekhabi, D., Njoku, E., O’Neill, P., 2009. The soil moisture active and passive Mission (SMAP): science and applications. Proceeding of the 2009 IEEE Radar Conference 1–3. https://doi.org/10.1109/RADAR.2009.4977030.

Entekhabi, D., Njoku, E., O’Neill, P., Kellogg, K., Crow, W., Edelstein, W., Entin, J., Goodman, S., Jackson, T., Johnson, J., 2010. The soil moisture active passive (SMAP) mission. P. IEEE. 98, 704–716. https://doi.org/10.1109/JPROC.2010.2043918.

Gruber, A., Dorigo, W., Crow, W., Wagner, W., 2017. Triple collocation-based merging of satellite soil moisture retrievals. IEEE Trans. Geosci. Remote Sens. 55, 6780–6792. https://doi.org/10.1109/TGRS.2017.2734070.

Gruber, A., Scanlon, T., Schalie, R., Wagner, W., Dorigo, W., 2019. Evolution of the ESA CCI Soil Moisture climate data records and their underlying merging methodology. Earth Syst. Sci. Data. 11, 717–739. https://doi.org/10.5194/essd-11-717-2019.

Hawley, M., Jackson, T., McCuen, R., 1983. Surface soil moisture variation on small agricultural watersheds. J. Hydrol. 62, 179–200. https://doi.org/10.1016/0022-1694(83)90102-6.

Hersbach, H., Rosnay, P., Bell, B., Schepers, D., Simmons, A., Soci, C., Abdalla, S., Alonso-Balmaseda, M., Balsamo, G., Bechtold, P., Berrisford, P., Bidlot, J., de Boisséson, E., Bonavita, M., Browne, P., Buizza, R., Dahlgren, P., Dee, D., Dragani, R., Diamantakis, M., Flemming, J., Forbes, R., Geer, A., Haiden, T., Hólm, E., Haimberger, L., Hogan, R., Horányi, A., Janiskova, M., Laloyaux, P., Lopez, P., Munoz-Sabater, J., Peubey, C., Radu, R., Richardson, D., Thépaut, J., Vitart, F., Yang, X., Zsótér, E., Zuo, H., 2018. Operational Global Reanalysis: Progress, Future Directions and Synergies with NWP. Available at: https://www.ecmwf.int/node/18765.

Hollmann, R., Merchant, C., Saunders, R., Downy, C., Buchwitz, M., Cazenave, A., Chuvieco, E., Defourny, P., de Leeuw, G., Forsberg, R., 2013. The ESA climate change initiative: satellite data records for essential climate variables. Bull. Amer. Meteor. 94, 1541–1552. https://doi.org/10.1175/BAMS-D-11-00254.1.

Jackson, T., 1993. Measuring surface soil moisture using passive microwave remote sensing. Hydrol. Process. 7, 139–152. https://doi.org/10.1002/hyp.3360070205.

Kawanishi, T., Sezai, T., Ito, Y., Imaoka, K., Takeshima, T., Ishido, Y., Shibata, A., Miura, M., Inahata, H., Spencer, R., 2003. The Advanced Microwave Scanning Radiometer for the Earth observing System (AMSR-E), NASDA's contribution to the EOS for global energy and water cycle studies. IEEE Trans. Geosci. Remote Sens. 41, 184–194. https://doi.org/10.1109/TGRS.2002.808331.

Kerr, Y., Waldteufel, P., Richaume, P., Wigneron, J., Ferrazzoli, P., Mahmoodi, A., Al Bitar, A., Cabot, F., Gruhier, C., Juglea, S., 2012. The SMOS soil moisture retrieval algorithm. IEEE Trans. Geosci. Remote Sens. 50, 1384–1403. https://doi.org/10.1109/TGRS.2012.2184548.

Kottek, M., Grieser, J., Beck, C., Rudolf, B., Rubel, F., 2006. World Map of the Köppen-Geiger climate classification updated. Meteorol. Z. 15, 259–263. https://doi.org/10.1127/0941-2948/2006/0130.

Lacava, T., Matgen, P., Brocca, L., Bittelli, M., Pergola, N., Moramarco, T., Tramutoli, V., 2012. A first assessment of the SMOS soil moisture product with in situ and modeled data in Italy and Luxembourg. IEEE Trans. Geosci. Remote Sens. 50, 1612–1622. https://doi.org/10.1109/TGRS.2012.2186819.

Larson, K., Small, E., Gutmann, E., Bilich, A., Braun, J., Zavorotny, V., 2008. Use of GPS receivers as a soil moisture network for water cycle studies. Geophys. Res. Lett. 35, L24405 https://doi.org/10.1029/2008GL036013.

Legates, D., Mahmood, R., Levia, D., de Liberty, T., Quiring, S., Houser, C., Nelson, F., 2011. Soil moisture: a central and unifying theme in physical geography. Prog. Phys. Geog. 35, 65–86. https://doi.org/10.1177/0309133310386514.

Leng, P., Song, X., Duan, S., Li, Z.-L., 2016. Preliminary validation of two temporal parameter-based soil moisture retrieval models using a satellite product and in situsoil moisture measurements over the REMEDHUS network. Int. J. Remote Sens. 37, 5902–5917. https://doi.org/10.1080/01431161.2016.1253896.

Leng, P., Li, Z.L., Liao, Q.Y., Gao, M.F., Duan, S.B., Zhang, X., Shang, G.F., 2019. Determination of all-sky surface soil moisture at fine spatial resolution synergistically using optical/thermal infrared and microwave measurements. J. Hydrol. 579, 124167 https://doi.org/10.1016/j.jhydrol.2019.124167.

Li, M., Wu, P., Ma, Z., 2020. A comprehensive evaluation of soil moisture and soil temperature from third-generation atmospheric and land reanalysis data sets. Int. J. Climatol. https://doi.org/10.1002/joc.6549.

Liu, Y., Dorigo, W., Parinussa, R., de Jeu, R., Wagner, W., McCabe, M., Evans, J., van Dijk, A., 2012. Trend-preserving blending of passive and active microwave soil moisture retrievals. Remote Sens. Environ. 123, 280–297. https://doi.org/10.1016/j.rse.2012.03.014.

Liu, J., Zhan, X., Hain, C., Yin, J., Fang, L., Li, Z., Zhao, L., 2016. NOAA soil moisture operational product system (SMOPS) and its validations. 2016 IEEE International Geoscience and Remote Sensing Symposium (IGARSS). 3477-3480. https://doi.org/10.1109/IGARSS.2016.7729899.

Martens, B., Gonzalez Miralles, D., Lievens, H., van Der Schalie, R., de Jeu, R., Fernández-Prieto, D., Beck, H.E., Dorigo, W., Verhoest, N., 2017. GLEAM v3: satellite-based land evaporation and root-zone soil moisture. Geosci. Model. Dev. Discuss. 10, 1903–1925. https://doi.org/10.5194/gmd-10-1903-2017.

Martínez-Fernández, J., 2003. Temporal stability of soil moisture in a large-field experiment in Spain. Soil Sci. Soc. Am. J. 67, 1647–1656. https://doi.org/10.2136/sssaj2003.1647.

Martínez-Fernández, J., González-Zamora, A., Sánchez, N., Gumuzzio, A., Herrero-Jiménez, C., 2016. Satellite soil moisture for agricultural drought monitoring: assessment of the SMOS derived Soil Water Deficit Index. Remote Sens. Environ. 177, 277–286. https://doi.org/10.1016/j.rse.2016.02.064.

Nair, A., Indu, J., 2016. Enhancing Noah land surface model prediction skill over Indian subcontinent by assimilating SMOPS blended soil moisture. Remote Sens. 8, 976. https://doi.org/10.3390/rs8120976.

Njoku, E., Jackson, T., Lakshmi, V., Chan, T., Nghiem, S., 2003. Soil moisture retrieval from AMSR-E. IEEE Trans. Geosci. Remote Sens. 41, 215–229. https://doi.org/10.1109/TGRS.2002.808243.

Osenga, E., Arnott, J., Endsley, K., Katzenberger, J., 2019. Bioclimatic and soil moisture monitoring across elevation in a mountain watershed: opportunities for research and resource management. Water Resour. Res. 55, 2493–2503. https://doi.org/10.1029/2018WR023653.

Peng, J., Niesel, J., Loew, A., 2015a. Evaluation of soil moisture downscaling using a simple thermal-based proxy–the REMEDHUS network (Spain) example. Hydrol. Earth Syst. Sc. 19, 4765–4782. https://doi.org/10.5194/hess-19-4765-2015.

Peng, J., Niesel, J., Loew, A., Zhang, S., Wang, J., 2015b. Evaluation of satellite and reanalysis soil moisture products over southwest China using ground-based measurements. Remote Sens. 7, 15729–15747. https://doi.org/10.3390/rs71115729.

Roberts, J., 1983. Forest transpiration: a conservative hydrological process? J. Hydrol. 66, 133–141. https://doi.org/10.1016/0022-1694(83)90181-6.

Rodell, M., Houser, P., Jambor, U., Gottschalck, J., Mitchell, K., Meng, C., Arsenault, K., Cosgrove, B., Radakovich, J., Bosilovich, M., Entin, J., Walker, J., Lohmann, D., Toll, D., 2004. The global land data assimilation system. Bull. Am. Meteorol. Soc. 85, 381–394. https://doi.org/10.1175/BAMS-85-3-381.

Rubel, F., Kottek, M., 2010. Observed and projected cllmate shifts 1901-2100 depicted by world maps of the Köppen-Geiger climate classifications. Meteorol. Z. 19, 135–141. https://doi.org/10.1127/0941-2948/2010/0430.

Schaefer, G., Paetzold, R., 2001. SNOTEL (SNOwpack TELemetry) and SCAN (soil climate analysis network). In: Proceeding of the Int. Workshop on Auto. Weather Stations for Applications in Agriculture and Water Resources Management. High Plains Climate Center, Uni. of Nebraska-Lincoln, USA and the World Meteorol. Org. (WMO), AGM-3 WMO/TD No. 1074.

Seneviratne, S., Corti, T., Davin, E., Hirschi, M., Jaeger, E., Lehner, I., Orlowsky, B., Teuling, A., 2010. Investigating soil moisture-climate interactions in a changing climate: a review. Earth-Sci. Rev. 99, 125–161. https://doi.org/10.1016/j.earscirev.2010.02.004.

Smith, A., Walker, J., Western, A., Young, R., Ellett, K., Pipunic, R., Grayson, R., Siriwardena, L., Chiew, F., Richter, H., 2012. The Murrumbidgee soil moisture monitoring network data set. Water Resour. Res. 48, 1–6. https://doi.org/10.1029/2012WR011976.

Stillman, S., Zeng, X., Bosilovich, M., 2016. Evaluation of 22 precipitation and 23 soil moisture products over a semiarid area in southeastern Arizona. J. Hydrometeorol. 17, 211–230. https://doi.org/10.1175/JHM-D-15-0007.1.

Wagner, W., Scipal, K., Pathe, C., 2003. Evaluation of the aggreement between the first global remotely sensed soil moisture data with model and precipitation data. J. Geophys. Res. 108, 4611. https://doi.org/10.1029/2003JD003663.

Wagner, W., Dorigo, W., de Jeu, R., Fernandez, D., Benveniste, J., Haas, E., Ertl, M., 2012. Fusion of active and passive microwave observations to create an essential climate variable data record on soil moisture. ISPRS Annals 7, 315–321. https://doi.org/10.5194/isprsannals-I-7-315-2012.

Wagner, W., Hahn, S., Kidd, R., Melzer, T., Bartalis, Z., Hasenauer, S., Figa-Saldaña, J., de Rosnay, P., Jann, A., Schneider, S., 2013. The ASCAT soil moisture product: a review of its specifications, validation results, and emerging applications. Meteorol. Z. 22, 5–33. https://doi.org/10.1127/0941-2948/2013/0399.

Wang, Y., Peng, J., Song, X., Leng, P., Ludwig, R., Loew, A., 2018. Surface soil moisture retrieval using optical/thermal infrared remote sensing data. IEEE Trans. Geosci. Remote Sens. 56, 5433–5442. https://doi.org/10.1109/TGRS.2018.2817370.

Wen, X., Lu, H., Li, C., Koike, T., Kaihotsu, I., 2014. Inter-comparison of soil moisture products from SMOS, AMSR-E, ECWMF and GLDAS over the Mongolia plateau. Proceedings of SPIE 9260. https://doi.org/10.1117/12.2068952.

Wigneron, J., Dayan, S., Kruszewski, A., Aluome, C., Yaari, M., Fan, L., Guven, S., Chipeaux, C., Moisy, C., Guyon, D., Loustau, D., 2018. The aqui network: soil moisture sites in the "Les landes" forest and graves vineyards (Bordeaux aquitaine region, France). 2018 IEEE International Geoscience and Remote Sensing Symposium(IGARSS) 3739–3742. https://doi.org/10.1109/IGARSS.2018.8517392.

Yin, J., Zhan, X., Zheng, Y., Liu, J., Hain, C., Fang, L., 2014. Impact of quality control of satellite soil moisture data on their assimilation into land surface model. Geophys. Res. Lett. 41, 7159–7166. https://doi.org/10.1002/2014GL060659.

Yin, J., Zhan, X., Liu, J., Schull, M., 2019. An intercomparison of Noah model skills with benefits of assimilating SMOPS blended and individual soil moisture retrievals. Water Resour. Res. 55, 2572–2592. https://doi.org/10.1029/2018WR024326.

Young, R., Walker, J., Yeoh, N., Smith, A., Ellett, K., Merlin, O., Western, A., 2008. Soil Moisture and Meteorological Observations from the Murrumbidgee Catchment. Department of Civil and Environmental Engineering, The University of Melbourne.

Zacharias, S., Bogena, H., Samaniego, L., Mauder, M., Fuß, R., Pütz, T., Frenzel, M., Schwank, M., Baessler, C., Butterbach-Bahl, K., 2011. A network of terrestrial environmental observatories in Germany. Vadose Zone J. 10, 955–973. https://doi.org/10.2136/vzj2010.0139.

Zhang, J., Becker-Reshef, I., Justice, C., 2015. Evaluation of the ASCAT surface soil moisture product for agricultural drought monitoring in USA. 2018 IEEE International Geoscience and Remote Sensing Symposium (IGARSS) 669–672. https://doi.org/10.1109/IGARSS.2015.7325852.

Zhang, R., Kim, S., Sharma, A., 2019. A comprehensive validation of the SMAP enhanced Level-3 soil moisture product using ground measurements over varied climates and landscapes. Remote Sens. Enviorn 223, 82–94. https://doi.org/10.1016/j.rse.2019.01.015.

Zhao, T., Shi, J., Lv, L., Xu, H., Chen, D., Cui, Q., Jackson, T., Yan, G., Jia, L., Chen, L., Zhao, K., Zheng, X., Zhao, L., Zheng, C., Ji, D., Xiong, C., Wang, T., Li, R., Pan, J., Wen, J., Yu, C., Zheng, Y., Jing, L., Chia, L., Lu, H., Yao, P., Ma, J., Lv, H., Wu, J., Zhao, W., Yan, G.N., Guo, P., Li, Y., Hu, L., Geng, D., Zhang, Z., 2020. Soil moisture

experiment in the Luan River supporting new satellite mission opportunities. Remote Sens. Enviorn 240, 111680. https://doi.org/10.1016/j.rse.2020.111680.
Zheng, W., Zhan, X., Liu, J., Ek, M., 2018. A preliminary assessment of the impact of assimilating satellite soil moisture data products on NCEP global forecast system. Adv. Meteorol. https://doi.org/10.1155/2018/7363194.
Zohaib, M., Kim, H., Choi, M., 2017. Evaluating the patterns of spatiotemproal trends of root zone soil moisture in major climate regions in East Asia. J. Geophys. Res-Atmos. 122, 7705–7722. https://doi.org/10.1002/2016JD026379.

4.4 Paper IV: IEEE GRSL - A method for downscaling satellite soil moisture based on land surface temperature and net surface shortwave radiation

A Method for Downscaling Satellite Soil Moisture Based on Land Surface Temperature and Net Surface Shortwave Radiation

Yawei Wang, Pei Leng, *Member, IEEE,* Jianwei Ma, and Jian Peng

***Abstract*— Due to the coarse spatial resolution of currently available microwave (mostly passive) soil moisture (SM) products, it is difficult to apply these SM data in watersheds or at local scales. To this end, a number of downscaling approaches have been developed to improve the spatial resolution of microwave SM products. Specifically, the optical-/thermal-based downscaling methods are most widely used in recent decades. However, such methods normally rely on instantaneous optical/thermal land surface parameters, which are commonly inapplicable under cloudy conditions. The purpose of this study is to develop a new downscaling method based on the temporal variation in geostationary satellite-derived land surface temperature and net surface shortwave radiation. The proposed method has a certain potential to improve data availability under cloudy conditions, because geostationary satellites are capable of providing land surface parameters at high temporal resolution. The proposed method was tested over the REMEDHUS network in Spain. The scaling strategy of cumulative distribution function matching was used to remove systematic differences in spatial mismatch between satellite pixels and *in situ* SM measurements. Results indicate that the downscaled SM agrees well with *in situ* measurements and has comparable accuracy with the original microwave SM product. The overall root mean square errors with the *in situ* measurements for the original microwave SM and the downscaled SM are 0.054 and 0.057 m^3/m^3, respectively. This method not only has a successful attempt to downscale microwave SM data using temporal information but also has the potential to avoid the failure of traditional instantaneous observations-based downscaling procedure due to clouds.**

***Index Terms*— Downscaling, geostationary satellites, land surface temperature (LST), microwave soil moisture (SM), net surface shortwave radiation (NSSR), temporal information.**

Manuscript received May 28, 2020; revised August 14, 2020 and December 3, 2020; accepted February 23, 2021. This work was supported in part by the National Natural Science Foundation of China under Grant 41601397 and Grant 41701431 and in part by the Fundamental Research Funds for Central Nonprofit Scientific Institution under Grant 1610132019012. The work of Yawei Wang was supported by the China Scholarship Council (CSC). *(Corresponding author: Pei Leng.)*

Yawei Wang is with the Department of Geography, Ludwig-Maximilians-University Munich, 80331 Munich, Germany (e-mail: yawei.wang1@gmail.com).

Pei Leng is with the Institute of Agricultural Resources and Regional Planning, Chinese Academy of Agricultural Sciences, Beijing 100081, China (e-mail: lengpei@caas.cn).

Jianwei Ma is with the China Institute of Water Resources and Hydropower Research, Beijing 100038, China (e-mail: majw@iwhr.com).

Jian Peng is with the Department of Remote Sensing, Helmholtz Centre for Environmental Research-UFZ, 04318 Leipzig, Germany, and also with the Remote Sensing Centre for Earth System Research, Leipzig University, 04109 Leipzig, Germany (e-mail: jian.peng@ufz.de).

Color versions of one or more figures in this letter are available at https://doi.org/10.1109/LGRS.2021.3062453.

Digital Object Identifier 10.1109/LGRS.2021.3062453

I. Introduction

SOIL moisture (SM) plays a significant role in hydrology, agriculture, and global climate change [1], [2]. A number of methods have been developed to determine SM and its dynamics with varying spatial and temporal resolutions, including *in situ* observations/networks and satellite retrieval [3], [4]. The remote sensing technology makes it possible to obtain SM at scales ranging from regional to global. Currently, although a number of algorithms have been developed to estimate SM with satellite observations, only microwave sensors can provide operational SM products at coarse spatial resolution of tens of kilometers. However, SM data at the finer spatial resolution of approximately 1–10 km are commonly required in applications at the watershed or local scale [5]–[7]. To this end, various downscaling methods have been proposed to enhance the spatial resolution of currently available microwave SM products [3], [4], [8]. Specifically, the key issue for developing these downscaling methods is to find a statistical correlation or a physically based model between the higher resolution auxiliary variables and coarse-scale SM.

In general, most of the currently available remote sensing downscaling methods can be divided into three major categories. The first category of methods is based on the combination of active and passive microwave data, such as using high spatial resolution backscatter data from an active sensor to downscale the coarse SM product from a passive sensor, or using brightness temperature from a passive sensor in combination with backscatter data. For this category, low temporal coverage of radar imagery and high sensitivity to vegetation cover and surface roughness of microwave observations are the two main drawbacks. The second category is based on optical/thermal remote sensing data, which can provide land surface parameters at higher spatial resolution as auxiliary variables. For this category, several methods such as the polynomial fitting downscaling method, temperature/vegetation index triangular feature space method [9], simpler downscaling method (UCLA) [10], and the disaggregation based on physical and theoretical scale change (DISPATCH) method have been widely used with various optical/thermal observations. However, for this category, nonavailability of optical/thermal observations under cloudy sky, impacts of vegetation cover on the optical/thermal observations, and indirect relationship of optical/thermal observations to SM

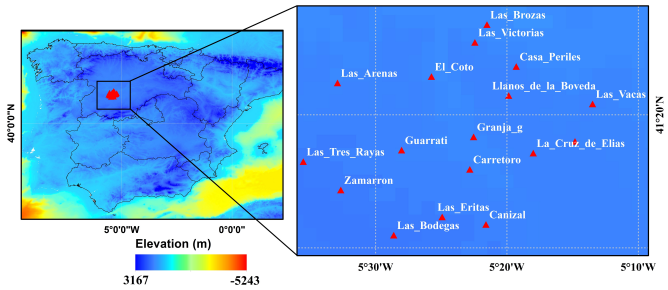

Fig. 1. Location of the REMEDHUS observation network and distribution of SM stations.

variations are the three main shortages. The third category is based on machine/deep learning, which can capture the abstract features of the satellite imageries and learn the potential associations between different observations. Among the various machine/deep learning approaches, artificial neural network, random forests, and support vector machine are the most widely used approaches [4], [11], [12]. Because a large number of data and computation are required for training, machine/deep learning-based downscaling methods are commonly complicated to apply.

The purpose of this study is to develop a new downscaling method based on the temporal variation of geostationary satellite-derived land surface temperature (LST) and net surface shortwave radiation (NSSR) over the midmorning period, which is expected to enhance the temporal coverage of land surface parameters related to SM in the downscaling procedure, since geostationary satellites are capable of providing land surface parameters at much higher frequencies (48–96 times per day). As a result, the multiobservations provided by the geostationary satellites can potentially avoid cases where the traditional instantaneous observation from the polar-orbit satellite is not available. Specifically, this study was motivated by the fact that the rate of change of LST with respect to NSSR over the midmorning period is considered highly sensitive to SM following several previous studies [13], [14].

II. Study Area and Data

A. Study Area

The REMEDHUS network (41–41.5°N and 5.0–5.7°W) was selected as the study area (Fig. 1). REMEDHUS is located in the semiarid parts of the Duero Basin in Spain, which is mainly covered by croplands and shrublands with relatively flat elevation ranging from 700 to 900 m. The climate pattern for the REMEDHUS region is semiarid continental Mediterranean, with dry and warm summers, which cool to mild and wet winters. The average annual temperature is 12 °C, and mean annual rainfall is 385 mm. The REMEDHUS network has been in operation since March 2005 and has been widely used for various applications [9]. In the present study, SM measurements in the top soil layer (0–5 cm) collected at 17 stations during the growing season from April to October 2018 were obtained from the International Soil Moisture Network.

B. MSG Data

In the present study, three land surface parameters derived from Meteosat Second Generation (MSG) data were used to downscale the coarse microwave SM products. Three parameters, namely, LST, land surface albedo, and down-welling surface shortwave radiative flux (DSSF), were obtained from the Land Surface Analysis Satellite Applications Facility. The MSG products used in this study have a spatial resolution of 3 km. Specifically, NSSR was derived from DSSF and land surface albedo and was subsequently used to develop the downscaling method in combination with LST.

C. Microwave SM Product

The climate change initiative (CCI) SM product developed by the European Space Agency, which has a daily time stamp with a spatial resolution of 0.25°, was used in this study. Specifically, the combined active/passive SM product with the latest version (v4.5) from April to October 2018 was used for downscaling [15].

III. Methodology

A. Theoretical Basis of the Proposed Downscaling Method

In an earlier study, based on simulated data from a 1-D boundary layer surface soil model, it was found that the rate of change of LST with respect to absorbed solar radiation over the midmorning period is more highly sensitive to SM than the other physical parameters retrieved from the Geostationary Operational Environmental Satellite [14]. In this study, the effects of SM produced 90% of the total variation in the morning slope of the temperature curve. Later, based on the Noah land surface model and the Gaussian emulation machine for sensitivity analysis, it was found that LST follows a linear relationship to NSSR during the midmorning period. Moreover, the LST rising rate (calculated as the difference in the NSSR during the midmorning period) was the most sensitive parameter to SM, contributing 80.72% to the total SM variance [13]. Following these previous investigations, a downscaling method was developed according to the linear relationship of LST and NSSR in the midmorning period, as follows:

$$\mathrm{LST} = k \times \mathrm{NSSR} + b \tag{1}$$

where k and b are the slope and intercept of the linear relationship between LST and NSSR, respectively. Specifically, LST and NSSR data sets from 8:30 A.M. to 11:00 A.M. were selected for analysis.

To simplify the expression and to facilitate the determination of the linear relationship between temporal LST and NSSR, LST and NSSR were primarily nondimensionalized as follows:

$$\mathrm{LST}_{\mathrm{new}} = \frac{\mathrm{LST} - \mathrm{LST}_{\mathrm{min}}}{\mathrm{LST}_{\mathrm{max}} - \mathrm{LST}_{\mathrm{min}}} \tag{2}$$

$$\mathrm{NSSR}_{\mathrm{new}} = \frac{\mathrm{NSSR} - \mathrm{NSSR}_{\mathrm{min}}}{\mathrm{NSSR}_{\mathrm{max}} - \mathrm{NSSR}_{\mathrm{min}}} \tag{3}$$

where $\mathrm{LST}_{\mathrm{new}}$ and $\mathrm{NSSR}_{\mathrm{new}}$ are the dimensionless LST and NSSR, $\mathrm{LST}_{\mathrm{max}}$ and $\mathrm{LST}_{\mathrm{min}}$ are the maximum and minimum

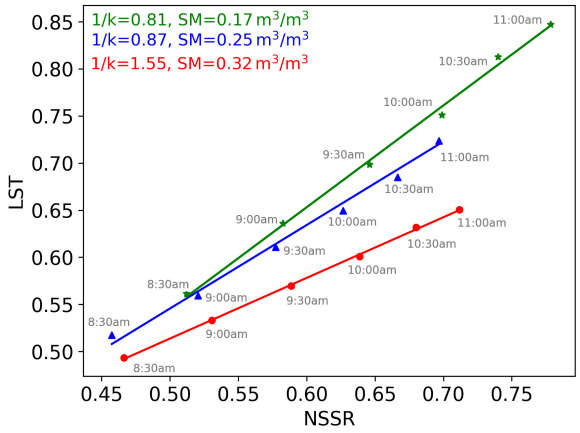

Fig. 2. Illustration of the derivative of slope ($1/k$) of the linear relationship for three sites (with varying SM conditions) between MSG-derived LST and NSSR in the midmorning period from 8:30 A.M. to 11.00 A.M. on July 8, 2018.

LST that can be set as 325 and 275 K, respectively, $\mathrm{NSSR}_{\max}$ and $\mathrm{NSSR}_{\min}$ are the maximum and minimum NSSR that can be set as 1200 and 0 W/m^2, respectively.

Specifically, NSSR was obtained from MSG-derived DSSF and land surface albedo (α) as follows [16]:

$$\mathrm{NSSR} = (1-\alpha) \times \mathrm{DSSF}. \tag{4}$$

Fig. 2 depicts an example of the derivative of slope ($1/k$) derived from MSG data in the midmorning period on July 8, 2018. It is obvious that LST is well correlated with NSSR with a linear form in this period under clear sky conditions. It also demonstrates that the derivative of the slope ($1/k$) of the linear relationship increases with increasing SM. This may be explained by the fact that under the same radiation absorbed by the land surface, due to the effects of soil thermal inertia, a slower increase in LST can be commonly observed when SM content is higher.

To downscale the coarse CCI product, the spatially averaged $1/k$ of MSG pixels within the same CCI pixel ($\overline{1/k}$) is first obtained as follows:

$$\overline{1/k} = \frac{1}{n}\sum_{i=1}^{n}(1/k)_i \tag{5}$$

where n is the number of MSG pixels within a CCI pixel.

For each MSG pixel within a given CCI pixel, the SM at the MSG pixel can be estimated as follows:

$$\theta_{\mathrm{MSG}} = (1/k) \times \frac{\theta_{\mathrm{CCI}}}{\overline{1/k}} \tag{6}$$

where θ_{MSG} is the downscaled SM at the MSG pixel and θ_{CCI} is CCI SM.

B. Simulation Analysis Based on Physically Based Model

Simulated data from the widely used common land model (CoLM) were used to investigate the effects of underlying surfaces on the derivative of slope ($1/k$) and SM [17]. With the required meteorological observations and initialization of underlying surface conditions, the CoLM can produce LST, NSSR, and SM time series following each scenario under a given atmospheric condition. Specifically, 12 soil textures following the classification system of Food and Agriculture Organization and different fraction vegetation cover (FVC) (varying from 0 to 1 with an interval of 0.1) were implemented in the simulation. For each scenario, a unique combination of soil texture, FVC, and SM status was used to represent a possible underlying surface condition. It is noted that for each soil type, the variation in SM is from wilting point to field capacity.

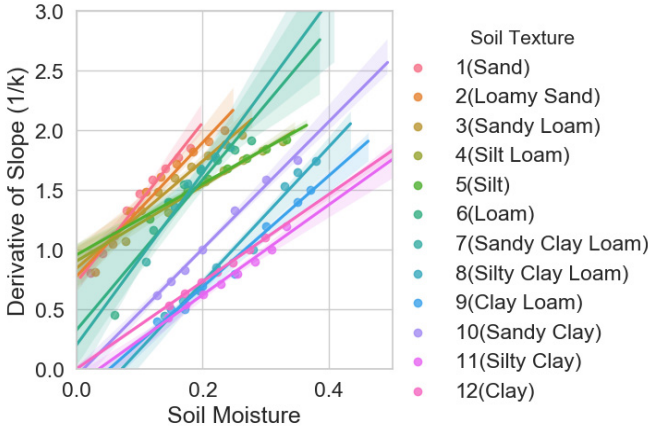

Fig. 3. Relationship between the derivative of slope ($1/k$) and SM for 12 different soil textures with CoLM-simulated data.

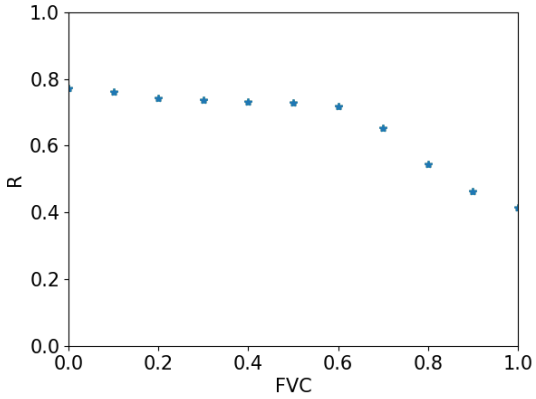

Fig. 4. Correlation coefficient (R) between SM and $1/k$ for all soil textures with different FVC.

Fig. 3 depicts cases over bare soils. It is obvious that SM correlates well with $1/k$ for each soil texture. Moreover, it is also reasonable that mixed bare soils can probably decrease the overall linear relationships between SM and $1/k$. Fig. 4 further depicts the effects of mixed pixels on the relationship between SM and $1/k$. As can be seen from this result, when considering all the soil textures, it is evident that the overall correlation coefficient between SM and $1/k$ generally decreases with the increase in FVC. Specifically, when FVC exceeds 0.6, the correlation coefficient between SM and $1/k$ reveals a dramatical decrease. All these results indicate that the relationship between SM and $1/k$ is generally stable over the regions with relatively low heterogeneity.

IV. Results

A. Spatial Patterns of SM

On the basis of the proposed method, the CCI SM was downscaled to the higher spatial resolution of 3 km during the

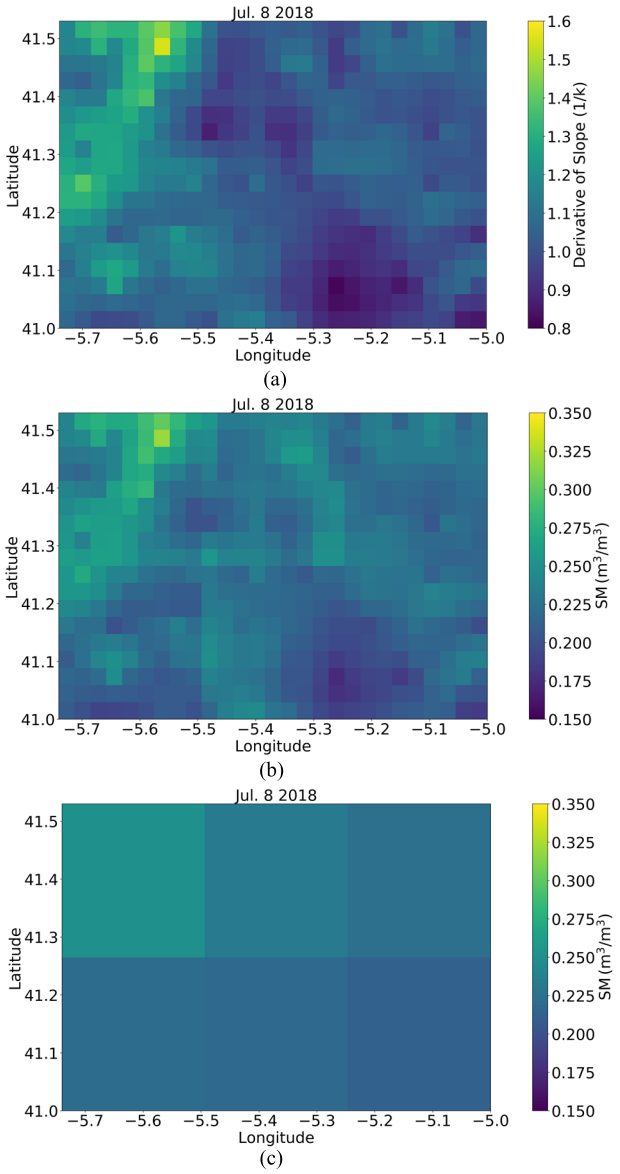

Fig. 5. Distribution of (a) derivative of slope ($1/k$), (b) downscaled SM, and (c) CCI SM, on July 8, 2018.

study period (i.e., from April to October 2018). Fig. 5 depicts the spatial distributions of $1/k$, downscaled SM, and original CCI SM on July 8, 2018. It is obvious that the downscaled SM reveals similar spatial patterns as the original CCI SM. For both the original SM product and the downscaled result, SM in the north shows higher values than in the south. The highest and lowest SM values occur in the northwest and southeast, respectively. These results indicate that the proposed downscaling method can well capture the spatial pattern of the original CCI SM.

B. Validation With in Situ Measurements

As the cumulative distribution function (CDF) matching method has been widely used to remove the systematic differences between satellite imagery and site-specific observations for SM assessments [18], CDF was implemented in this study to eliminate the scale issue before validation. It is evident from Fig. 6 that both CCI SM and downscaled SM agree well with

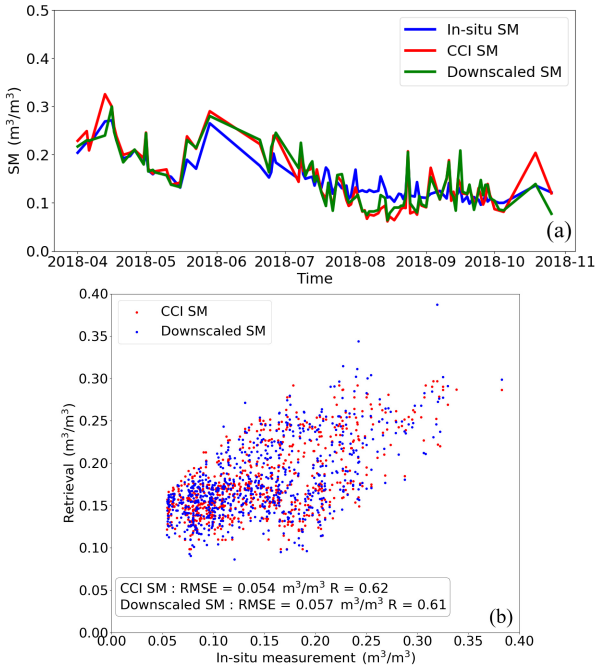

Fig. 6. Comparison of *in situ* SM measurements and satellite SM data. (a) Time series of the CCI SM, downscaled SM, and *in situ* SM at REMEDHUS network scale during the study period, and (b) scatter plots of downscaled SM at MSG pixel versus *in situ* SM measurements, and of CCI SM versus *in situ* measurements.

the *in situ* SM over the study period. The station-averaged CCI SM and downscaled SM have similar trends with the *in situ* measurements [Fig. 6(a)]. As shown in Fig. 6(b), the root mean square errors (RMSEs) with the *in situ* SM measurements are 0.054 and 0.057 m^3/m^3 for CCI SM and downscaled SM, respectively. The correlation coefficient between *in situ* measurements and CCI SM (downscaled SM) is 0.62 (0.61). These results indicate that the downscaling approach can obtain SM at higher spatial resolution with comparable accuracy to the original coarse microwave product.

V. Discussion

The proposed method has comparable accuracy with the published downscaling methods implemented over the REMEDHUS network [8], [9]. However, the present study reveals at least two advantages compared with previous investigations. The primary advantage is that temporal information ($1/k$) derived from land surface parameters, rather than direct land surface parameters (e.g., LST and NSSR), were used to downscale the coarse microwave SM data. It is known that errors normally exist in instantaneous satellite-derived land surface products. For example, an overall RMSE of 1–2 K was reported with the MSG-derived LST product, whereas the moderate-resolution imaging spectroradiometer LST data are commonly recognized to have an RMSE of ~1 K. It is most likely that the errors in the instantaneous satellite-derived land surface parameters can lead to various uncertainties when they are used to downscale microwave SM products. For the proposed approach, the temporal information ($1/k$) can theoretically reduce the effects of errors in the instantaneous

polar-orbit satellite-derived land surface parameters during the downscaling procedure. Another advantage is that more chances can be found in the proposed method, since geostationary satellites can observe the Earth with a fixed angle at much higher frequencies (48–96 times per day) than polar-orbit satellites (1–2 times per day). As shown in Fig. 2, even if optical/thermal infrared observations are unavailable at several times due to the effects of clouds (e.g., around 10:30 A.M. when MODIS transits), the linear relationship can still be determined with MSG observations at other times. Nevertheless, it should be noted that (6) is under the assumption of the constant relation between SM and $1/k$ for all MSG pixels within a CCI pixel. Hence, the proposed method is not recommended for application over the regions where large heterogeneity appears. Moreover, the simulated results have also confirmed that the relationship between SM and $1/k$ is more stable over the regions with low heterogeneity.

VI. Conclusion

In the present study, a new SM downscaling approach was developed from the temporal variation in geostationary satellite-derived LST and NSSR. This approach is developed on the basis of a physical mechanism where a slower LST rising rate can be observed when SM is higher under the same absorbed energy condition. With MSG products, downscaled SM at MSG pixels from the CCI products can well capture the spatial patterns of the original SM data but with better spatial details. A preliminary validation with *in situ* SM measurements implies that the downscaled SM maintains a comparable accuracy, with an RMSE at around 0.057 m^3/m^3 during the growing season from April to October in 2018. Compared to the previous downscaling methods that primarily use instantaneous optical/thermal infrared parameters, the proposed approach shows several advantages, such as the ability to decrease the effects of errors included in the optical/thermal infrared parameters when they are used to downscale microwave SM data. Furthermore, although the proposed method has not been investigated under cloudy or partially cloudy conditions where the traditional polar-orbit satellites-based SM downscaling approaches are probably not available, it has the potential to reduce the effects of clouds, since multiple observations are available from geostationary satellites. Specifically, future studies can focus on this issue to explore SM downscaling with satellite-derived temporal information under specific cloudy conditions.

References

[1] D. R. Legates *et al.*, "Soil moisture: A central and unifying theme in physical geography," *Prog. Phys. Geography, Earth Environ.*, vol. 35, no. 1, pp. 65–86, Feb. 2011.

[2] S. I. Seneviratne *et al.*, "Investigating soil moisture-climate interactions in a changing climate: A review," *Earth-Sci. Rev.*, vol. 99, nos. 3–4, pp. 125–161, 2010.

[3] S. Sabaghy, J. P. Walker, L. J. Renzullo, and T. J. Jackson, "Spatially enhanced passive microwave derived soil moisture: Capabilities and opportunities," *Remote Sens. Environ.*, vol. 209, pp. 551–580, May 2018.

[4] Q. Yuan *et al.*, "Deep learning in environmental remote sensing: Achievements and challenges," *Remote Sens. Environ.*, vol. 241, May 2020, Art. no. 111716.

[5] D. Raynaud, J. Thielen, P. Salamon, P. Burek, S. Anquetin, and L. Alfieri, "A dynamic runoff co-efficient to improve flash flood early warning in Europe: Evaluation on the 2013 central European floods in Germany," *Meteorological Appl.*, vol. 22, no. 3, pp. 410–418, Jul. 2015.

[6] C. M. Taylor *et al.*, "Modeling soil moisture-precipitation feedback in the Sahel: Importance of spatial scale versus convective parameterization," *Geophys. Res. Lett.*, vol. 40, no. 23, pp. 6213–6218, Dec. 2013.

[7] M. Zink *et al.*, "The German drought monitor," *Environ. Res. Lett.*, vol. 11, no. 7, Jul. 2016, Art. no. 074002.

[8] J. Peng, A. Loew, O. Merlin, and N. E. C. Verhoest, "A review of spatial downscaling of satellite remotely sensed soil moisture," *Rev. Geophysics*, vol. 55, no. 2, pp. 341–366, Jun. 2017.

[9] J. Peng, J. Niesel, and A. Loew, "Evaluation of soil moisture downscaling using a simple thermal-based proxy–the REMEDHUS network (Spain) example," *Hydrol. Earth Syst. Sci.*, vol. 19, no. 12, pp. 4765–4782, Dec. 2015.

[10] J. Kim and T. S. Hogue, "Improving spatial soil moisture representation through integration of AMSR-E and MODIS products," *IEEE Trans. Geosci. Remote Sens.*, vol. 50, no. 2, pp. 446–460, Feb. 2012.

[11] P. K. Srivastava, D. Han, M. R. Ramirez, and T. Islam, "Machine learning techniques for downscaling SMOS satellite soil moisture using MODIS land surface temperature for hydrological application," *Water Resour. Manage.*, vol. 27, no. 8, pp. 3127–3144, Jun. 2013.

[12] Y. Liu, Y. Yang, W. Jing, and X. Yue, "Comparison of different machine learning approaches for monthly satellite-based soil moisture downscaling over northeast China," *Remote Sens.*, vol. 10, no. 2, p. 31, Dec. 2017.

[13] W. Zhao and Z.-L. Li, "Sensitivity study of soil moisture on the temporal evolution of surface temperature over bare surfaces," *Int. J. Remote Sens.*, vol. 34, nos. 9–10, pp. 3314–3331, May 2013.

[14] P. J. Wetzel, D. Atlas, and R. H. Woodward, "Determining soil moisture from geosynchronous satellite infrared data: A feasibility study," *J. Climate Appl. Meteorol.*, vol. 23, no. 3, pp. 375–391, Mar. 1984.

[15] A. Gruber, T. Scanlon, R. van der Schalie, W. Wagner, and W. Dorigo, "Evolution of the ESA CCI soil moisture climate data records and their underlying merging methodology," *Earth Syst. Sci. Data*, vol. 11, no. 2, pp. 717–739, May 2019.

[16] R. T. Pinker, R. Frouin, and Z. Li, "A review of satellite methods to derive surface shortwave irradiance," *Remote Sens. Environ.*, vol. 51, no. 1, pp. 108–124, Jan. 1995.

[17] Y. Dai *et al.*, "The common land model," *Bull. Amer. Meteorol. Soc.*, vol. 84, pp. 1013–1024, Aug. 2003.

[18] L. Brocca *et al.*, "Soil moisture estimation through ASCAT and AMSR-E sensors: An intercomparison and validation study across Europe," *Remote Sens. Environ.*, vol. 115, no. 12, pp. 3390–3408, Dec. 2011.

5. Conclusion

This thesis focused on the exploitation of geostationary satellite data for monitoring SM. The contributions of this thesis are presented in the following conclusions according to the research questions outlined in section 3.1.

Q1: Is it possible to propose an optical/thermal infrared-based SM retrieval method (or downscaling method) which can be applied to cloudy days?

Most optical/thermal-based methods rely on instantaneous optical/thermal land surface parameters (e.g. a single daily, maximum or minimum thermal data). These methods are inapplicable to the regions covered by clouds at the overpass time of satellites. However, only five sets of LST and NSSR in the daytime and two sets in the mid-morning period are required for the ellipse model and downscaling method, separately. Therefore, two methods in this thesis using the temporal information provided by geostationary satellite can break the cloud-free day limits.

Q2: Can the drawbacks of traditional optical/thermal infrared-based SM retrieval methods to estimate SM directly instead of SM-related indices be overcome by a novel retrieval approach?

In Figure 8, the elliptical relationship between the diurnal cycles of LST and NSSR has been proposed by four ellipse parameters, namely the ellipse center horizontal and vertical coordinate (x_0 and y_0), semi-major axis (a) and rotation angle (θ). As shown in Figure 9, the ellipse varies with different SM in a specific soil texture. Similarly, each ellipse is fitted with different soil textures for the same SM in Figure 10. Thus, the ellipse parameters are most likely capable of determining SM for various soil types under given atmospheric conditions. According to the diurnal cycles of LST and NSSR, the SM can be estimated based on an individual ellipse for each pixel. Therefore, the ellipse model can directly estimate quantitative volumetric SM without establishing empirical relationships between in-situ SM measurements and satellite-derived proxies of SM, which is independent of soil texture and ground-based measurements.

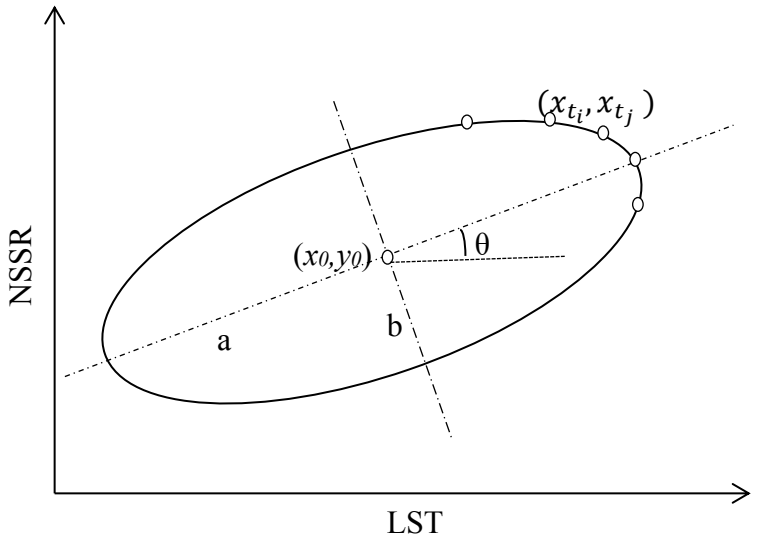

Figure 8. Sketches of the elliptical relationship between the diurnal cycles of LST and NSSR; x_0, y_0, a and θ are the ellipse parameters of the elliptical relationship between diurnal LST and NSSR cycles, which respectively represent the ellipse center horizontal and vertical coordinate, semi-major axis, semi-minor axis and rotation angle; x_{ti} and y_{ti} are LST and NSSR at five different time (i=0,1,2,3,4).

Additionally, the ellipse parameters describe the physical processes and states. The value of x_0 or y_0 positively correlates with the mean LST or NSSR. a and semi-minor axis (b) describe the diurnal variation of LST and NSSR. If the ratio of a and b is larger, the ellipse will be flatter, which indicates the rate of change of LST with respect to NSSR becomes slower. In the same soil texture, volumetric heat capacity increases with increased SM content, and thereby slowing down the diurnal variation of LST. At the same time, due to the increased SM, a smaller soil reflectance makes NSSR larger. This results in the bigger θ. Therefore, θ can directly represent different SM under the same soil texture conditions as shown in Figure 9.

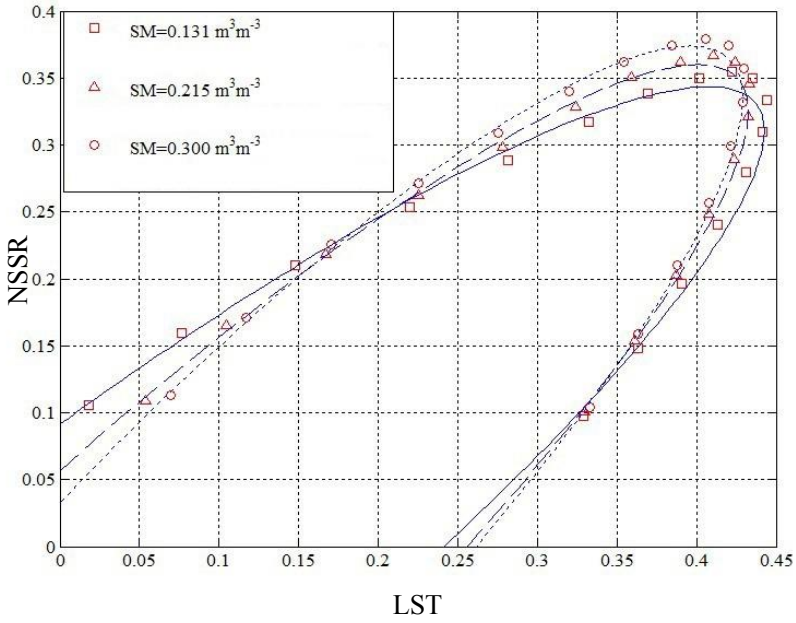

Figure 9. Ellipse fitting with diurnal cycles of non-dimensional LST and NSSR for clay soil

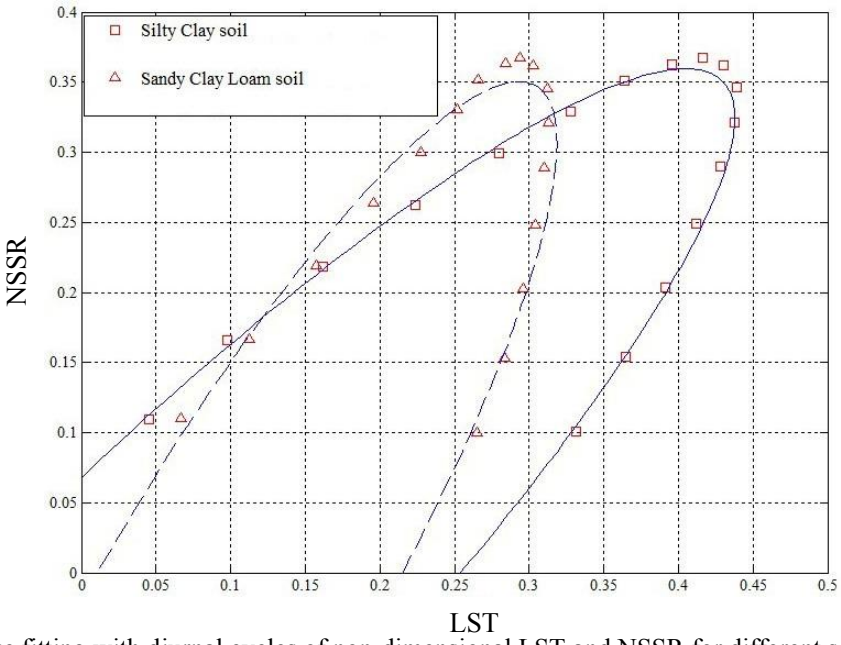

Figure 10. Ellipse fitting with diurnal cycles of non-dimensional LST and NSSR for different soil textures but same SM

Q3: Among all remote sensing SM products, blended CCI and SMOPS global SM products have either better temporal or better spatial coverage than those derived from a single sensor. Which one is more suitable for application? Can these two blended SM products synergize with each other in the application?

Based upon the results from both in-situ SM measurements and reanalysis SM data, CCI is recommended when both CCI and SMOPS are available, since CCI generally has better errors statistics compared to SMOPS across most of the regions worldwide. Specifically, CCI is prioritized in all equatorial climate, several arid climates, most of the warm temperate climate, and some continental climate regions. The primary reason is the enhanced quality control of the CCI SM product. For instance, the stricter TC analysis based error characterization guaranteed the quality of the CCI SM product. In contrast, SMOPS only performs better under three continental climate regions covering 0.6% of the global regions. It might due to the fact that CCI (v4.5 version) merged data from only one or two sensors over these continental climate regions, while SMOPS merged more available sensors including SMAP and GPM Microwave Imager. Compared to the daily CCI data, SMOPS can provide both daily and 6 hourly interval data. Additionally, considering the better spatial coverage of SMOPS, it can provide SM estimates with comparable accuracy over the gaps remaining by CCI. Hence, it is concluded that the two blended SM products have the potential to complement each other for a variety of applications.

Q4: Currently most microwave SM products are at coarse spatial resolution of tens of kilometers. How to improve their spatial resolution to meet the criteria of the applications at the regional or local scale?

A number of downscaling approaches have been developed to improve the spatial resolution of microwave SM products. Specifically, the optical/thermal-based downscaling methods are most widely used in recent decades. However, such methods normally rely on instantaneous optical/thermal land surface parameters, which are commonly inapplicable under cloudy conditions. The proposed method in paper IV is developed based on the temporal variation of geostationary satellite-derived LST and NSSR. A linear relationship between LST and NSSR in the mid-morning period has been found in Figure 11, which also demonstrated that the derivative of the slope (1/k) of the linear relationship increased with increasing SM. This may be explained by the fact that under the same radiation absorbed by the land surface, due to the effects of soil thermal inertia, a slower increase of LST can be commonly observed when SM content is higher. This is the theoretical foundation, which supports to disaggregate 25 km CCI SM product to 3 km.

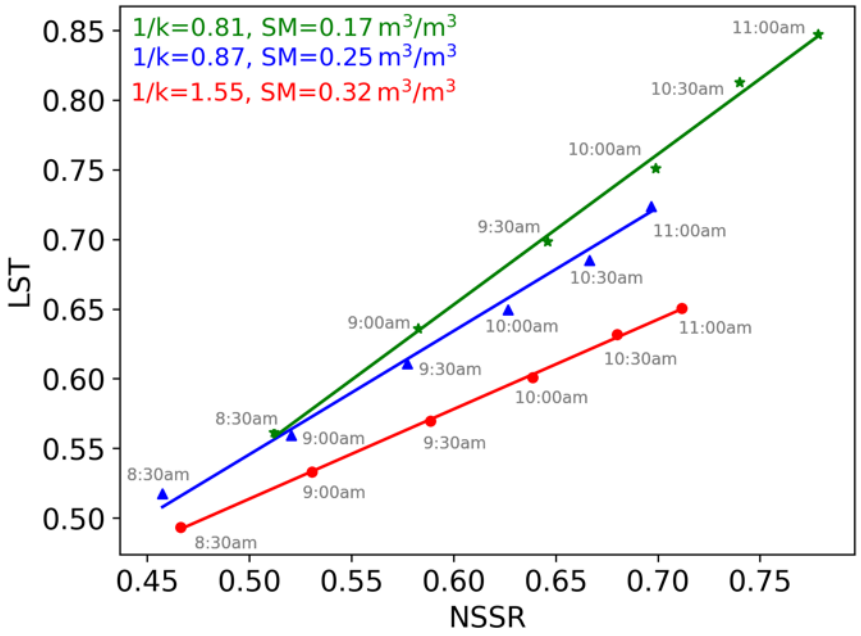

Figure 11. Illustration of the derivative of slope ($1/k$) of the linear relationship for three sites (with varying SM conditions) between MSG derived-LST and NSSR in the mid-morning period from 8:30 a.m. to 11.00 a.m. on July 8, 2018.

Overall, the most promising development in SM retrieval using Earth observation data is possibly the progress in synergistic approaches, in which two or more Earth observation datasets with different imaging characteristics are exploited. In the future, two topics should be addressed. First, the downscaling method only works in the lower vegetated regions with low heterogeneous of land cover and topography. Therefore, how to improve the transferability over heterogeneous areas should be further explored. Second, optical/thermal data have a limited surface penetration depth, high perturbation of the signal by clouds and signal attenuation by the earth's atmosphere. Although microwave emissions can penetrate clouds and rain to provide continuous SM, the microwave-based SM products have some limitations as mentioned before. Even though several methods based on the synergistic use of optical/thermal and microwave data have already been developed, no practical approach has been proposed to estimate SM directly from satellite observations at fine spatial resolution in cloudy days. Therefore, a new method suitable in all-weather based on optical/thermal infrared data and microwave data is great interest for future research.

6. Bibliography

Adegoke, J.O., Carleton, A.M., 2002. Relations between soil moisture and satellite vegetation indices in the US Corn Belt. Journal of hydrometeorology 3, 395–405.

Ångström, A., 1925. The albedo of various surfaces of ground. Geografiska Annaler 7, 323–342.

Arthur-Hartranft, S.T., Carlson, T.N., Clarke, K.C., 2003. Satellite and ground-based microclimate and hydrologic analyses coupled with a regional urban growth model. Remote Sensing of Environment 86, 385–400.

Attema, E.P.W., Ulaby, F.T., 1978. Vegetation modeled as a water cloud. Radio science 13, 357–364.

Baghdadi, N., King, C., Chanzy, A., Wigneron, J.-P., 2002. An empirical calibration of the integral equation model based on SAR data, soil moisture and surface roughness measurement over bare soils. International Journal of Remote Sensing 23, 4325–4340.

Baghdadi, N., Saba, E., Aubert, M., Zribi, M., Baup, F., 2011. Evaluation of radar backscattering models IEM, Oh, and Dubois for SAR data in X-band over bare soils. IEEE Geoscience and Remote Sensing Letters 8, 1160–1164.

Baghdadi, N., Zribi, M., 2006. Evaluation of radar backscatter models IEM, OH and Dubois using experimental observations. International Journal of Remote Sensing 27, 3831–3852. https://doi.org/10.1080/01431160600658123

Baghdadi, N., Zribi, M., Loumagne, C., Ansart, P., Anguela, T.P., 2008. Analysis of TerraSAR-X data and their sensitivity to soil surface parameters over bare agricultural fields. Remote sensing of environment 112, 4370–4379.

Balenzano, A., Mattia, F., Satalino, G., Davidson, M.W.J., 2011. Dense Temporal Series of C- and L-band SAR Data for Soil Moisture Retrieval Over Agricultural Crops. IEEE Journal of Selected Topics in Applied Earth Observations and Remote Sensing 4, 439–450. https://doi.org/10.1109/JSTARS.2010.2052916

Berg, A., Sheffield, J., 2018. Soil Moisture–Evapotranspiration Coupling in CMIP5 Models: Relationship with Simulated Climate and Projections. Journal of Climate 31, 4865–4878. https://doi.org/10.1175/JCLI-D-17-0757.1

Bindlish, R., Barros, A.P., 2000. Multifrequency Soil Moisture Inversion from SAR Measurements with the Use of IEM. Remote Sensing of Environment 71, 67–88. https://doi.org/10.1016/S0034-4257(99)00065-6

Bindlish, R., Jackson, T.J., Wood, E., Gao, H., Starks, P., Bosch, D., Lakshmi, V., 2003. Soil moisture estimates from TRMM Microwave Imager observations over the Southern United States. Remote Sensing of Environment 85, 507–515. https://doi.org/10.1016/S0034-4257(03)00052-X

Bowers, S.A., Hanks, R.J., 1971. Reflection of radiant energy from soils (PhD Thesis). Kansas State University.

Brocca, L., Ciabatta, L., Massari, C., Camici, S., Tarpanelli, A., 2017. Soil moisture for hydrological applications: open questions and new opportunities. Water 9, 140.

Brocca, L., Melone, F., Moramarco, T., Wagner, W., Naeimi, V., Bartalis, Z., Hasenauer, S., 2010. Improving runoff prediction through the assimilation of the ASCAT soil moisture product. Hydrology and Earth System Sciences 14, 1881–1893.

Calvet, J.-C., Wigneron, J.-P., Chanzy, A., Haboudane, D., 1995. Retrieval of surface parameters from microwave radiometry over open canopies at high frequencies. Remote sensing of environment 53, 46–60.

Capehart, W.J., Carlson, T.N., 1997. Decoupling of surface and near-surface soil water content: A remote sensing perspective. Water Resources Research 33, 1383–1395.

Capehart, W.J., Carlson, T.N., 1994. Estimating near-surface soil moisture availability using a meteorologically driven soil-water profile model. Journal of hydrology 160, 1–20.

Carlson, T., 2007. An overview of the" triangle method" for estimating surface evapotranspiration and soil moisture from satellite imagery. Sensors 7, 1612–1629.

Carlson, T.N., Arthur, S.T., 2000. The impact of land use—land cover changes due to urbanization on surface microclimate and hydrology: a satellite perspective. Global and planetary change 25, 49–65.

Carlson, T.N., Buffum, M.J., 1989. On estimating total daily evapotranspiration from remote surface temperature measurements. Remote Sensing of Environment 29, 197–207.

Carlson, T.N., Gillies, R.R., Schmugge, T.J., 1995. An interpretation of methodologies for indirect measurement of soil water content. Agricultural and forest meteorology 77, 191–205.

Carlson, T.N., Perry, E.M., Schmugge, T.J., 1990. Remote estimation of soil moisture availability and fractional vegetation cover for agricultural fields.

Carlson, T.N., Ripley, D.A., 1997. On the relation between NDVI, fractional vegetation cover, and leaf area index. Remote sensing of Environment 62, 241–252.

Chan, S.K., Bindlish, R., O'Neill, P.E., Njoku, E., Jackson, T., Colliander, A., Chen, F., Burgin, M., Dunbar, S., Piepmeier, J., 2016. Assessment of the SMAP passive soil moisture product. IEEE Transactions on Geoscience and Remote Sensing 54, 4994–5007.

Chauhan, N.S., Miller, S., Ardanuy, P., 2003. Spaceborne soil moisture estimation at high resolution: a microwave-optical/IR synergistic approach. International Journal of Remote Sensing 24, 4599–4622.

Chen, F., Crow, W.T., Starks, P.J., Moriasi, D.N., 2011. Improving hydrologic predictions of a catchment model via assimilation of surface soil moisture. Advances in Water Resources 34, 526–536.

Cohen, Y., Alchanatis, V., Meron, M., Saranga, Y., Tsipris, J., 2005. Estimation of leaf water potential by thermal imagery and spatial analysis. Journal of experimental botany 56, 1843–52. https://doi.org/10.1093/jxb/eri174

Colaizzi, P.D., Barnes, E.M., Clarke, T.R., Choi, C.Y., Waller, P.M., 2003. Estimating soil moisture under low frequency surface irrigation using crop water stress index. Journal of irrigation and drainage engineering 129, 27–35.

Das, N.N., 2019. SMAP-Sentinel L2 Radar/Radiometer Soil Moisture (Active/Passive) Data Products: L2_SM_SP 62.

Das, N.N., Entekhabi, D., Dunbar, R.S., Chaubell, M.J., Colliander, A., Yueh, S., Jagdhuber, T., Chen, F., Crow, W., O'Neill, P.E., Walker, J.P., Berg, A., Bosch, D.D., Caldwell, T., Cosh, M.H., Collins, C.H., Lopez-Baeza, E., Thibeault, M., 2019. The SMAP and Copernicus Sentinel 1A/B microwave active-passive high resolution surface soil moisture product. Remote Sensing of Environment 233, 111380. https://doi.org/10.1016/j.rse.2019.111380

Das, N.N., Entekhabi, D., Njoku, E.G., Shi, J.J.C., Johnson, J.T., Colliander, A., 2014. Tests of the SMAP Combined Radar and Radiometer Algorithm Using Airborne Field Campaign Observations and Simulated Data. IEEE Transactions on Geoscience and Remote Sensing 52, 2018–2028. https://doi.org/10.1109/TGRS.2013.2257605

de Jeu, R.A., Holmes, T.R., Parinussa, R.M., Owe, M., 2014. A spatially coherent global soil moisture product with improved temporal resolution. Journal of Hydrology 516, 284–296.

Dorigo, W.A., Gruber, A., De Jeu, R.A.M., Wagner, W., Stacke, T., Loew, A., Albergel, C., Brocca, L., Chung, D., Parinussa, R.M., 2015. Evaluation of the ESA CCI soil moisture product using ground-based observations. Remote Sensing of Environment 162, 380–395.

Dubois, P.C., Van Zyl, J., Engman, T., 1995. Measuring soil moisture with imaging radars. IEEE transactions on geoscience and remote sensing 33, 915–926.

Engman, E.T., 1994. The potential of SAR in hydrology, in: Proceedings of IGARSS'94-1994 IEEE International Geoscience and Remote Sensing Symposium. IEEE, pp. 283–285.

Engman, E.T., 1991. Applications of microwave remote sensing of soil moisture for water resources and agriculture. Remote Sensing of Environment 35, 213–226. https://doi.org/10.1016/0034-4257(91)90013-V

Entekhabi, D., Njoku, E.G., O'Neill, P.E., Kellogg, K.H., Crow, W.T., Edelstein, W.N., Entin, J.K., Goodman, S.D., Jackson, T.J., Johnson, J., 2010. The soil moisture active passive (SMAP) mission. Proceedings of the IEEE 98, 704–716.

Entekhabi, D., Yueh, S., De Lannoy, G., 2014. SMAP handbook.

Fang, B., Lakshmi, V., Bindlish, R., Jackson, T.J., Cosh, M., Basara, J., 2013. Passive Microwave Soil Moisture Downscaling Using Vegetation Index and Skin Surface Temperature. Vadose Zone Journal 12, vzj2013.05.0089. https://doi.org/10.2136/vzj2013.05.0089

Foucras, M., Zribi, M., Albergel, C., Baghdadi, N., Calvet, J.-C., Pellarin, T., 2020. Estimating 500-m Resolution Soil Moisture Using Sentinel-1 and Optical Data Synergy. Water 12, 866. https://doi.org/10.3390/w12030866

Fung, A.K., Li, Z., Chen, K.S., 1992. Backscattering from a Randomly Rough Dielectric Surface. IEEE Transactions on Geoscience and Remote Sensing 30, 356–369. https://doi.org/10.1109/36.134085

Gao, H., Wood, E.F., Drusch, M., Crow, W., Jackson, T.J., 2004. Using a microwave emission model to estimate soil moisture from ESTAR observations during SGP99. Journal of Hydrometeorology 5, 49–63.

Gao, Z., Xu, X., Wang, J., Yang, H., Huang, W., Feng, H., 2013. A method of estimating soil moisture based on the linear decomposition of mixture pixels. Mathematical and Computer Modelling 58, 606–613.

Gao, Q., Zribi, M., Escorihuela, M.J., Baghdadi, N., 2017. Synergetic Use of Sentinel-1 and Sentinel-2 Data for Soil Moisture Mapping at 100 m Resolution. Sensors 17, 1966. https://doi.org/10.3390/s17091966

Gillies, R.R., Carlson, T.N., 1995. Thermal remote sensing of surface soil water content with partial vegetation cover for incorporation into climate models. Journal of Applied Meteorology 34, 745–756.

Gillies, R.R., Kustas, W.P., Humes, K.S., 1997. A verification of the'triangle'method for obtaining surface soil water content and energy fluxes from remote measurements of the Normalized Difference Vegetation Index (NDVI) and surface e. International journal of remote sensing 18, 3145–3166.

Girardin, M.P., Wotton, B.M., 2009. Summer Moisture and Wildfire Risks across Canada. Journal of Applied Meteorology and Climatology 48, 517–533. https://doi.org/10.1175/2008JAMC1996.1

Gloersen, P., Cavalieri, D., Wilheit, T., Chang, A., Campbell, W., Johannessen, O., Katsaros, K., Kunzi, K., Ross, D., Staelin, D., 1984. A summary of results from the first NIMBUS 7 SMMR observations. Journal of Geophysical Research 89. https://doi.org/10.1029/JD089iD04p05335

Godt, J.W., Baum, R.L., Chleborad, A.F., 2006. Rainfall characteristics for shallow landsliding in Seattle, Washington, USA. Earth Surface Processes and Landforms: The Journal of the British Geomorphological Research Group 31, 97–110.

Goward, S.N., Cruickshanks, G.D., Hope, A.S., 1985. Observed relation between thermal emission and reflected spectral radiance of a complex vegetated landscape. Remote Sensing of Environment 18, 137–146.

Gruber, A., Scanlon, T., van der Schalie, R., Wagner, W., Dorigo, W., 2019. Evolution of the ESA CCI Soil Moisture climate data records and their underlying merging methodology. Earth System Science Data 1–37.

He, L., Qin, Q., Panciera, R., Tanase, M., Walker, J.P., Hong, Y., 2017. An Extension of the Alpha Approximation Method for Soil Moisture Estimation Using Time-Series SAR Data Over Bare Soil Surfaces. IEEE Geoscience and Remote Sensing Letters 14, 1328–1332. https://doi.org/10.1109/LGRS.2017.2711006

Hollmann, R., Merchant, C.J., Saunders, R., Downy, C., Buchwitz, M., Cazenave, A., Chuvieco, E., Defourny, P., de Leeuw, G., Forsberg, R., 2013. The ESA climate change initiative: Satellite data records for essential climate variables. Bulletin of the American Meteorological Society 94, 1541–1552.

Idso, S.B., Schmugge, T.J., Jackson, R.D., Reginato, R.J., 1975. The utility of surface temperature measurements for the remote sensing of surface soil water status. Journal of Geophysical Research 80, 3044–3049.

Imaoka, K., Kachi, M., Kasahara, M., Ito, N., Nakagawa, K., Oki, T., 2010. Instrument performance and calibration of AMSR-E and AMSR2. International Archives of the Photogrammetry, Remote Sensing and Spatial Information Science 38, 13–18.

Jackson, T.J., 1997. Soil moisture estimation using special satellite microwave/imager satellite data over a grassland region. Water resources research 33, 1475–1484.

Jackson, T.J., Chang, A., Schmugge, T.J., 1981. Aircraft active microwave measurements for estimating soil moisture. Photogrammetric Engineering and Remote Sensing 47, 801–805.

Jackson, T.J., Schmugge, T.J., 1989. Passive microwave remote sensing system for soil moisture: Some supporting research. IEEE Transactions on Geoscience and Remote Sensing 27, 225–235.

Jaeger, J.C., 1953. Conduction of heat in a solid with periodic boundary conditions, with an application to the surface temperature of the moon. Mathematical Proceedings of the Cambridge Philosophical Society 49, 355–359. https://doi.org/10.1017/S0305004100028450

Karthikeyan, L., Pan, M., Wanders, N., Kumar, D.N., Wood, E.F., 2017. Four decades of microwave satellite soil moisture observations: Part 1. A review of retrieval algorithms. Advances in water resources 109, 106–120.

Kelly, R.E.J., Davie, T.J.A., Atkinson, P.M., 2003. Explaining temporal and spatial variation in soil moisture in a bare field using SAR imagery. International Journal of Remote Sensing 24, 3059–3074.

Kim, H., Lee, S., Cosh, M.H., Lakshmi, V., Kwon, Y., McCarty, G.W., 2020. Assessment and Combination of SMAP and Sentinel-1A/B-Derived Soil Moisture Estimates With Land Surface Model Outputs in the Mid-Atlantic Coastal Plain, USA. IEEE Transactions on Geoscience and Remote Sensing 1–21. https://doi.org/10.1109/TGRS.2020.2991665

Kim, J., Hogue, T.S., 2012. Improving Spatial Soil Moisture Representation Through Integration of AMSR-E and MODIS Products. IEEE Transactions on Geoscience and Remote Sensing 50, 446–460. https://doi.org/10.1109/TGRS.2011.2161318

Kurucu, Y., Balik Sanli, F., Esetlili, M., Bolca, M., Göksel, Ç., 2009. Contribution of SAR images to determination of surface moisture on the Menemen Plain, Turkey. International Journal of Remote Sensing - INT J REMOTE SENS 30, 1805–1817. https://doi.org/10.1080/01431160802639764

Lakshmi, V., 2013. Remote sensing of soil moisture. ISRN Soil Science 2013.

Lakshmi, V., Jackson, T.J., Zehrfuhs, D., 2003. Soil moisture–temperature relationships: results from two field experiments. Hydrological Processes 17, 3041–3057. https://doi.org/10.1002/hyp.1275

Lawston, P. M., Santanello Jr, J. A., & Kumar, S. V. 2017). Irrigation signals detected from SMAP soil moisture retrievals. Geophysical Research Letters, 44(23), 11-860.

Lee, K.-H., Anagnostou, E.N., 2004. A combined passive/active microwave remote sensing approach for surface variable retrieval using Tropical Rainfall Measuring Mission observations. Remote Sensing of Environment 92, 112–125. https://doi.org/10.1016/j.rse.2004.05.003

Li, B., Rodell, M., 2013. Spatial variability and its scale dependency of observed and modeled soil moisture over different climate regions. Hydrology & Earth System Sciences 17.

Lindell, D.B., Long, D.G., 2016. High-Resolution Soil Moisture Retrieval With ASCAT. IEEE Geosci. Remote Sensing Lett. 13, 972–976. https://doi.org/10.1109/LGRS.2016.2557321

Liu, W., Baret, F., Xingfa, G., Qingxi, T., Lanfen, Z., Bing, Z., 2002. Relating soil surface moisture to reflectance. Remote sensing of environment 81, 238–246.

Liu, Y.Y., Dorigo, W.A., Parinussa, R.M., de Jeu, R.A.M., Wagner, W., McCabe, M.F., Evans, J.P., van Dijk, A.I.J.M., 2012. Trend-preserving blending of passive and active microwave soil moisture retrievals. Remote Sensing of Environment 123, 280–297. https://doi.org/10.1016/j.rse.2012.03.014

Liu, Z., Zhao, Y., 2006. Research on the method for retrieving soil moisture using thermal inertia model. SCI CHINA SER D 49, 539–545. https://doi.org/10.1007/s11430-006-0539-6

Lobell, D.B., Asner, G.P., 2002. Moisture effects on soil reflectance. Soil Science Society of America Journal 66, 722–727.

Macdonald, H.C., Waite, W.P., 1971. Soil Moisture Detection with Imaging Radars. Water Resources Research 7, 100–110. https://doi.org/10.1029/WR007i001p00100

Massari, C., Brocca, L., Moramarco, T., Tramblay, Y., Lescot, J.-F.D., 2014. Potential of soil moisture observations in flood modelling: Estimating initial conditions and correcting rainfall. Advances in Water Resources 74, 44–53.

McVicar, T.R., Jupp, D.L.B., 1998. The current and potential operational uses of remote sensing to aid decisions on drought exceptional circumstances in Australia: a review. Agricultural Systems 57, 399–468.

Merlin, O., Chehbouni, A., Walker, J.P., Panciera, R., Kerr, Y.H., 2008. A Simple Method to Disaggregate Passive Microwave-Based Soil Moisture. IEEE Trans. Geosci. Remote Sensing 46, 786–796. https://doi.org/10.1109/TGRS.2007.914807

Minacapilli, M., Iovino, M., Blanda, F., 2009. High resolution remote estimation of soil surface water content by a thermal inertia approach. Journal of hydrology 379, 229–238.

Mladenova, I.E., Jackson, T.J., Njoku, E., Bindlish, R., Chan, S., Cosh, M.H., Holmes, T.R.H., De Jeu, R.A.M., Jones, L., Kimball, J., 2014. Remote monitoring of soil moisture using passive microwave-based techniques—Theoretical basis and overview of selected algorithms for AMSR-E. Remote sensing of environment 144, 197–213.

Molero, B., Merlin, O., Malbéteau, Y., Al Bitar, A., Cabot, F., Stefan, V., Kerr, Y., Bacon, S., Cosh, M.H., Bindlish, R., 2016. SMOS disaggregated soil moisture product at 1 km resolution: Processor overview and first validation results. Remote Sensing of Environment 180, 361–376.

Montosi, E., Manzoni, S., Porporato, A., Montanari, A., 2012. An ecohydrological model of malaria outbreaks. Hydrology and Earth System Sciences 16, 2759.

Moran, M.S., Clarke, T.R., Inoue, Y., Vidal, A., 1994. Estimating crop water deficit using the relation between surface-air temperature and spectral vegetation index. Remote sensing of environment 49, 246–263.

Moran, M.S., Peters-Lidard, C.D., Watts, J.M., McElroy, S., 2004. Estimating soil moisture at the watershed scale with satellite-based radar and land surface models. Canadian journal of remote sensing 30, 805–826.

Moran, M.S., Rahman, A.F., Washburne, J.C., Goodrich, D.C., Weltz, M.A., Kustas, W.P., 1996. Combining the Penman-Monteith equation with measurements of surface temperature and reflectance to estimate evaporation rates of semiarid grassland. Agricultural and forest Meteorology 80, 87–109.

Moran, M.S., Vidal, A., Troufleau, D., Qi, J., Clarke, T.R., Pinter, P.J., Mitchell, T.A., Inoue, Y., Neale, C.M.U., 1997. Combining multifrequency microwave and optical data for crop management. Remote Sensing of Environment 61, 96–109. https://doi.org/10.1016/S0034-4257(96)00243-X

Myneni, R.B., Williams, D.L., 1994. On the relationship between FAPAR and NDVI. Remote Sensing of Environment 49, 200–211.

Narayanan, R.M., Horner, J.R., Germain, K.M.S., 1999. Simulation Study of a Robust Algorithm for Soil Moisture and Surface Roughness Estimation Using L-Band Radar Backscatter. Geocarto International 14, 6–13. https://doi.org/10.1080/10106049908542088

Narvekar, P.S., Entekhabi, D., Kim, S.-B., Njoku, E.G., 2015. Soil Moisture Retrieval Using L-Band Radar Observations. IEEE Transactions on Geoscience and Remote Sensing 53, 3492–3506. https://doi.org/10.1109/TGRS.2014.2377714

Njoku, E.G., Entekhabi, D., 1996. Passive microwave remote sensing of soil moisture. Journal of hydrology 184, 101–129.

Njoku, E.G., Li, L., 1999. Retrieval of land surface parameters using passive microwave measurements at 6-18 GHz. IEEE Transactions on Geoscience and Remote Sensing 37, 79–93.

Njoku, E.G., Wilson, W.J., Yueh, S.H., Dinardo, S.J., Li, F.K., Jackson, T.J., Lakshmi, V., Bolten, J., 2002. Observations of soil moisture using a passive and active low-frequency microwave airborne sensor during SGP99. IEEE Transactions on Geoscience and Remote Sensing 40, 2659–2673. https://doi.org/10.1109/TGRS.2002.807008

Njoku, E.G., Wilson, W.J., Yueh, S.H., Rahmat-Samii, Y., 2000. A large-antenna microwave radiometer-scatterometer concept for ocean salinity and soil moisture sensing. IEEE Transactions on Geoscience and Remote Sensing 38, 2645–2655.

Oh, Y., Sarabandi, K., Ulaby, F.T., 2002. Semi-empirical model of the ensemble-averaged differential Mueller matrix for microwave backscattering from bare soil surfaces. IEEE Transactions on Geoscience and Remote Sensing 40, 1348–1355.

Oh, Y., Sarabandi, K., Ulaby, F.T., 1992. An empirical model and an inversion technique for radar scattering from bare soil surfaces. IEEE transactions on Geoscience and Remote Sensing 30, 370–381.

Oki, T., Kanae, S., 2006. Global hydrological cycles and world water resources. science 313, 1068–1072.

Owe, M., de Jeu, R., Holmes, T., 2008. Multisensor historical climatology of satellite-derived global land surface moisture. Journal of Geophysical Research: Earth Surface 113.

Owe, M., de Jeu, R., Walker, J., 2001. A methodology for surface soil moisture and vegetation optical depth retrieval using the microwave polarization difference index. IEEE Transactions on Geoscience and Remote Sensing 39, 1643–1654.

Paloscia, S., Macelloni, G., Santi, E., Koike, T., 2001. A multifrequency algorithm for the retrieval of soil moisture on a large scale using microwave data from SMMR and SSM/I satellites. Geoscience and Remote Sensing, IEEE Transactions on 39, 1655–1661. https://doi.org/10.1109/36.942543

Paloscia, S., Pampaloni, P., Pettinato, S., Poggi, P., Santi, E., 2005. The retrieval of soil moisture from ENVISAT/ASAR data. EARSeL eProceedings 4, 44–51.

Pan, M., Sahoo, A.K., Wood, E.F., 2014. Improving soil moisture retrievals from a physically-based radiative transfer model. Remote Sensing of Environment 140, 130–140.

Panciera, R., Tanase, M.A., Lowell, K., Walker, J.P., 2013. Evaluation of IEM, Dubois, and Oh radar backscatter models using airborne L-band SAR. IEEE Transactions on Geoscience and Remote Sensing 52, 4966–4979.

Parida, B.R., 2006. Analysing the effect of severity and duration of agricultural drought on crop performance using terra-MODIS satellite data and meteorological data. ITC.

Parrens, M., Wigneron, J.-P., Richaume, P., Al Bitar, A., Mialon, A., Fernandez-Moran, R., Al-Yaari, A., O'neill, P., Kerr, Y., 2017. Considering combined or separated roughness and vegetation effects in soil moisture retrievals. International journal of applied earth observation and geoinformation 55, 73–86.

Patel, N.R., Parida, B.R., Venus, V., Saha, S.K., Dadhwal, V.K., 2012. Analysis of agricultural drought using vegetation temperature condition index (VTCI) from Terra/MODIS satellite data. Environmental monitoring and assessment 184, 7153–7163.

Peng, J., Albergel, C., Balenzano, A., Brocca, L., Cartus, O., Cosh, M.H., Crow, W.T., Dabrowska-Zielinska, K., Dadson, S., Davidson, M.W., 2020. A roadmap for high-resolution satellite soil moisture applications–confronting product characteristics with user requirements. Remote Sensing of Environment 112162.

Peng, J., Loew, A., Merlin, O., Verhoest, N.E., 2017. A review of spatial downscaling of satellite remotely sensed soil moisture. Reviews of Geophysics 55, 341–366.

Peng, J., Loew, A., Zhang, S., Wang, J., Niesel, J., 2015a. Spatial downscaling of satellite soil moisture data using a vegetation temperature condition index. IEEE Transactions on Geoscience and Remote Sensing 54, 558–566.

Peng, J., Niesel, J., Loew, A., 2015b. Evaluation of soil moisture downscaling using a simple thermal-based proxy-the REMEDHUS network (Spain) example. Hydrology and Earth System Sciences 19, 4765–4782.

Peters, A.J., Walter-Shea, E.A., Ji, L., Vina, A., Hayes, M., Svoboda, M.D., 2002. Drought monitoring with NDVI-based standardized vegetation index. Photogrammetric engineering and remote sensing 68, 71–75.

Petropoulos, G., Carlson, T.N., Wooster, M.J., Islam, Sjp., 2009. A review of Ts/VI remote sensing based methods for the retrieval of land surface energy fluxes and soil surface moisture. Progress in Physical Geography 33, 224–250.

Petropoulos, G.P., Ireland, G., Barrett, B., 2015. Surface soil moisture retrievals from remote sensing: Current status, products & future trends. Physics and Chemistry of the Earth, Parts A/B/C 83, 36–56.

Piles, M., Petropoulos, G.P., Sánchez, N., González-Zamora, Á., Ireland, G., 2016. Towards improved spatio-temporal resolution soil moisture retrievals from the synergy of SMOS and MSG SEVIRI spaceborne observations. Remote Sensing of Environment, Special Issue: ESA's Soil Moisture and Ocean Salinity Mission - Achievements and Applications 180, 403–417. https://doi.org/10.1016/j.rse.2016.02.048

Piles, M., Sánchez, N., Vall-llossera, M., Camps, A., Martínez-Fernández, J., Martínez, J., González-Gambau, V., 2014. A Downscaling Approach for SMOS Land Observations: Evaluation of High-Resolution Soil Moisture Maps Over the Iberian Peninsula. IEEE Journal of Selected Topics in Applied Earth Observations and Remote Sensing 7, 3845–3857. https://doi.org/10.1109/JSTARS.2014.2325398

Pohn, H.A., Offield, T.W., Watson, K., 1974. Thermal inertia mapping from satellite-discrimination of geologic units in Oman. J. Res. US Geol. Surv. 2, 147–158.

Ponziani, F., Pandolfo, C., Stelluti, M., Berni, N., Brocca, L., Moramarco, T., 2012. Assessment of rainfall thresholds and soil moisture modeling for operational hydrogeological risk prevention in the Umbria region (central Italy). Landslides 9, 229–237.

Portal, G., Jagdhuber, T., Vall-llossera, M., Camps, A., Pablos, M., Entekhabi, D., Piles, M., 2020. Assessment of Multi-Scale SMOS and SMAP Soil Moisture Products across the Iberian Peninsula. Remote Sensing 12, 570. https://doi.org/10.3390/rs12030570

Portal, G., Vall-Llossera, M., Piles, M., Camps, A., Chaparro, D., Pablos, M., Rossato, L., 2018. A spatially consistent downscaling approach for SMOS using an adaptive moving window. IEEE Journal of Selected Topics in Applied Earth Observations and Remote Sensing 11, 1883–1894.

Pratt, D.A., Ellyett, C.D., 1979. The thermal inertia approach to mapping of soil moisture and geology. Remote sensing of environment 8, 151–168.

Price, J.C., 1985. On the analysis of thermal infrared imagery: The limited utility of apparent thermal inertia. Remote Sensing of Environment 18, 59–73. https://doi.org/10.1016/0034-4257(85)90038-0

Price, J.C., 1977. Thermal inertia mapping: A new view of the Earth. Journal of Geophysical Research (1896-1977) 82, 2582–2590. https://doi.org/10.1029/JC082i018p02582

Rahman, M.M., Moran, M.S., Thoma, D.P., Bryant, R., Sano, E.E., Holifield Collins, C.D., Skirvin, S., Kershner, C., Orr, B.J., 2007. A derivation of roughness correlation length for parameterizing radar backscatter models. International Journal of Remote Sensing 28, 3995–4012.

Reginato, R.J., Idso, S.B., Vedder, J.F., Jackson, R.D., Blanchard, M.B., Goettelman, R., 1976. Soil water content and evaporation determined by thermal parameters obtained from ground-based and remote measurements. Journal of Geophysical Research 81, 1617–1620.

Rice, S.O., 1951. Reflection of electromagnetic waves from slightly rough surfaces. Communications on pure and applied mathematics 4, 351–378.

Rodríguez-Fernández, N., de Rosnay, P., Albergel, C., Richaume, P., Aires, F., Prigent, C., Kerr, Y., 2019. SMOS Neural Network Soil Moisture Data Assimilation in a Land Surface Model and Atmospheric Impact. Remote Sensing 11, 1334. https://doi.org/10.3390/rs11111334

Saatchi, S.S., Njoku, E.G., Wegmüller, U., Choudhury, B.J., 1994. Synergism of active and passive microwave data for estimating bare soil surface moisture, in: Proc. Passive Microwave Remote Sensing of Land-Atmosphere Interactions, ESA/NASA Int. Workshop. pp. 205–224.

Sandholt, I., Rasmussen, K., Andersen, J., 2002. A simple interpretation of the surface temperature/vegetation index space for assessment of surface moisture status. Remote Sensing of environment 79, 213–224.

Schanda, E., 1987. On the contribution of volume scattering to the microwave backscattered signal from wet snow and wet soil. International Journal of Remote Sensing 8, 1489–1500.

Scheidt, S., Ramsey, M., Lancaster, N., 2010. Determining soil moisture and sediment availability at White Sands Dune Field, New Mexico, from apparent thermal inertia data. Journal of Geophysical Research: Earth Surface 115. https://doi.org/10.1029/2009JF001378

Schmugge, T., Blanchard, B., Anderson, A., Wang, J., 1978. Soil Moisture Sensing with Aircraft Observations of the Diurnal Range of Surface Temperature1. JAWRA Journal of the American Water Resources Association 14, 169–178. https://doi.org/10.1111/j.1752-1688.1978.tb02135.x

Schmugge, T., O'Neill, P.E., Wang, J.R., 1986. Passive microwave soil moisture research. IEEE Transactions on Geoscience and Remote Sensing 12–22.

Seneviratne, S.I., Corti, T., Davin, E.L., Hirschi, M., Jaeger, E.B., Lehner, I., Orlowsky, B., Teuling, A.J., 2010. Investigating soil moisture–climate interactions in a changing climate: A review. Earth-Science Reviews 99, 125–161.

Short, N.M., Stuart, L.M., United States., 1983. The Heat Capacity Mapping Mission (HCMM) anthology, NASA SP.465. Scientific and Technical Information Branch, National Aeronautics & Space Administration, Washington, D.C.

Shoshany, M., Svoray, T., Curran, P.J., Foody, G.M., Perevolotsky, A., 2000. The relationship between ERS-2 SAR backscatter and soil moisture: generalization from a humid to semi-arid transect. International Journal of Remote Sensing 21, 2337–2343.

Sobrino, J.A., El Kharraz, M.H., Cuenca, J., Raissouni, N., 1998. Thermal inertia mapping from NOAA-AVHRR data. Advances in Space Research 22, 655–667. https://doi.org/10.1016/S0273-1177(97)01127-7

Sohrabinia, M., Rack, W., Zawar-Reza, P., 2014. Soil moisture derived using two apparent thermal inertia functions over Canterbury, New Zealand. JARS 8, 083624. https://doi.org/10.1117/1.JRS.8.083624

Song, X., Ma, J., Li, X., Leng, P., Zhou, F., Li, S., 2014. First results of estimating surface soil moisture in the vegetated areas using ASAR and hyperion data: The chinese heihe river basin case study. Remote Sensing 6, 12055–12069.

Srivastava, P.K., 2017. Satellite soil moisture: Review of theory and applications in water resources. Water Resources Management 31, 3161–3176.

Temimi, M., Leconte, R., Chaouch, N., Sukumal, P., Khanbilvardi, R., Brissette, F., 2010. A combination of remote sensing data and topographic attributes for the spatial and temporal monitoring of soil wetness. Journal of Hydrology 388, 28–40. https://doi.org/10.1016/j.jhydrol.2010.04.021

Thoma, D., Moran, M., Bryant, R., Collins, C.H., Rahman, M., Skirvin, S., 2004. Comparison of two methods for extracting surface soil moisture from C-band radar imagery, in: IGARSS 2004. 2004 IEEE International Geoscience and Remote Sensing Symposium. Presented at

the IGARSS 2004. 2004 IEEE International Geoscience and Remote Sensing Symposium, pp. 827–830. https://doi.org/10.1109/IGARSS.2004.1368532

Tomer, S.K., Al Bitar, A., Sekhar, M., Zribi, M., Bandyopadhyay, S., Sreelash, K., Sharma, A.K., Corgne, S., Kerr, Y., 2015. Retrieval and multi-scale validation of soil moisture from multi-temporal SAR data in a semi-arid tropical region. Remote Sensing 7, 8128–8153.

Tramblay, Y., Bouvier, C., Martin, C., Didon-Lescot, J.-F., Todorovik, D., Domergue, J.-M., 2010. Assessment of initial soil moisture conditions for event-based rainfall–runoff modelling. Journal of Hydrology 387, 176–187.

Tsiros, E., Domenikiotis, C., Spiliotopoulos, M., Dalezios, N.R., 2004. Use of NOAA/AVHRR-based vegetation condition index (VCI) and temperature condition index (TCI) for drought monitoring in Thessaly, Greece, in: EWRA Symposium on Water Resources Management: Risks and Challenges for the 21st Century, Izmir, Turkey. pp. 2–4.

Ulaby, F.T., 1982. Microwave remote sensing active and passive. Rader remote sensing and surface scattering and emission theory 848–902.

Ulaby, F.T., Batlivala, P.P., Dobson, M.C., 1978. Microwave backscatter dependence on surface roughness, soil moisture, and soil texture: Part I-bare soil. IEEE Transactions on Geoscience Electronics 16, 286–295.

Ulaby, F.T., Moore, R.K., Fung, A.K., 1986. Microwave remote sensing: Active and passive. Volume 3-From theory to applications.

Ulaby, F.T., Sarabandi, K., Mcdonald, K., Whitt, M., Dobson, M.C., 1990. Michigan microwave canopy scattering model. International Journal of Remote Sensing 11, 1223–1253.

Van Doninck, J., Peters, J., De Baets, B., De Clercq, E.M., Ducheyne, E., Verhoest, N.E.C., 2011. The potential of multitemporal Aqua and Terra MODIS apparent thermal inertia as a soil moisture indicator. International Journal of Applied Earth Observation and Geoinformation 13, 934–941. https://doi.org/10.1016/j.jag.2011.07.003

Verhoef, A., 2004. Remote estimation of thermal inertia and soil heat flux for bare soil. Agricultural and Forest Meteorology 123, 221–236. https://doi.org/10.1016/j.agrformet.2003.11.005

Verhoest, N.E., Lievens, H., Wagner, W., Álvarez-Mozos, J., Moran, M.S., Mattia, F., 2008. On the soil roughness parameterization problem in soil moisture retrieval of bare surfaces from synthetic aperture radar. Sensors 8, 4213–4248.

Veroustraete, F., Li, Q., Verstraeten, W.W., Chen, X., Bao, A., Dong, Q., Liu, T., Willems, P., 2012. Soil moisture content retrieval based on apparent thermal inertia for Xinjiang province in China. International Journal of Remote Sensing 33, 3870–3885. https://doi.org/10.1080/01431161.2011.636080

Verstraeten, W.W., Veroustraete, F., van der Sande, C.J., Grootaers, I., Feyen, J., 2006. Soil moisture retrieval using thermal inertia, determined with visible and thermal spaceborne data, validated for European forests. Remote Sensing of Environment 101, 299–314. https://doi.org/10.1016/j.rse.2005.12.016

Voronovich, A.G., 1985. Small-slope approximation in wave scattering by rough surfaces. Sov. Phys. JETP 62, 65–70.

Wagner, W., Dorigo, W., de Jeu, R., Fernandez, D., Benveniste, J., Haas, E., Ertl, M., 2012. Fusion of active and passive microwave observations to create an essential climate variable data

record on soil moisture. ISPRS Annals of the Photogrammetry, Remote Sensing and Spatial Information Sciences (ISPRS Annals) 7, 315–321.

Wagner, W., Hahn, S., Kidd, R., Melzer, T., Bartalis, Z., Hasenauer, S., Figa-Saldaña, J., de Rosnay, P., Jann, A., Schneider, S., Komma, J., Kubu, G., Brugger, K., Aubrecht, C., Züger, J., Gangkofner, U., Kienberger, S., Brocca, L., Wang, Y., Blöschl, G., Eitzinger, J., Steinnocher, K., 2013. The ASCAT Soil Moisture Product: A Review of its Specifications, Validation Results, and Emerging Applications. metz 22, 5–33. https://doi.org/10.1127/0941-2948/2013/0399

Wagner, W., Scipal, K., 2000. Large-scale soil moisture mapping in western Africa using the ERS scatterometer. IEEE Transactions on Geoscience and Remote Sensing 38, 1777–1782. https://doi.org/10.1109/36.851761

Wan, Z., Wang, P., Li, X., 2004. Using MODIS land surface temperature and normalized difference vegetation index products for monitoring drought in the southern Great Plains, USA. International journal of remote sensing 25, 61–72.

Wang, X., Xie, H., Guan, H., Zhou, X., 2007. Different responses of MODIS-derived NDVI to root-zone soil moisture in semi-arid and humid regions. Journal of hydrology 340, 12–24.

Watson, K., 1982. Regional thermal-inertia mapping from an experimental satellite. Geophysics 47, 1681–1687.

Watson, K., 1973. Periodic heating of a layer over a semi-infinite solid. Journal of Geophysical Research (1896-1977) 78, 5904–5910. https://doi.org/10.1029/JB078i026p05904

Wei, L., Zhang, B., Wang, M., 2007. Effects of antecedent soil moisture on runoff and soil erosion in alley cropping systems. Agricultural water management 94, 54–62.

Wen, J., Su, Z., Ma, Y., 2003. Determination of land surface temperature and soil moisture from Tropical Rainfall Measuring Mission/Microwave Imager remote sensing data. Journal of Geophysical Research: Atmospheres 108, ACL 2-1-ACL 2-10. https://doi.org/10.1029/2002JD002176

Wetzel, P.J., Woodward, R.H., 1987. Soil moisture estimation using GOES-VISSR infrared data: A case study with a simple statistical method. Journal of climate and applied Meteorology 26, 107–117.

Whiting, M.L., Li, L., Ustin, S.L., 2004. Predicting water content using Gaussian model on soil spectra. Remote sensing of environment 89, 535–552.

Wigneron, J.-P., Kerr, Y., Waldteufel, P., Saleh, K., Escorihuela, M.-J., Richaume, P., Ferrazzoli, P., De Rosnay, P., Gurney, R., Calvet, J.-C., 2007. L-band microwave emission of the biosphere (L-MEB) model: Description and calibration against experimental data sets over crop fields. Remote Sensing of Environment 107, 639–655.

Wigneron, J.-P., Waldteufel, P., Chanzy, A., Calvet, J.-C., Kerr, Y., 2000. Two-dimensional microwave interferometer retrieval capabilities over land surfaces (SMOS mission). Remote Sensing of Environment 73, 270–282.

Xue, Y., Cracknell, A.P., 1995. Advanced thermal inertia modelling. International Journal of Remote Sensing 16, 431–446. https://doi.org/10.1080/01431169508954411

Zhao, W., Li, Z.-L., 2013. Sensitivity study of soil moisture on the temporal evolution of surface temperature over bare surfaces. International Journal of Remote Sensing 34, 3314–3331. https://doi.org/10.1080/01431161.2012.716532

Zribi, M., Dechambre, M., 2002. A new empirical model to retrieve soil moisture and roughness from C-band radar data. Remote Sensing of Environment 84, 42–52.

Zribi, M., Taconet, O., Le Hégarat-Mascle, S., Vidal-Madjar, D., Emblanch, C., Loumagne, C., Normand, M., 1997. Backscattering behavior and simulation comparison over bare soils using SIR-C/X-SAR and ERASME 1994 data over Orgeval. Remote sensing of environment 59, 256–266.